

國立交通大學

應用數學系

博士論文

不可溶界面活性劑之流體模擬數值方法

Numerical Methods for Interfacial Flows with Insoluble Surfactant



研究生：曾昱豪

指導教授：賴明治 教授

中華民國九十八年七月

不可溶界面活性劑之流體模擬數值方法  
Numerical Methods for Interfacial Flows with Insoluble Surfactant


研究生：曾昱豪

Student : Yu-Hau Tseng

指導教授：賴明治

Advisor : Ming-Chih Lai

國立交通大學  
應用數學系  
博士論文



A Dissertation  
Submitted to Department of Applied Mathematics  
National Chiao Tung University  
in partial Fulfillment of the Requirements  
for the Degree of  
Doctor of Philosophy  
in

Applied Mathematics

July 2009

Hsinchu, Taiwan, Republic of China

中華民國九十八年七月

# 不可溶界面活性劑之流體模擬數值方法

學生：曾昱豪

指導教授：賴明治 教授

國立交通大學

應用數學系 博士班

## 摘要

本論文之主要目的在於發展一個簡易且精確的數值方法，來處理含有不可溶界面活性劑的界面流問題。長久以來，界面流問題的數值模擬已經成為了解各種相關流體之現象的熱門管道。在這個論文中，我們先介紹一個有關界面流問題(包含 moving contact line problems)的數學模型，並且提出一種 immersed boundary method 來處理二維流體中帶有不可溶界面活性劑之界面的數值模擬。這個數學模型可以寫成一般常見的 immersed boundary method 的公式，包含 Eulerian 座標系下的流體方程式以及建立在 Lagrangian 座標系中有關界面的變數，而這兩個座標系之間各個變數的轉換，則是藉由 Dirac delta function 來連結。界面上的作用力主要依靠表面張力的影響，而界面上的表面張力則隨著界面活性劑的分佈而有所不同。對於 moving contact line problems，我們必需在 contact line 附近額外提供一個 unbalanced Young force 來趨動界面。利用 Lagrangian markers 來追蹤界面，我們可以導出一個簡單的界面活性劑方程。整個數值方法主要可分為幾個部分，首先計算界面所提供給流體的力量，再利用投影法算出流體的速度並內插求得界面移動的速度；算出新的界面位置之後，在界面的切線方向引入人工的速度場以達到界面上網格的均勻分佈；此間，界面活性劑方程也會受到這個人工切線速度的影響，所以活性劑方程需要做一些調整，而活性劑在界面上的濃度則經由這個調整過後的方程式來決定。在研究界面活性劑影響界面流問題的過程中，最重要的一個關鍵在於保持界面活性劑的不可溶特性，而本論文主要的貢獻在於提出一個新的對稱的數值離散方法，來處理界面活性劑方程式，基於這個方法，活性劑在數值模擬過程中可以完全的被保持住。在數值結果方面，包括剪切流中水泡的形變及附著在固態物質上液滴等。本論文提出的數值方法可以有效的處理有表面活性劑的 moving contact line problems。

## 誌 謝

當我寫英文致謝的時候，心裡就暗自構想要怎麼在中文致謝中大書特書，然而就在動筆的當下，那五味雜陳的感覺卻讓人不知該從何下筆，每寫一個字就像是在為我的學生生涯倒數，每個思緒都牽引出過去的點滴，是寫不完的幸福與感謝。

先來說說我的老大，賴明治大教授(這是最後一次以學生的身分狗腿一下)。我們的相遇應該是上帝的安排吧！十幾年前，我像是脫韁野馬奔馳在遠離宜蘭的嘉義平原上，心中早已忘卻父母親對我的殷殷期盼(當個高中數學老師)，熱愛籃球的我，自詡是球場管理員，一個星期到球場報到六天，每天三小時，有時還得去球隊練球，就這樣三年的時間轉瞬間消逝！而我卻在大學時代的第四年，像是迷途知返的浪子重新投奔書本的懷抱，不太記得是什麼力量將我拉回來，或許就是一個單純的念頭「時候到了」。還記得那門選修課「應用數學導論」，一個年輕且活力十足的傢伙(也就是當年還很幼齒的賴老大)，講述著生活中哪些事情是可以數學來描述的，而如何把我們所學的數學應用在這些實際的例子則是這堂課的目的，這是生平第一次覺得數學也能變得很活潑。然而當時的我只把這門課當成是曇花一現的美麗，眼前只擔心有研究所考試，只為了不想去當兵！

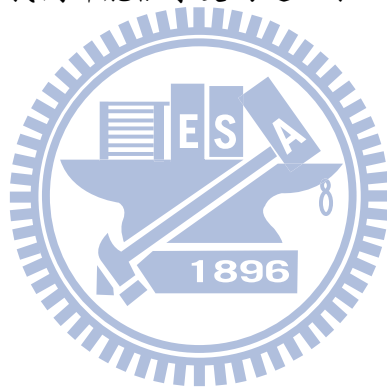
不得不承認冥冥之中似有什麼力量讓我只能選擇交大，而賴老大也在這時候被挖腳到交大，當大家都在為了選哪位指導教授而苦惱的時候，沒有概念的我不假思索就跟了賴老大！全然沒有接觸過的領域，讓我足足熬了一年多才適應過來，才對科學計算有初步的了解，或許在很多人眼中，那是苦難是折磨，對於吃苦當吃補的我，則是一直期待著苦盡甘來。一路走來，我始終不為自己設限，耳濡目染老大的行事風格處事態度，讓我見識到很多待人接物的學問，隨著賴老大南征北討，接觸了許多對我來說很新奇的事物，也拓展我的國際觀，漸漸地從一開始的只為了畢業的作研究，一直到樂在研究當中，我才發現這就是我以後要走的方向，有多少人能有這般的幸運能把糊口的工作當成樂趣呢!?

在這漫長的學生生涯中，我還得感謝一起合作過的老師。首先感謝吳佳宏老師，曾經幫他算了一些關於探討 General Navier-Stokes 方程 blow up 現象的模擬，雖然很難算，結果也不是那麼好，不過這倒是讓我初步認識用數值結果也能證實一些分析上 asymptotic approach。接下來要謝謝吳金典老師(因為跟他比較熟了，我就不需要太拘束的形容他，基本上我覺得他是個怪腳，有點宅，卻又口若懸河，有明顯的政治立場，又很熱心助人，有時候也有讓人很噴飯行為)，合作期間(以 multigrid method 來解圓柱座標上的橢圓 pde)，不僅讓我學會 multigrid method 的基本概念，也幫助我在研究上態度的修正。最近主要的研究工作是有關 moving contact line problem 與界面活性劑的問題，黃華雄老師在此間給與了很多有助於研究成果更完善的協助，同時也提供了一些未來可以深入探討的相關問題。感謝我的口試委員，對本論文的指教及提供了許多有關接下來要作的研究的意見，也感謝楊淵能老師幫我訂正論文中的錯誤。感謝系辦小姐們時常幫我處理和收拾我的迷糊帳，也感謝系上參與我生活的學弟妹們。由於本人腦細胞品質不佳，記憶區塊嚴重的退化，可能遺漏了很多直接或間接幫助過我的老師或同學，在此一並感謝你們。

「千里馬計劃」是博士班生涯的一個驚喜！老大鼓勵我出去看看外面的世界，我也就呆呆的向前衝。那段期間，我學會如何快速的適應截然不同的環境，語言上的溝通、研究領域的上的差異、一個人生活的孤獨、不同文化上人與人之間的包容等，這讓我意識到每個人的未來是有無限的可能，別把自己局限在自己所認為的世界中。感謝 John 在研究上的指導，感謝 Fang、Maggie、Jinsun、Lin、Xiang、Ming、Nelson、Jenny、Yu-Wen 等，當然還有 Ken 老大嘍，陪我談天說地、遊山玩水、逛街。另外，感謝國科會及台灣國際扶輪社提供的支持與協助，讓我在他鄉的生活無虞。

接下來要感謝我的家人和多年來親愛的朋友。感謝我的爸爸、媽媽、姊姊和弟弟，長久以來包容我的懶散、粗心及晴時多雲偶陣雨的脾氣，不斷的給我支持與鼓勵，讓我無後顧之憂的從事研究工作。我也要謝謝陪我一起打球、遊行、念書的伙伴們，帥哥、仲尹、科寶、鎮綸、阿國、偉偉…等，雖然我不常關心你們，你們總是不介意我的冷漠，依然與我同樂。

最後，我要感謝在我生命中過去十幾年來，對我非常重要的Y和W。雖然離別了，我會記住過去的美好，也希望以後的我們都能很幸福；雖然始終沒有太大的交集，我會記住生命中曾出現讓我奮不顧身的人，希望未來的我們都能很享受的過日子。



# Acknowledgements

First of all, I would like to express my deep and sincere gratitude to my advisor, professor Ming-Chih Lai, for his invaluable guidance and continuous support throughout my PhD studies. His great knowledge, personality and experience have inspired me not only to throw myself deep into research but to broaden my world view. It is hard to show the gratefulness in words, so the better way to express my thanks is keep working hard for him.

During my PhD studies, many professors generously aided me at the right moment. I am grateful to professor Huaxiong Huang for his valuable ideas and fruitful discussions on the computational results of the moving contact-line problem presented in this dissertation. I would also like to thank professor Chin-Tien Wu for many interesting discussions on implementing techniques of the multigrid method on a cylinder. I extend my thanks to professor John Lowengrub for his guidance when I visited University of California, Irvine. Also, I want to thank all friends (especially, Fang, Maggie, Jinsun, Lin, and Xiang) who made my life colorful in CA. Thanks for the supports from National Science Council of Taiwan and Rotary International Taiwan. In addition, I appreciate the committees of my defense, they gave lots of advices to make this thesis complete and many brilliant ideas to guide the future work.

I am indebted to all of my colleagues at the department for their timely help and encouragement. I also like to give my thanks to Professor Yuan-Nan Young for his aid in the correction of this thesis.

Next, my thanks go to my family and friends for their long-term support and encouragement. All my family (my parents, sister, and brother) keep tolerating my laziness, carelessness, and weird temper. They helped me to solve lots of problems on which I even payed no attention. I am very fortune to have such a wonderful family. I have to mention my dear friends, Iamtheman, Ken, Li-Wei, Nelson, Yu-Wen, Cepeda, Thomas, Yukao,...., etc. They accompanied me to study, to play, to travel, and to exploit my life.

Finally, I have to give an immense gratitude to Y and W. They played important roles in my life in the past years, I really learned a lot from them.

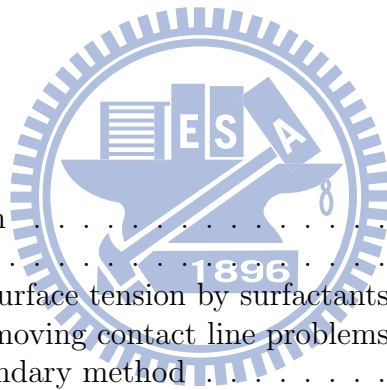
# Abstract

Numerical simulations of the interfacial flows have been a popular way to study a variety of fluid-world phenomena for a long time. In this dissertation, a mathematical model for interfacial flow problems (including the moving contact line problem) is demonstrated and an immersed boundary method is proposed for the simulation of two-dimensional fluid interfaces with insoluble surfactant. The governing equations are written in a usual immersed boundary formulation where a mixture of Eulerian flow and Lagrangian interfacial variables are used and the linkage between these two set of variables is provided by the Dirac delta function. The immersed boundary force comes from the surface tension which is affected by the distribution of surfactant along the interface. In particular, the unbalanced Young force should be applied in the moving contact line problems to derive the interface movement near moving contact lines. By tracking the interface in a Lagrangian manner, a simplified surfactant transport equation is derived. The numerical method involves solving the Navier-Stokes equations on a staggered grid by a semi-implicit pressure increment projection method where the immersed interfacial forces are calculated at the beginning of each time step. Once the velocity field and interfacial configurations are obtained, an equi-distributed technique of the Lagrangian markers is applied to force the markers to reach a uniform distribution in physical space. Meantime, the surfactant transport equation should be modified due to the effect of the tangential velocity arising from the equi-distributed process. Then the surfactant concentration is updated using the modified transport equation.

The essential purpose of this dissertation is to study the effects of insoluble surfactants in the interfacial flow problems. Since it is important to maintain the insolubility of the surfactant concentration, the main contribution of this work is to propose a new symmetric discretization for the surfactant concentration equation such that the total mass of surfactant is conserved numerically. In numerical experiments, a bubble rises in a gravitational field, a vesicle deforms in a shear flow, and a hydrophilic or hydrophobic drop adheres to a solid substrate, are typical examples to observe the effects of the surfactant. To our best knowledge, the numerical method we propose here provides a wonderful chance for the simulations of moving contact line problems with insoluble surfactant.

# Contents

<b>Acknowledgements</b>	<b>i</b>
<b>Abstract</b>	<b>ii</b>
<b>Contents</b>	<b>iii</b>
<b>List of Tables</b>	<b>iv</b>
<b>List of Figures</b>	<b>v</b>
<b>1 Introduction</b>	<b>1</b>
1.1 Surface tension . . . . .	2
1.2 Surfactant . . . . .	4
1.3 Reduction of surface tension by surfactants . . . . .	5
1.4 Surfactant in moving contact line problems . . . . .	9
1.5 Immersed boundary method . . . . .	10
1.6 Numerical experiments . . . . .	11
<b>2 Mathematical model for interfacial flow</b>	<b>13</b>
2.1 Governing equations of bulk fluids . . . . .	14
2.1.1 Conservation of mass . . . . .	15
2.1.2 Conservation of momentum . . . . .	16
2.2 A two-dimensional incompressible two-phase flow . . . . .	20
2.3 Moving contact line problems . . . . .	25
2.4 Governing equation of surfactant concentration . . . . .	27
2.5 Boundary conditions . . . . .	29
2.5.1 For Navier-Stokes equations . . . . .	29
2.5.2 For surfactant concentration equation . . . . .	30
<b>3 Immersed boundary method</b>	<b>32</b>
3.1 Equation of motion . . . . .	32
3.1.1 Derivation of interfacial forces . . . . .	33

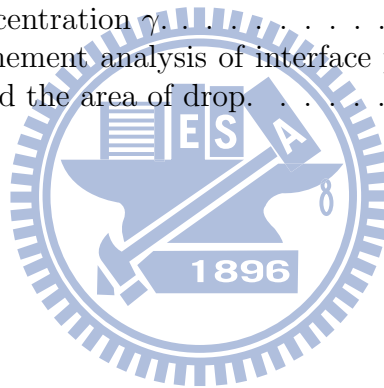




3.1.2	Connection between fluid and interface . . . . .	35
3.1.3	Dimensionless variables . . . . .	35
3.1.4	Dimensionless equations of motion . . . . .	36
3.2	Construction of $\delta$ -function . . . . .	38
3.2.1	Postulates of $\phi(r)$ . . . . .	38
3.2.2	Construction of $\phi(r)$ . . . . .	40
3.2.3	Other conventional $\phi(r)$ . . . . .	41
<b>4</b>	<b>Numerical method</b> . . . . .	<b>44</b>
4.1	Fluid solver . . . . .	44
4.1.1	Staggered grid . . . . .	45
4.1.2	MAC formulation . . . . .	47
4.1.3	Projection method . . . . .	48
4.2	Lagrangian manners . . . . .	51
4.3	Connection between fluid and interface . . . . .	52
4.4	An equi-distributed technique for Lagrangian markers . . . . .	52
4.5	Modified surfactant concentration equation . . . . .	54
4.6	Mass-preserving numerical scheme for surfactant equation . . . . .	55
4.7	Ghost values from boundary conditions . . . . .	56
4.8	Indicator function . . . . .	57
4.9	Numerical time integration . . . . .	58
<b>5</b>	<b>Numerical results</b> . . . . .	<b>61</b>
5.1	Convergent test . . . . .	61
5.1.1	For a bubble in a shear flow . . . . .	61
5.1.2	For the moving contact line problem . . . . .	62
5.2	Capillary and Maragoni effect . . . . .	64
5.3	Deformation of a bubble in a shear flow . . . . .	67
5.3.1	Clean vs. contaminated interface . . . . .	67
5.3.2	Linear vs. nonlinear equation of state . . . . .	70
5.3.3	Effect of capillary number on drop deformation . . . . .	71
5.4	A drop adheres to a solid surface . . . . .	72
5.4.1	Hydrophilic case . . . . .	75
5.4.2	Hydrophobic case . . . . .	78
5.4.3	Hydrophobic-hydrophilic case . . . . .	80
5.5	A rising bubble in a fluid with gravity effect . . . . .	85
<b>6</b>	<b>Summary and future work</b> . . . . .	<b>88</b>
	<b>Bibliography</b> . . . . .	<b>90</b>

# List of Tables

1.1	Surface tension of a few common liquids (at $20^{\circ}C$ unless otherwise noted) and interfacial tension of the water/oil system. . .	3
5.1	The mesh refinement analysis of the velocity $u$ , $v$ , and the surfactant concentration $\gamma$ . . . . .	62
5.2	The mesh refinement analysis of the velocity $u$ , $v$ , and the surfactant concentration $\gamma$ . . . . .	63
5.3	The mesh refinement analysis of interface positions, the contact angles, and the area of drop. . . . .	63



# List of Figures

1.1	An unhappy molecule at the surface: it is missing half its attractive interaction. . . . .	2
1.2	(a) Two bugs stay on the water-air surface. (b) A cross-sectional view of one leg of a bug. . . . .	3
1.3	The diagram of the alveoli. . . . .	5
1.4	Simplified diagram of the interface between two condensed phases <i>a</i> and <i>b</i> . . . . .	6
1.5	Diagrammatic representation of heptane-water interface with adsorbed surfactant. . . . .	8
1.6	The effect of detergence in a water-tetradecane system. On increasing the concentration of surfactant (SPAN 80), the system goes from a partial wetting regime to a total wetting regime of tetradecane on the substrate. The water droplet thus tends to detach itself from the substrate. . . . .	10
2.1	The diagram of nine components of stress. . . . .	17
2.2	The diagram of a bubble in a two-phase interfacial flow. . . . .	21
2.3	(a) The surface tension with which an element of the interface acts on its boundary is normal to the boundary and tangential to the interface; it tries to minimize the area of this element. (b) The resultant action of the surface tension on a surface element from a surrounding surface has a normal component if the interface is not flat, and a tangential component if the surface tension varies along the interface. . . . .	23
2.4	The diagram of contact lines and the problem setting. . . . .	26
3.1	(a) Hat function. (b) Cosine approximation. (c) Second-order approximation with 4-point support. (d) Second-order approximation with 3-point support. . . . .	43
4.1	A diagram of the staggered grid. . . . .	45

5.1	Comparison of stretching factor $ \mathbf{X}_\alpha $ with ( $U^A = 0$ , dashed line) and ( $U^A \neq 0$ , solid line), where $h = 1/128$ . . . . .	64
5.2	The time evolution of a bubble in a quiescent flow. The dash-line is the configuration of the steady state which is a circle with $r_e = 0.4243$ . (a) Relative error of area loss. (b) Total length of the bubble. . . . .	65
5.3	(a) A bubble with bulk surfactant in the second quadrant moves to the left-top corner of the box. (b) The corresponding evolution of surfactant concentration of (a). (c) A bubble with bulk surfactant in the third quadrant moves to the left-bottom corner of the box. (d) The corresponding evolution of surfactant concentration of (c). . . . .	66
5.4	The time evolution of a drop in a shear flow with clean ( $\eta = 0$ , '·') and contaminated interface ( $\eta = 0.25$ , '·-', $\eta = 0.5$ , '-·'). . .	68
5.5	The vorticity plot for the drop with surfactant near the left and right tips ( $\eta = 0.5, T = 12$ ). . . . .	68
5.6	Distributions of the surfactant concentration (left) and the corresponding surface tension (right). Notations and parameters are same as in Fig. 5.14. . . . .	70
5.7	The corresponding capillary force (left) and Marangoni force (right). Notations and parameters are same as in Fig. 5.14. . .	71
5.8	(a) Total mass of the surfactant. (b) Time plot of $m(t) - m(0)$ . (c) Total area of the bubble. (d) Total length of the interface. Notations and parameters are same as in Fig. 5.14. . . . .	72
5.9	The time evolution of a bubble under a shear flow with linear ('·') and nonlinear ('-·') equation of state. . . . .	73
5.10	Distributions of the surfactant concentration (left) and the corresponding surface tension (right). Notations and parameters are same as in Fig. 5.9. . . . .	73
5.11	The corresponding capillary force (left) and Marangoni force (right). Notations and parameters are same as in Fig. 5.9. . .	74
5.12	(a) Total mass of the surfactant. (b) Time plot of $m(t) - m(0)$ . (c) Total area of the bubble. (d) Total length of the interface. Notations and parameters are same as in Fig. 5.9. . . . .	74
5.13	The effect of capillary number $Ca$ on the deformation of the bubble. ( $Ca = 0.05$ : '·', $Ca = 0.25$ : '·-', $Ca = 0.5$ : '-·', $Ca = 1.0$ : '-·-') . . . . .	75
5.14	The time evolution of a hydrophilic drop with clean ( $\eta = 0$ , dashed line) and contaminated interface ( $\eta = 0.3$ , solid line). . . . .	76
5.15	The velocity field for the drop with surfactant near the left and right contact lines ( $\eta = 0.3, T = 1.5625$ ). . . . .	77

5.16	Distribution of the surfactant concentration (top) and the corresponding surface tension (bottom). . . . .	78
5.17	(a) Left contact line speed of the drop. (b) Right contact line speed of the drop. (c) Contact angle of the drop. (d) Total length of the drop. Notations and parameters are same as in Fig. 5.14. . . . .	79
5.18	The time evolution of a hydrophobic drop with clean ( $\eta = 0$ , dashed line) and contaminated interface ( $\eta = 0.3$ , solid line). . . . .	80
5.19	The velocity field for the drop with surfactant near the left and right contact lines ( $\eta = 0.3, T = 1.5625$ ). . . . .	81
5.20	(a) Left contact line speed of the drop. (b) Right contact line speed of the drop. (c) Contact angles of the drop. (d) Total length of the drop. Notations and parameters are same as in Fig. 5.18. . . . .	82
5.21	Wettability and the initial drop set up. . . . .	83
5.22	The time evolution of a hydrophilic drop with clean ( $\eta = 0$ , dashed line) and contaminated interface ( $\eta = 0.3$ , solid line). . . . .	83
5.23	The velocity field for the drop with surfactant near the left and right contact lines at $T = 1.0938, 3.5938$ . . . . .	84
5.24	Distribution of the surfactant concentration (top) and the corresponding surface tension (bottom). . . . .	85
5.25	(a) Left contact line speed of the drop. (b) Right contact line speed of the drop. (c) Left contact angle of the drop. (d) Right contact angle of the drop. . . . .	86
5.26	(a) A rising bubble with $E_o = 0.1$ . (b) A rising bubble with $E_o = 10$ . . . . .	87

# Chapter 1

## Introduction

The real world is abundant in phenomena of free surfaces, interfaces and moving boundaries (generally called interfaces), that interact with a surrounding substances, like gas, fluid, or solid. These interfaces separate one fluid from another, for instance air and water form the case of bubbles or free surface flows, and behave as boundaries between two materials of different physical properties. In some respects, the interface may be a rigid wall that moves with some specified time dependent motion, or an elastic membrane that deforms and stretches in response to the fluid motion. In addition, motion of interface may involve not only the dynamics of the liquid and surrounding air but also their interaction with adjacent solid surfaces. Many industrial processes, ranging from spin coating of microchips to de-icing of aircraft surfaces, rely on the ability to control these interactions.

Fluid flows with moving interfaces play important roles in many scientific, biomedical, and engineering applications. The interaction of muscle tissue with blood in the heart and arteries, coating of solid substrates with liquids, film boiling and crystal growth, micro-organisms utilize for locomotion the anisotropic drag properties of their long flexible flagella, are part of interesting applications. If an incompressible fluid flow contains an interface and the interface is between fluid 1 and fluid 2, then the flow often refers to be a free surface flow. The position of the interface is determined by the capillary force (a force acts in the direction perpendicular to the tangent plane of an interface point), which results from the balance between the normal stress and the surface tension on the interface. Generally speaking, these problems are usually described by the time-dependent incompressible Navier-Stokes equations together with interface jump conditions (can be viewed as a balance of forces on the interface). These types of problems are generally called free-boundary problems, multi-phase flow problems or interfacial flow problems.

## 1.1 Surface tension

In the microscopic sense of a matter, molecules attract one another all the time. When the attraction is stronger than thermal agitation, molecules switch from a gas phase to a more dense phase, so called a liquid. A molecule in the midst of a liquid interacts with all its neighbors and finds itself in a "happy" state. By contrast, a molecule that floats at the surface loses half of its cohesive interactions, see Fig 1.1, and becomes "unhappy". That is

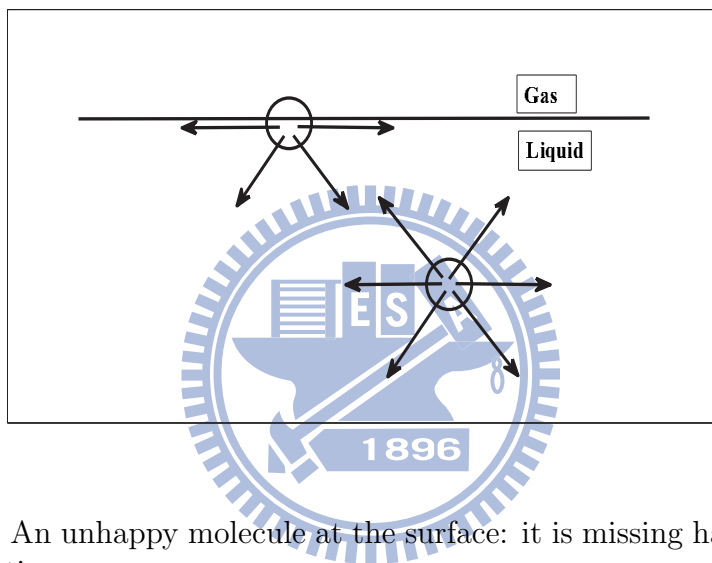


Figure 1.1: An unhappy molecule at the surface: it is missing half its attractive interaction.

the fundamental reason that liquids adjust their shape in order to expose the smallest possible surface area.

In physics, a liquid molecule is in an unfavorable energy state when it moves to the surface. If the cohesion energy per molecule is  $U$  inside the liquid, a molecule sitting at the surface goes short of energy roughly  $U/2$ . The surface tension is a direct measure of this energy shortfall per unit surface area. If  $r$  is the molecule's size and  $r^2$  is its exposed area (like one face of a cube), the surface tension is of order  $\sigma \cong U/(2r^2)$ . For most oils, for which the interactions are of the van der Waals type, we have  $U \cong kT$ , which is the thermal energy. At a temperature of  $25^\circ\text{C}$ ,  $kT$  is equal to  $1/40 \text{ eV}$ , which gives  $\sigma = 20 \text{ mJ/m}^2$ . Because water involves hydrogen bonds, its surface tension is larger ( $\sigma \approx 72 \text{ mJ/m}^2$ ). For mercury, which is a strongly cohesive liquid metal,  $U \approx 1 \text{ eV}$  and  $\sigma \approx 500 \text{ mJ/m}^2$ . Note that  $\sigma$  can

equivalently be expressed in units of  $mN/m$ . Similarly, the surface energy between two non-miscible liquids  $a$  and  $b$  is characterized by an interfacial tension  $\sigma_{ab}$ . Table 1.1 [47] lists the surface tensions of some ordinary liquids (including those usually used in the experiments of related applications), as

Table 1.1: Surface tension of a few common liquids (at  $20^\circ C$  unless otherwise noted) and interfacial tension of the water/oil system.

Liquid	Helium (4K)	Ethanol	Acetone	Cyclohexane	Glycerol
$\sigma(\frac{mN}{m})$	0.1	23	24	25	63
Liquid	Water	Water ( $100^\circ C$ )	Molten glass	Mercury	Water/oil
$\sigma(\frac{mN}{m})$	73	58	$\sim 300$	485	$\sim 50$

well as the interface tension between water and oil. Although its origin can be explained at the molecular level, the surface tension  $\sigma$  is a macroscopic

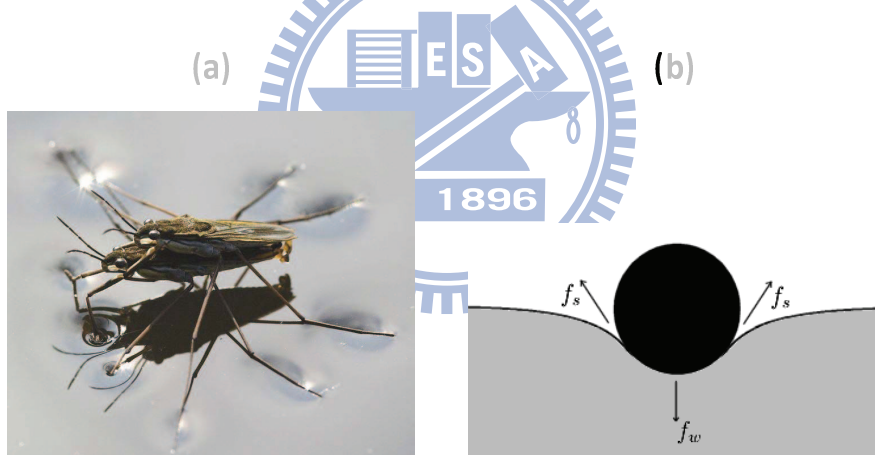


Figure 1.2: (a) Two bugs stay on the water-air surface. (b) A cross-sectional view of one leg of a bug.

parameter defined on a macroscopic scale. In Fig. 1.2(a), two waterstriders can mat on the water mainly due to the effect of surface tension. One can think the surface tension as the force acting parallel to the water-air surface and perpendicular to the line (the long leg of the bug), see Fig. 1.2(b),  $f_s$  and  $f_w$  reach a balance so that the leg is static on the water-air interface.

So far, one knows that supplying energy is necessary to create surfaces.



Suppose one wants to distort a liquid to increase its surface area by an amount  $dA$ . The work required is proportional to the number of molecules that must be brought up to the surface, i.e., to  $dA$ ; and one can write:

$$\delta W = \sigma dA$$

where  $\sigma$  is the surface (or interfacial) tension. Dimensionally,  $[\sigma] = E/L^2$ . The surface tension  $\sigma$  is thus expressed in units of  $mJ/m^2$ . In words,  $\sigma$  is the energy that must be supplied to increase the surface area by one unit.

## 1.2 Surfactant

Surfactants are the most versatile products of the chemical industry, appearing in various products such as the motor oils in the automobiles, the pharmaceuticals for patients, the detergents for cleaning our laundry and our homes, and the flotation agents used in benefit of ores [9]. In a liquid-liquid system, surfactant allows small droplets to be formed and used as an emulsion. Surfactant also plays an important role in water purification and other applications where micro-sized bubbles are generated by lowering the surface tension of the liquid-gas interface. In microsystems with the presence of interfaces, it is extremely important to consider the effect of surfactant since in such cases the capillary effect dominates the inertia of the fluids [51]. The last decades have seen the extension of surfactant applications to such high-technology areas as electronic printing, magnetic recording, biotechnology, micro-electronics, and viral research.

An example of surfactant for babies is the surfactant production in the unborn baby's lung. In pregnancy, the components of surfactant start to appear at approximately week twentieth, however it is not until much later in pregnancy that the surfactant becomes mature enough to work correctly. In the lungs, surfactant is a complex substance containing phospholipid and four different types of surfactant proteins: hydrophilic (water-attracting) proteins SP-A and SP-D and the hydrophobic (water-repelling) proteins SP-B and SP-C. These latter proteins, SP-B and SP-C (also present in Curosurf), are essential for the uniform spreading of the surfactant throughout the lung. The main role of surfactant is to prevent collapse of the alveoli thereby reducing the effort needed to expand the lungs during inspiration (breathing in) and allow gas exchange to take place. Surfactant therefore helps breathing to be relatively effortless. During expiration (breathing out) the lungs have a tendency to collapse, if they are allowed to do so then a much greater inspiratory effort is required to open them with the next breath. Surfactant

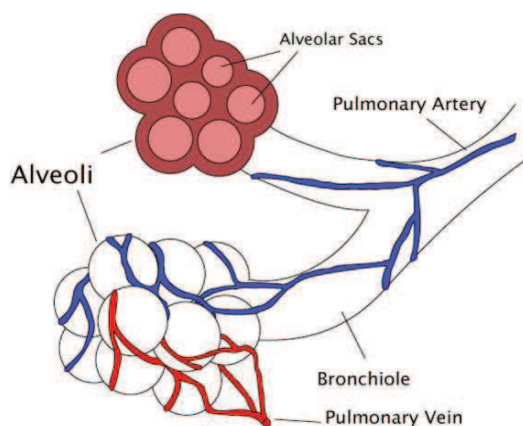


Figure 1.3: The diagram of the alveoli.

prevents this by reducing surface tension throughout the lung; surface tension is the force present within the alveoli of the lungs that causes them to collapse and stick together during expiration. Surfactant forms a very thin film which covers the surface of the alveolar cells; the components of surfactant work together to reduce surface tension and therefore reduce the tendency of the alveoli to collapse during expiration. The lungs are less stiff (improved pulmonary compliance) and therefore reduced effort is needed to expand the lungs and making breathing easier. The natural production of surfactant increases at approximately week 30 to 32 and babies born after the end of the 32nd week usually have sufficient surfactant to breath normally.

### 1.3 Reduction of surface tension by surfactants

Surfactant are surface active agents that adhere to the fluid interface and affect the interfacial tension. Reduction of surface or interfacial tension is one of the most commonly measured properties of surfactants in solution. Since it depends directly on the replacement of molecules of solvent at the interface by molecules of surfactant, and therefore on the surface (or interfacial) excess concentration of the surfactant, as shown by the Gibbs equation

$$d\sigma = - \sum_i \sigma_i d\mu_i,$$

it is also one of the most fundamental of interfacial phenomena.

As we know, the molecules at the surface of a liquid have potential energies greater than those of similar molecules in the interior of the liquid. (This is because attractive interactions of molecules at the surface with those in the interior of the liquid are greater than those with the widely separated molecules in the gas phase.) Because the potential energies of molecules at the surface are greater than those in the interior of the phase, an amount of work equal to this difference in potential energy must be expended to bring a molecule from the interior to the surface. The surface free energy per unit area, or surface tension, is a measure of this work; it is the minimum amount of work required to bring sufficient molecules to the surface from the interior to expand it by unit area. Although more correctly thought of as a surface free energy per unit area, surface tension is often conceptualized as a force per unit length at a right angle to the force required to pull apart the surface molecules in order to permit expansion of the surface by movement into it of molecules from the phase underneath it.

At the interface between two condensed, phases, the dissimilar molecules

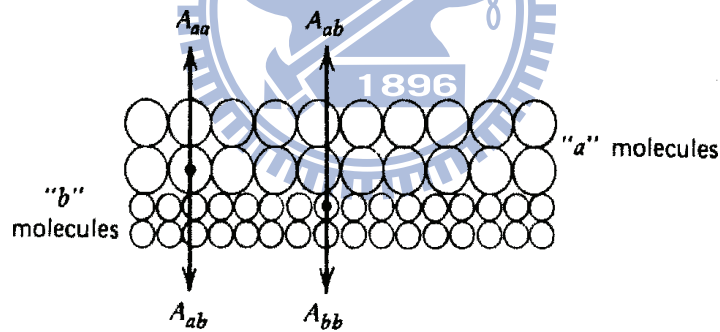


Figure 1.4: Simplified diagram of the interface between two condensed phases  $a$  and  $b$ .

in the adjacent layers facing each other across the interface (Fig. 1.4) also have potential energies different from those in their respective phases. Each molecule at the interface has a potential energy greater than that of a similar molecule in the interior of its bulk phase by an amount equal to its interaction energy with the molecules in the interior of its bulk phase minus its interaction energy with the molecules in the bulk phase across the interface. For most purposes, however, only interactions with adjacent molecules need be

taken into account. If we consider an interface between two pure liquid phases  $a$  and  $b$  (Fig. 1.4), then the increased potential energy of the  $a$  molecules at the interface over those in the interior of that phase is  $A_{aa}$  and  $A_{ab}$ , where  $A_{aa}$  symbolizes the molecular interaction energy between  $a$  molecules at the interface and similar molecules in the interior of the bulk phase and  $A_{ab}$  symbolizes the molecular interaction energy between  $a$  molecules at the interface and  $b$  molecules across the interface. Similarly, the increased potential of  $b$  molecules at the interface over those in the interior is  $A_{bb} - A_{ab}$ . The increased potential energy of all the molecules at the interface over those in the interior of the bulk phases, the interfacial free energy, is then  $(A_{aa} - A_{ab}) + (A_{bb} - A_{ab})$  or  $A_{aa} + A_{bb} - 2A_{ab}$ , and this is the minimum work required to create the interface. The interfacial free energy per unit area of interface, the interfacial tension  $\sigma_I$  is then given by the expression

$$\sigma_I = \sigma_a + \sigma_b - 2\sigma_{ab}, \quad (1.1)$$

where  $\sigma_a$  and  $\sigma_b$  are the surface free energies per unit area (the surface tensions) of the pure liquids  $a$  and  $b$ , respectively, and  $\sigma_{ab}$  is the  $a - b$  interaction energy per unit area across the interface.

The value of the interaction energy per unit area across the interface  $\sigma_{ab}$  is large when molecules  $a$  and  $b$  are similar in nature to each other (e.g., water and short-chain alcohols). When  $\sigma_{ab}$  is large, we can see from equation (1.1) that the interfacial tension  $\sigma_I$  will be small; when  $\sigma_{ab}$  is small,  $\sigma_I$  is large. The value of the interfacial tension is therefore a measure of the dissimilarity of the two types of molecules facing each other across the interface.

In the case where one of the phases is a gas (the interface is a surface), the molecules in that phase are so far apart relative to those in the condensed phase that tensions produced by molecular interaction in that phase can be disregarded. Thus if phase  $a$  is a gas,  $\sigma_a$  and  $\sigma_{ab}$  can be disregarded and  $\sigma_I \approx \sigma_b$ , the surface tension of the condensed phase  $b$ .

When the two phases are immiscible liquids,  $\sigma_a$  and  $\sigma_b$ , their respective surface tensions, are experimentally determinable, permitting the evaluation of  $\sigma_{ab}$ , at least in some cases. If one of the phases is solid, on the other hand, experimental evaluation of  $\sigma_{ab}$  is difficult, if not impossible. However here, too, the greater the similarity between  $a$  and  $b$  in structure or in the nature of their intermolecular forces, the greater the interaction between them (i.e., the greater the value of  $\sigma_{ab}$ ) and the smaller the resulting interfacial tension between the two phases. When  $2\sigma_{ab}$  becomes equal to  $\sigma_a + \sigma_b$ , the interfacial region disappears and the two phases spontaneously merge to form a single one.

If we now add to a system of two immiscible phases (e.g., heptane and

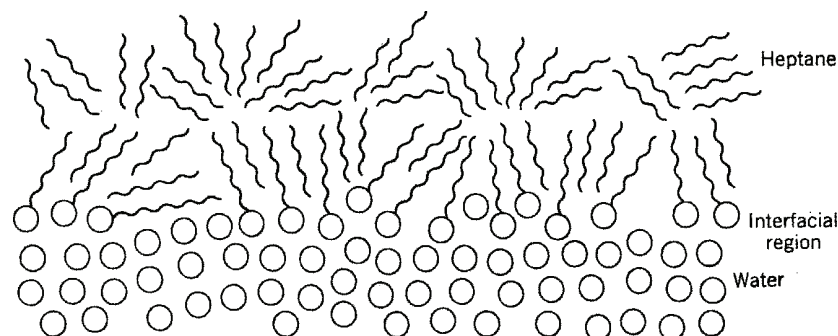


Figure 1.5: Diagrammatic representation of heptane-water interface with adsorbed surfactant.

water), a surface-active agent that is adsorbed at the interface between them, it will orient itself there, mainly with the hydrophilic group toward the water and the hydrophobic group toward the heptane (Fig. 1.5). When the surfactant molecules replace water and/or heptane molecules of the original interface, the interaction across the interface is now between the hydrophilic group of the surfactant and water molecules on one side of the interface and between the hydrophobic group of the surfactant and heptane on the other side of the interface. Since these interactions are now much stronger than the original interaction between the highly dissimilar heptane and water molecules, the tension across the interface is significantly reduced by the presence there of the surfactant. Since air consists of molecules that are mainly non-polar, surface tension reduction by surfactants at the air-aqueous solution interface is similar in many respects to interfacial tension reduction at the heptane-aqueous solution interface.

We can see from this simple model why a necessary but not sufficient condition for surface or interfacial tension reduction is the presence in the surfactant molecule of both lyophobic and lyophilic portions. The lyophobic portion has two functions: (1) to produce spontaneous adsorption of the surfactant molecule at the interface and (2) to increase interaction across the interface between the adsorbed surfactant molecules there and the molecules in the adjacent phase. The function of the lyophilic group is to provide strong interaction between the molecules of surfactant at the interface and the molecules of solvent. If any of these functions is not performed, then the marked reduction of interfacial tension characteristic of surfactants will

probably not occur. Thus, we would not expect ionic surfactants containing hydrocarbon chains to reduce the surface tensions of hydrocarbon solvents, in spite of the distortion of the solvent structure by the ionic groups in the surfactant molecules. Adsorption of such molecules at the airhydrocarbon interface with the ionic groups oriented toward the predominantly non-polar air molecules would result in decreased interaction across the interface, compared to that with their hydrophobic groups oriented toward the air.

For significant surface activity, a proper balance between lyophilic and lyophobic character in the surfactant is essential. Since the lyophilic (or lyophobic) character of a particular structural group in the molecule varies with the chemical nature of the solvent and such conditions of the system as temperature and the concentrations of electrolyte and/or organic additives, the lyophilic-lyophobic balance of a particular surfactant varies with the system and the conditions of use. In general, good surface or interfacial tension reduction is shown only by those surfactants that have an appreciable, but limited, solubility in the system under the conditions of use. Thus surfactants which may show good surface tension reduction in aqueous systems may show no significant surface tension reduction in slightly polar solvents such as ethanol and polypropylene glycol in which they may have high solubility.

## 1.4 Surfactant in moving contact line problems

In our daily lives, there are full of the motion of liquid under the influence of surface tension. For example, drink a cup of coffee, take a shower, wash clothes, design a thermometer, wax cars, or cook with nonstick cook ware, etc.. These phenomena always involve a key, the interface of the two fluid phases intersects the solid phase to introduce the motion of a contact line, where a triple juncture of the solid/gas, solid/liquid, and liquid/gas interfaces. A typical paradox arises from no-slip boundary conditions near the contact line, implies that an infinite force is required to move a contact line [8, 47]. In recent decades, many scientists put lots of effort on curing this paradox. Several models have been proposed to study the motion of moving contact lines. Most of them involve adding an additional effect on a microscopic length-scale, for instance, weakening the no-slip boundary condition via a slip condition effective at small scales [11, 12, 43] or incorporating the effect of long-range Van der Waals forces between the liquid and solid.

When a fluid-fluid interface is in contact with a solid substrate, surfactant

can change the wetting properties by altering the value of the contact angle. This simple fact has found many interesting applications in our daily life and industrial processes. For example, we add detergents (surfactant) in washing machine to clean our clothes more effectively. The detergent helps to remove drops of grease from clothes by increasing the contact angle (measured from inside the drop). An idealization of this problem can be found in a photo shown in Fig. 1.6 [51] or a figure in [14] where it is demonstrated that a

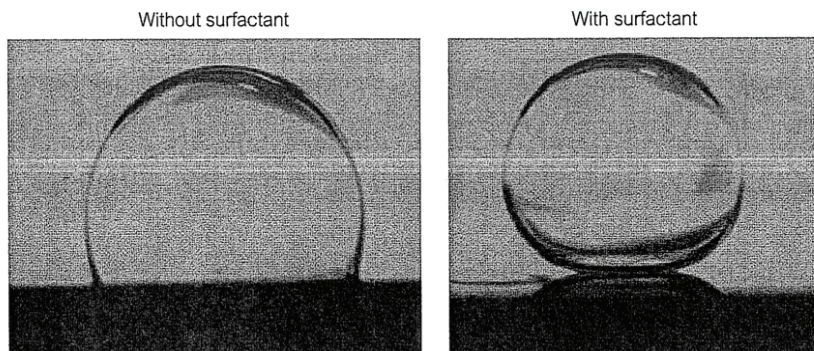


Figure 1.6: The effect of detergent in a water-tetradecane system. On increasing the concentration of surfactant (SPAN 80), the system goes from a partial wetting regime to a total wetting regime of tetradecane on the substrate. The water droplet thus tends to detach itself from the substrate.

drop on clothes can become less wetting (from the drop point of view) by increasing surfactant concentration. By adding surfactant, a drop which sticks to clothes becomes less sticky and the water currents can wash away the drop readily. The physical situation corresponding to this idealized system includes a solid-drop (grease)-water system and the surfactant. Mathematically, as discussed more detail in the main text of this dissertation, this is a moving contact line problem since the solid-drop (grease)-water triple intersection forms a contact line. One of the main issues we will try to address in this dissertation is how surfactant, by changing the contact angle, affects the movement of the contact line.

## 1.5 Immersed boundary method

The immersed boundary (IB) method proposed by Peskin [35], has been applied successfully to blood-valve interaction and other biological problems. The IB formulation employs a mixture of Eulerian and Lagrangian variables,

where the immersed boundary is represented by a set of discrete Lagrangian markers embedding in the Eulerian fluid domain. Those markers can be treated as force generators to the fluid while being carried by the fluid motion. The interaction between the Lagrangian force generators (markers) and the fluid motion, described by variables defined on the fixed Eulerian grid, is linked by a properly chosen discretized delta function. Most IB applications in the literature belong to the fluid-structure problems, and they can be found in a recent review of Peskin [36]. However, there is comparatively less work on the application of the IB method to viscous, incompressible multi-phase flow problems. Perhaps the most successful one is the front-tracking method proposed by Tryggvason *et al.* [53, 52] which uses an approach similar to the immersed boundary method.

## 1.6 Numerical experiments

In the case of interfacial flows with surfactant, Ceniceros [5] used a hybrid level set and front tracking approach to study the effects of surfactant on the formation of capillary waves. Lee and Pozrikids [30] used Peskin's immersed boundary idea to study the effects of surfactant on the deformation of drops and bubbles in Navier-Stokes flows. The surfactant convection-diffusion equation in these papers is based on the formulation proposed by Wong *et al.* [54], and the conservation of total mass of surfactant on the interface has not been rigorously investigated numerically.

James and Lowengrub [24] have proposed a surfactant-conserving volume-of-fluid method for interfacial flows with insoluble surfactant. Instead of solving the surfactant concentration equation based on Stone's derivation [49] directly, the authors relate the surfactant concentration to the ratio of the surfactant mass and surface area so that they are tracked independently. The method has been applied to study the axis-symmetric drop deformation in extensional flows. Recently, Xu *et al.* [56] develop a level-set method for interfacial Stokes flows with surfactant. Their method couples surfactant transport, solved in an Eulerian domain [57] with Stokes flow field, solved by the immersed interface method [28] with jump conditions across the interface. However, the method does not conserve the mass automatically and numerical scaling is used to enforce the conservation of surfactant on the interface numerically. Recently, Muradoglu and Tryggvason [33] have proposed a front-tracking method for computation of interfacial flows with soluble surfactant. They consider the axis-symmetric motion and deformation of a viscous drop moving in a circular tube.



Numerical simulation of two-phase flows with moving contact lines have also been developed in the literature. Finite element method [39], level set method [48], front tracking method [20], volume-of-fluid method [45, 50, 58], phase field method [23, 42], sharp interface Cartesian grid method [26] and molecular dynamics [40, 41, 43] have been tools to address these problems. However, to the best of our knowledge there is no numerical result taking the contaminant into account in the fluid, even only on the interface. In hydrodynamic cleaning, a shear flow is exploited for the removal of remnant droplets of a contaminant or impurity. The removal of droplets from the narrow passages of a porous medium determines the efficiency of tertiary oil recovery and plays an important role in the micro-mechanics of groundwater flow.



## Chapter 2

# Mathematical model for interfacial flow

The essential purpose of this chapter is to derive the mathematical model for physical problems we are interested in. First, we derive the governing equations of fluid flows which result from invoking the physical laws of conservation of mass, and momentum. Basically, we use the continuum method, which ignores individual molecules and assumes that the fluid consists of continuous matter, to describe equations which govern the motion of fluid. Since there is an interface immersed in the fluid, we use two reference frames simultaneously, the Eulerian framework is employed for fluid variables while variables defined on the interface are based on the Lagrangian framework. A general theorem, called the Reynolds' transport theorem [7], is used to relate derivatives of Lagrangian and Eulerian frameworks to yield the so-called continuity equation and the Navier-Stokes equations. Further, the boundary conditions across a interface for a two-phase flow will be determined, and it can be converted into a singular force by the use of a continuum surface forces formulation [4, 35].

Next, the conservation of mass of surfactant concentration comes from its insolubility on the interface, and the corresponding governing equation will be represented in a simple form [31]. For moving contact line problems, the interface movement involves not only the fluid-fluid surface tension but surface tensions between solid substrate and liquids. A driver called the unbalanced Young force for the contact line will be introduced to mimic the tendency of the Young condition. To close the system, appropriate boundary conditions, respectively, for fluid field [15] (especially Navier-slip boundary condition for the moving contact line problems) and surfactant concentration, will be introduced at the end of this chapter.

## 2.1 Governing equations of bulk fluids

We first introduce the concept of a control volume  $V$  which is arbitrary in shape, and each conservation principle is applied to the integral over a control volume. The result of applying each conservation principle will be an integro-differential equation of the type  $\int_V L\psi dV = 0$  where  $L$  is some differential operator and  $\psi$  is some property of fluid, like density or velocity. Since  $V$  is arbitrarily chosen, the only way this equality can be satisfied is to set  $L\psi = 0$ , which is a differential equation of the corresponding conservation law. The following is a principal theorem, so-called Reynolds' transport theorem, to derive differential equations of conservation laws.

**Theorem.** *Suppose that  $\psi$  is any property of the fluid dependent on space and time, i.e.  $\psi = \psi(\mathbf{x}, t)$ , and  $V$  is the control volume, then the rate of change of the integral of  $\psi$  is*

$$\frac{D}{Dt} \int_{V(t)} \psi(\mathbf{x}, t) dV = \int_{V(t)} \left( \frac{\partial \psi}{\partial t} + \nabla \cdot (\psi \mathbf{u}) \right) dV, \quad (2.1)$$

where  $D/Dt$  is the lagrangian derivative and  $\mathbf{u}$  is the velocity of the control volume.

**proof:** Assume that the control volume is a function of  $t$ , and  $V(t)$  is the control volume at time  $t$ , then  $V(t + \delta t)$  is the control volume after flowing a small time  $\delta t$  away from  $t$ . By definition of the differentiation,

$$\begin{aligned} \frac{D}{Dt} \int_{V(t)} \psi(\mathbf{x}, t) dV &= \lim_{\delta t \rightarrow 0} \frac{1}{\delta t} \left( \int_{V(t+\delta t)} \psi(\mathbf{x}, t + \delta t) dV - \int_{V(t)} \psi(\mathbf{x}, t) dV \right) \\ &= \lim_{\delta t \rightarrow 0} \frac{1}{\delta t} \left( \int_{V(t+\delta t)} \psi(\mathbf{x}, t + \delta t) - \psi(\mathbf{x}, t) dV + \int_{V(t+\delta t)-V(t)} \psi(\mathbf{x}, t) dV \right), \end{aligned}$$

the first term of the right-hand side is actually the integral of the partial derivative of  $\psi(\mathbf{x}, t)$  with respect to  $t$ , and the second term can be converted to a surface integral by the use of the approximation  $dV = \mathbf{u} \cdot \mathbf{n} \delta t dS$ , therefore,

$$\lim_{\delta t \rightarrow 0} \frac{1}{\delta t} \int_{V(t+\delta t)-V(t)} \psi(\mathbf{x}, t) dV = \lim_{\delta t \rightarrow 0} \frac{1}{\delta t} \int_{S(t)} \psi(\mathbf{x}, t) \mathbf{u} \cdot \mathbf{n} \delta t dS.$$

Moreover, the divergence theorem transfer the surface integral back to a volume integral

$$\int_{S(t)} \psi(\mathbf{x}, t) \mathbf{u} \cdot \mathbf{n} dS = \int_{V(t)} \nabla \cdot (\psi(\mathbf{x}, t) \mathbf{u}) dV$$

and then the proof is completed.

### 2.1.1 Conservation of mass

The conservation of mass is a fundamental concept of physics. Its main spirit states that mass can neither be created nor destroyed except the special theory of relativity of Albert Einstein, the mass of a body changes as the energy possessed by the body changes. Such nuclear reactions usually occur in subatomic phenomena, and matter may be created, for instance, by the materialization of a photon (quantum of electromagnetic energy) into an electron-positron pair; or it may be destroyed, by the annihilation of this pair of elementary particles to produce a pair of photons.

To comprehend the conservation of mass in fluid mechanics, we consider a specific mass of fluid whose volume  $V$  is arbitrarily chosen. This piece of fluid is followed as it flows, meantime, its shape or size will be changed. Suppose there are no nuclear reactions in the process, the principle of mass conservation means that no matter this given piece of fluid changes its size or shape, its mass will remain the same. The mathematical equivalence of the statement of mass conservation is to take the lagrangian derivative  $D/Dt$  to the mass of fluid contained in  $V$ , which is  $\int_V \rho dV$ , equal to zero, where  $\rho$  is the density per unit volume. That is, the equation which expresses conservation of mass is

$$\frac{D}{Dt} \int_V \rho dV = 0. \quad (2.2)$$

By use of Eq. (2.1), we transfer a derivative in lagrangian manner of an integral to an integral of derivatives in eulerian manner

$$\frac{D}{Dt} \int_V \rho dV = \int_V \left( \frac{\partial \rho}{\partial t} + \nabla \cdot (\rho \mathbf{u}) \right) dV = 0,$$

and since  $V$  is arbitrary, we obtain a local differential form of conservation of mass as

$$\frac{\partial \rho}{\partial t} + \nabla \cdot (\rho \mathbf{u}) = 0. \quad (2.3)$$

Alternatively, using the Einstein notation convention, (2.3) can be rewritten as

$$\frac{\partial \rho}{\partial t} + \frac{\partial}{\partial x_k} (\rho u_k) = 0. \quad (2.4)$$

Note that this partial differential equation forces the velocity field to be at least continuous. So, Eq. (2.3) is usually called the continuity equation.

## 2.1.2 Conservation of momentum

The conservation of momentum is another important concept of physics along with the conservation of mass. Momentum is defined to be the product of the mass of an object and its corresponding velocity. The conservation of momentum states that within some problem domain, the amount of momentum remains constant. In other words, momentum is neither created nor destroyed, but only changed through the action of forces. In fact, the principle of conservation of momentum is an application of Newton's second law of motion to an object. In fluid mechanics, Newton's second law of motion can be easily derived by an element of the fluid. That is, if we consider a given mass of fluid in a lagrangian framework, the rate of change of the momentum of the fluid mass is equal to the net external force acting on the mass. Some people prefer to think of forces only and restate this law in the form that the inertia force is equal to the net external force acting on the element.

Basically, the external forces acting on a mass of the fluid can be simply categorized into two classes. One is the class of body forces, such as gravitational or electromagnetic forces. The other is the class of surface forces, such as pressure forces or viscous stresses. Let  $\mathbf{f}$  be a vector which represents the resultant of the body forces per unit mass, then the net external body force acting on a mass of volume  $V$  is  $\int_V \rho \mathbf{f} dV$ . On the other hand, if a surface vector  $\mathbf{T}$  represents the resultant surface force per unit area, then the net external surface force acting on the surface  $S$  containing  $V$  is  $\int_S \mathbf{T} dS$ . Also, we assume that the mass per unit volume is  $\rho$  and its momentum is  $\rho \mathbf{u}$ , so that the momentum contained in the volume  $V$  is  $\int_V \rho \mathbf{u} dV$ . According to statements of Newton's second law of motion, the rate of the change of momentum (or inertia force) is equal to the sum of the resultant forces. If the mass of the arbitrarily chosen volume  $V$  is observed in the lagrangian framework, the rate of change of momentum of the mass contained within  $V$  will be  $(D/Dt) \int_V \rho \mathbf{u} dV$ . Therefore, we can obtain a mathematical equation which arises from imposing the physical law of conservation of momentum in the form

$$\frac{D}{Dt} \int_V \rho \mathbf{u} dV = \int_S \mathbf{T} dS + \int_V \rho \mathbf{f} dV, \quad (2.5)$$

In general, we can use a stress tensor [7] to represent surface forces acting on the fluid, and there are nine components of stress at any given point, one normal component and two shear components on each coordinate plane. These nine components of stress can be easily illustrated by the use of a cubical element in Fig. 2.1, then the stress components will act at a point as the length of the cube tends to zero. In Fig. 2.1 the cartesian coordinates

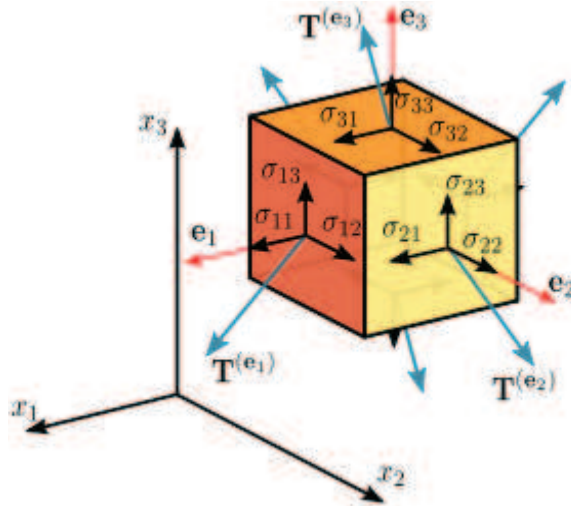


Figure 2.1: The diagram of nine components of stress.

$(x, y, z)$  have been denoted by  $(x_1, x_2, x_3)$ . This allows us to describe the components of stress as a double-subscript notation. In this notation, a particular component of the stress may be represented by the quantity  $\sigma_{ij}$ , in which the first subscript indicates that this stress component acts on the plane  $x_i = C$ , where  $C$  is a constant, and the second subscript indicates that it acts in the  $x_j$ -direction. The fact that the stress may be represented by the quantity  $\sigma_{ij}$ , in which  $i$  and  $j$  may be 1, 2, or 3, means that the stress at a point may be represented by a tensor of rank 2. However, it was observed that there would be a vector force at each point on the surface of the control volume, and this force was represented by  $\mathbf{T}$ . The surface force vector  $\mathbf{T}$  may be related to the stress tensor  $\sigma_{ij}$  as follows: The three stress components acting on the plane  $x_1 = \text{constant}$  are  $\sigma_{11}$ ,  $\sigma_{12}$ , and  $\sigma_{13}$ . Since the unit normal vector acting on this surface is  $n_1$ , the resulting force acting in the  $x_1$  direction is  $T_1 = \sigma_{11}n_1$ . Likewise, the forces acting in the  $x_2$  direction and the  $x_3$  direction are, respectively,  $T_2 = \sigma_{12}n_1$  and  $T_3 = \sigma_{13}n_1$ . Then, for an arbitrarily oriented surface whose unit normal has components  $n_1$ ,  $n_2$ , and  $n_3$ , the surface force will be given by  $T_j = \sigma_{ij}n_i$  in which  $i$  is summed from 1 to 3. That is, in tensor notation the equation expressing conservation of momentum becomes

$$\frac{D}{Dt} \int_V \rho u_j dV = \int_S \sigma_{ij} n_i dS + \int_V \rho f_j dV$$

Again, the left-hand side of this equation can be converted to a volume integral of only eulerian derivatives by using Eq. (2.1), meanwhile, the surface integral on the right-hand side can be changed to a volume integral by making use of Gauss' theorem. In this way the equation which evolved from Newton's second law becomes

$$\int_V \left( \frac{\partial}{\partial t} (\rho u_j) + \frac{\partial}{\partial x_k} (\rho u_j u_k) \right) dV = \int_V \frac{\partial \sigma_{ij}}{\partial x_i} dV + \int_V \rho f_j dV$$

Collect these volume integrals to express this equation in the form  $\int_V \{\} dV = 0$ , where the integrand is a differential equation in eulerian coordinates. As before, the arbitrariness of the control volume  $V$  implies that the integrand of the above integro-differential equation have to present the basic law of dynamics in an equivalent differential equations

$$\frac{\partial}{\partial t} (\rho u_j) + \frac{\partial}{\partial x_k} (\rho u_j u_k) = \frac{\partial \sigma_{ij}}{\partial x_i} + \rho f_j,$$

If we consider  $\rho u_j u_k$  as the product of  $\rho u_k$  and  $u_j$ , and expand the left-hand side of the equation above, we obtain

$$\rho \frac{\partial u_j}{\partial t} + u_j \frac{\partial \rho}{\partial t} + u_j \frac{\partial}{\partial x_k} (\rho u_k) + \rho u_k \frac{\partial u_j}{\partial x_k} = \frac{\partial \sigma_{ij}}{\partial x_i} + \rho f_j$$

Note that the sum of the second and third terms on the left-hand side of this equation is zero due to the continuity equation (2.4). With this simplification, the expression of conservation of momentum becomes

$$\rho \frac{\partial u_j}{\partial t} + \rho u_k \frac{\partial u_j}{\partial x_k} = \frac{\partial \sigma_{ij}}{\partial x_i} + \rho f_j \quad (2.6)$$

It is useful to recall that this equation came from an application of Newton's second law to an element of the fluid. The left-hand side of Eq. (2.6) represents the rate of change of momentum of a unit volume of the fluid (or the inertia force per unit volume). The first term is the familiar temporal acceleration term, while the second term is a convective acceleration and accounts for local accelerations even when the flow is steady. Note also that this second term is nonlinear, since the velocity appears quadratically. On the right-hand side of Eq. (2.6) are the forces which are causing the acceleration. The first of these is due to the gradient of surface shear stresses and the second is due to body forces, such as gravity, which act on the mass of the fluid. A clear understanding of the physical significance of each of the terms in Eq. (2.6) is essential when approximations to the full governing equations must be made. In the following, we will list some assumptions and the surface-stress tensor  $\sigma_{ij}$  will be related to an expression of pressure and velocities.

1. When the fluid is at rest, the stress is hydrostatic and the pressure exerted by the fluid is the thermodynamic pressure. This implies that the stress tensor  $\sigma_{ij}$  is of the form

$$\sigma_{ij} = -p\delta_{ij} + \tau_{ij} \quad (2.7)$$

where  $\tau_{ij}$  depends on the motion of the fluid only and is called the shear-stress tensor. The quantity  $p$  is the thermodynamic pressure and  $\delta_{ij}$  is the Kronecker delta.

2. The stress tensor  $\sigma_{ij}$  is linearly related to the deformation-rate tensor  $e_{kl}$  and depends only on that tensor. This is the distinguishing feature of newtonian fluids. There are nine elements in the shear-stress tensor  $\tau_{ij}$ , and each of these elements may be expressed as a linear combination of the nine elements in the deformation-rate tensor  $e_{kl}$  (just as a vector may be represented as a linear combination of components of the base vectors). That is, each of the nine elements of  $\tau_{ij}$  will in general be a linear combination of the nine elements of  $e_{kl}$  so that 81 parameters are needed to relate  $\tau_{ij}$  to  $e_{kl}$ . This means that a tensor of rank 4 is required so that the general form of  $\tau_{ij}$  will be

$$\tau_{ij} = \alpha_{ijkl} \frac{\partial u_k}{\partial x_l} \quad (2.8)$$

3. Since there is no shearing action in a solid body rotation of the fluid, no shear stresses will act during such a motion. Then

$$\tau_{ij} = \frac{1}{2} \beta_{ijkl} \left( \frac{\partial u_k}{\partial x_l} - \frac{\partial u_l}{\partial x_k} \right) \quad (2.9)$$

4. There are no preferred directions in the fluid, so that the fluid properties are point functions. This condition is the so-called condition of isotropy, which guarantees that the results obtained should be independent of the orientation of the coordinate system chosen. The most general isotropic tensor of rank 4 is of the form, see appendix in [7],

$$\lambda \delta_{ij} \delta_{kl} + \mu (\delta_{ik} \delta_{jl} + \delta_{il} \delta_{jk}) + \gamma (\delta_{ik} \delta_{jl} - \delta_{il} \delta_{jk}) \quad (2.10)$$

Using the fact that  $\delta_{kl} = 0$  unless  $l = k$ , the expression for the shear-stress tensor becomes

$$\tau_{ij} = \lambda \delta_{ij} \frac{\partial u_k}{\partial x_k} + \mu \left( \frac{\partial u_i}{\partial x_j} + \frac{\partial u_j}{\partial x_i} \right) \quad (2.11)$$

Thus the constitutive relation for stress in a newtonian fluid becomes

$$\sigma_{ij} = -p\delta_{ij} + \lambda \delta_{ij} \frac{\partial u_k}{\partial x_k} + \mu \left( \frac{\partial u_i}{\partial x_j} + \frac{\partial u_j}{\partial x_i} \right) \quad (2.12)$$



## 2.2 A two-dimensional incompressible two-phase flow

Consider an incompressible two-phase flow problem consisting of fluids 1 and 2 in a fixed two-dimensional square domain  $\Omega = [a, b] \times [c, d] = \Omega_1 \cup \Omega_2$  where an interface  $\Sigma$  separates  $\Omega_1$  from  $\Omega_2$ , see Fig. 2.2. Actually, almost all materials in reality are compressible to some extent, and the incompressibility refers to flow, not the material property. This means that under certain circumstances, a compressible material can nearly behave as an incompressible flow. Strictly speaking, an incompressible fluid is a fluid which is not reduced in volume by an increase in pressure. With this ideal assumption, the density of the fluid element is a constant as it moves from one point to another. This implies that the material derivative of density is zero,  $D\rho/Dt = 0$ . Then Eq. (2.3) can be reduced in the following:

$$0 = \frac{\partial \rho}{\partial t} + \nabla \cdot (\rho \mathbf{u}) = \frac{D\rho}{Dt} + \rho \nabla \cdot \mathbf{u} \Rightarrow \nabla \cdot \mathbf{u} = 0.$$

Take advantage of the divergence free property of the velocity,  $\lambda \delta_{ij} \frac{\partial u_k}{\partial x_k}$  is zero, then Eq. (2.12) is simply reduced as

$$\sigma_{ij} = -p\delta_{ij} + \mu \left( \frac{\partial u_i}{\partial x_j} + \frac{\partial u_j}{\partial x_i} \right).$$

Since these equation are satisfied in each bulk fluid, we can write the corresponding Navier-Stokes equations of the two-phase flow as

$$\rho_i \left( \frac{\partial \mathbf{u}_i}{\partial t} + (\mathbf{u}_i \cdot \nabla) \mathbf{u}_i \right) = \nabla \cdot \mathbf{T}_i + \rho_i \mathbf{f}_i \quad \text{in } \Omega_i \quad (2.13)$$

$$\nabla \cdot \mathbf{u}_i = 0, \quad \text{in } \Omega_i, \quad (2.14)$$

where for  $i = 1, 2$  in each fluid domain,  $\mathbf{T}_i = -p_i \mathbf{I} + \mu_i (\nabla \mathbf{u}_i + \nabla \mathbf{u}_i^T)$  is the stress tensor,  $p_i$  is the pressure,  $\mathbf{u}_i$  is the fluid velocity,  $\rho_i$  is the density,  $\mu_i$  is the viscosity, and  $\mathbf{f}_i$  is the external force such as the gravitational force.

### Jump conditions cross the interface

When two fluids contact with each other, they form a thin layer (a few nanometers for most fluids) due to the influence from the bulk phases. Although this layer is very thin, the intermolecular forces acting on it from the bulk phases are so strong that asymmetry in these forces is very important

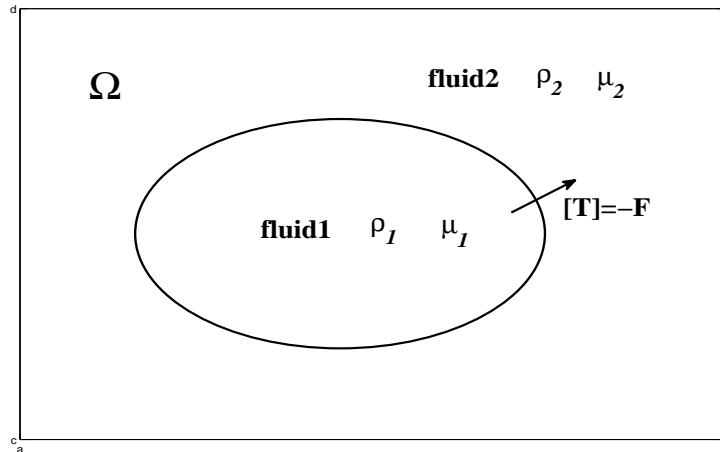


Figure 2.2: The diagram of a bubble in a two-phase interfacial flow.

for the overall dynamics of the system. For simplicity, the interface is considered as a geometric surface without thickness, and the boundary conditions for the bulk parameters to be formulated on this surface have to incorporate both the universal conservation laws as well as the specific physics of the processes in the interfacial layer for a particular system. Let  $\phi(\mathbf{r}, t)$  be a level function such that  $\phi(\mathbf{r}, t) = 0$  represents the interface to separate fluid 1 ( $\phi \leq 0$ ) and fluid 2 ( $\phi \geq 0$ ) with the superscript + and -, respectively;  $\mathbf{n} = \nabla\phi/|\nabla\phi|$  is a unit normal pointing from fluid 1 to fluid 2.

Suppose that  $\delta r$  is a distance which an element of the interface at position  $\mathbf{r}$  traveled in the normal direction  $\mathbf{n}$  in a very short period  $\delta t$ . Then both  $\phi(\mathbf{r}, t)$  and  $\phi(\mathbf{r} + \delta t\mathbf{n}, t + \delta t)$  are zeros, and we have

$$0 = \phi(\mathbf{r} + \delta t\mathbf{n}, t + \delta t) = \phi(\mathbf{r}, t) + \frac{\partial\phi}{\partial t}(\mathbf{r}, t)\delta t + \delta r\mathbf{n} \cdot \nabla\phi(\mathbf{r}, t) + o(\delta r, \delta t),$$

Divide the above equality by  $\delta t$  and take  $\delta t \rightarrow 0$ , we obtain an approximation of the shape of the interface

$$\frac{\partial\phi}{\partial t} + \mathbf{v}^s \cdot \nabla\phi = 0, \quad (2.15)$$

where  $\mathbf{v}^s$  is the normal projection of the interface velocity.

The conservation laws can be translated into the corresponding boundary conditions in several equivalent ways. Here, an approach based on considering

fluxes across the interface will be used.

Since the interface is very thin and massless (or the density there is of the same order as in the bulk), a sink or source of mass can be neglected compared to the mass fluxes across the boundary. As a result, in the general case of a permeable interface we have the continuity of mass flux across it

$$\rho^+ (\mathbf{u}^+ - \mathbf{v}^s) \cdot \mathbf{n} = \rho^- (\mathbf{u}^- - \mathbf{v}^s) \cdot \mathbf{n} \quad \text{at } \phi(\mathbf{r}, t) = 0. \quad (2.16)$$

Note that Eq. (2.16) holds for both permeable and impermeable interface, it is sufficient to prescribe a specific mass flux for the concerned physics,

$$\rho^+ (\mathbf{u}^+ - \mathbf{v}^s) \cdot \mathbf{n} = \chi, \quad (2.17)$$

where  $\chi$  has to be specified in terms of parameters determining a particular physical mechanism responsible for mass transfer across the interface, such as, chemical reactions, evaporation-condensation, mutual dissolution of fluids, etc. In particular, a case of an impermeable interface has  $\chi = 0$ , and this implies that

$$\mathbf{u}^+ \cdot \mathbf{n} = \mathbf{u}^- \cdot \mathbf{n}, \quad \frac{\partial \phi}{\partial t} + \mathbf{u}^+ \cdot \nabla \phi = 0, \quad \text{at } \phi(\mathbf{r}, t) = 0 \quad (2.18)$$

Alternatively, we consider another formulation for the movement of the interface and also consider a continuous tangential velocity, then the jump condition of the velocity is

$$[\mathbf{u}]_{\Sigma} = \mathbf{u}|_{\Sigma,2} - \mathbf{u}|_{\Sigma,1} = 0. \quad (2.19)$$

Similarly, the conservation of momentum can be translated into the boundary conditions by using the momentum flux tensor  $\Pi$  defined by  $\Pi = \rho \mathbf{u} \mathbf{u} - \mathbf{T}$ . The momentum fluxes in fluid 1 and 2 across a moving interface are  $\mathbf{n} \cdot \Pi^+$  and  $\mathbf{n} \cdot \Pi^-$ , respectively, where

$$\Pi^{\pm} = \rho^{\pm} (\mathbf{u}^{\pm} - \mathbf{v}^s) (\mathbf{u}^{\pm} - \mathbf{v}^s) - \mathbf{T}^{\pm}. \quad (2.20)$$

Note that if the source or sink effect of momentum from the interface is neglected compared with  $\mathbf{n} \Pi^{\pm}$ , then the momentum flux across an interface is continuous:

$$\mathbf{n} \cdot \Pi^+ = \mathbf{n} \cdot \Pi^-, \quad (2.21)$$

for instance, flows with very large length scales such as tidal waves, lava flows, large-scale free-surface flows industry, etc. However, in many situations the dynamics of the interfaces contributes significantly to the overall dynamics

of the system, and we have to consider this contribution here.

The source/sink of momentum due to the presence of an interface simply composes of two components, external forces  $\mathbf{F}^s$  and surface tension  $\sigma$ .

For the external forces, the interface may possess properties which in a dynamic sense would "compensate" its negligible thickness. For example, an electrically charged interface with electric current in a electrically neutral and nonconducting fluid can significantly influence the dynamics of the system by an external electromagnetic field. If the interface has no properties concerning external forces, then one can neglect the effect from external forces due to the negligible thickness of the interface. For instance, the effect of gravity is proportional to the mass of liquid contained in the interfacial layer and hence practically never plays any role in the interfacial dynamics.

The second way in which an interface can contribute to the overall dynamics of the system is through its intrinsic dynamic properties the most important being the surface tension. Physically, the surface tension appears as a result of an asymmetric action on the interfacial layer of intermolecular forces from the bulk phases. These forces are singularly strong compared to those considered in fluid mechanics so that their strength compensates the negligible thickness of the interfacial layer making the resultant dynamic effect finite.

Mathematically,  $\sigma$  is a function defined along the interface and, in

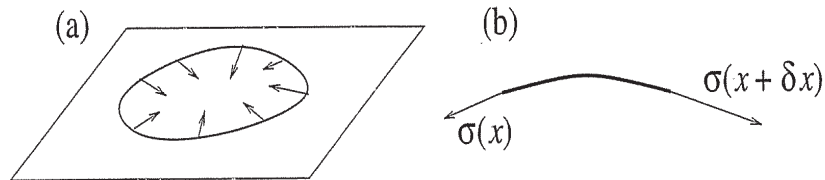


Figure 2.3: (a) The surface tension with which an element of the interface acts on its boundary is normal to the boundary and tangential to the interface; it tries to minimize the area of this element. (b) The resultant action of the surface tension on a surface element from a surrounding surface has a normal component if the interface is not flat, and a tangential component if the surface tension varies along the interface.

the framework of fluid-mechanical modeling, it has to be included in a two-dimensional surface stress tensor  $\mathbf{T}^s$ . In order to imbed  $\mathbf{T}^s$  into the three-

dimensional space, it is convenient to use a tensor  $(\mathbf{I} - \mathbf{n}\mathbf{n})$ , where as before  $\mathbf{I}$  is the metric tensor in space, and  $\mathbf{n}$  is a unit normal to the interface. This tensor generates a metric on the surface and singles out the tangential components of vectors: if  $\mathbf{a} = a_n\mathbf{n} + \mathbf{a}_{\parallel}$ , where  $\mathbf{a}_{\parallel}$  is tangential to the interface, then  $(\mathbf{I} - \mathbf{n}\mathbf{n}) \cdot \mathbf{a} = \mathbf{a}_{\parallel}$ .

Taking

$$\mathbf{T}^s = \sigma (\mathbf{I} - \mathbf{n}\mathbf{n}), \quad (2.22)$$

we have  $\mathbf{n} \cdot \mathbf{T}^s = 0$ , while for any two unit vectors  $\mathbf{t}_1$  and  $\mathbf{t}_2$  lying in the interface and normal to each other, we have  $\mathbf{t}_1 \cdot \mathbf{T}^s \cdot \mathbf{t}_2 = 0$  and  $\mathbf{t}_1 \cdot \mathbf{T}^s \cdot \mathbf{t}_1 = \sigma$ . Hence for a line lying in the interface and normal to  $\mathbf{t}_1$  the stress tensor defined by (2.22) describes a force directed along  $\mathbf{t}_1$  with the magnitude  $\sigma$  per unit length of the line. This is exactly how we defined the surface tension. In what follows, it is important to remember also that since  $\sigma$  is defined only on the interface, its derivative in the direction normal to it is zero by definition, that is  $\mathbf{n} \cdot \nabla\sigma = 0$ . This constraint allows one to use  $\sigma$  formally as a function of all three space coordinates. The same applies to other surface characteristics if the interface possesses other mechanical and/or thermal properties, and in particular one has  $\mathbf{n} \cdot \nabla\mathbf{n}$ .

Consider the momentum flux across an interface. Given the requirement of momentum conservation and taking into account the contribution from the interface, we have

$$\mathbf{n} \cdot (\Pi^+ - \Pi^-) = \nabla \cdot \mathbf{T}^s + \mathbf{F}^s. \quad (2.23)$$

Here  $\mathbf{F}^s$  is the density of external forces per unit area acting on the interface; the contribution from the surface stress in the form of  $\nabla \cdot \mathbf{T}^s$  is analogous to the corresponding contribution of bulk stresses.

Substituting expressions (2.20) and (2.22) for  $\Pi^{\pm}$  and  $\mathbf{T}^s$  and take the advantage of the mass flux continuity condition (2.16), we have

$$\rho^+ \mathbf{u}^+ (\mathbf{u}^+ - \mathbf{v}^s) \cdot \mathbf{n} - \rho^- \mathbf{u}^- (\mathbf{u}^- - \mathbf{v}^s) \cdot \mathbf{n} - \mathbf{n} \cdot (\mathbf{T}^+ - \mathbf{T}^-) = \nabla\sigma - \sigma \mathbf{n} \cdot \nabla \mathbf{n} + \mathbf{F}^s. \quad (2.24)$$

The first two terms on the left-hand side written down as

$$\rho^+ \mathbf{u}^+ (\mathbf{u}^+ - \mathbf{v}^s) \cdot \mathbf{n} - \rho^- \mathbf{u}^- (\mathbf{u}^- - \mathbf{v}^s) \cdot \mathbf{n} = \chi (\mathbf{u}^+ - \mathbf{u}^-), \quad (2.25)$$

show that mass transfer across an interface has an impact on the momentum balance when (a) it is significant in itself, and (b) it is associated with a considerable hump in the bulk velocity. This is the case, for example, in shock waves. On the contrary, for liquid-fluid interfaces the effect of mass

transfer on the momentum balance is practically always negligible compared to capillary effects and especially to the bulk stress. The first two terms on the right-hand side give the tangential and normal components of the force acting on a surface element due to surface tension and its gradient, see Fig. 2.3 (b). In writing them down we used that (a)  $(\mathbf{I} - \mathbf{n}\mathbf{n}) \cdot \nabla \sigma = \nabla \sigma$  since the surface-tension gradient is directed along the interface and (b)  $\mathbf{n} \cdot \nabla \mathbf{n} = 0$ .

In the simplest case of an impermeable interface ( $\chi = 0$ ) and negligible external surface forces ( $\mathbf{F}^s = 0$ ), the normal projection of Eq. (2.23),

$$-(p^+ - p^-) + \mathbf{n} \cdot (\boldsymbol{\sigma}^+ - \boldsymbol{\sigma}^-) \cdot \mathbf{n} = \sigma \nabla \cdot \mathbf{n}, \quad (2.26)$$

is known as the capillarity equation, and the normal stress jump is balanced by the interfacial force  $\mathbf{F}$  (defined only on  $\Sigma$ ) as

$$[\mathbf{T}\mathbf{n}]_{\Sigma} + \mathbf{F} = 0, \quad (2.27)$$

where  $\mathbf{n}$  is the unit normal vector on  $\Sigma$  directed towards fluid 2.

Since it is not easy to solve the Navier-Stokes equations (2.13)-(2.14) in  $\Omega$  with jump conditions (2.19) and (2.27) on  $\Sigma$ , especially when the interface is moving. In order to formulate the problem using the immersed boundary approach, we simply treat the interface as an immersed boundary that exerts force  $\mathbf{F}$  to the fluids and moves with local fluid velocity. We will discuss the detail later.

## 2.3 Moving contact line problems

If we consider two immiscible fluids (say fluid 1 and 2) that are placed on a solid substrate in which the interface of the two fluids intersects the substrate at so called the contact lines. (More precisely, it should be called the contact points in two-dimensional flow.) In the absence of external forces and the contact lines are static, the surface forces acting at the contact lines follow the well-known Young's condition [9]

$$\sigma_{s2} = \sigma_{s1} + \sigma \cos \theta_e, \quad (2.28)$$

where  $\sigma_{s1}$ ,  $\sigma_{s2}$ , and  $\sigma$  are the corresponding surface tension between the solid-fluid 1, solid-fluid 2 and fluid interfaces, and  $\theta_e$  is the static equilibrium contact angle. However, when the contact line moves, we have to model both the fluid dynamics and contact line dynamics simultaneously. Here, we assume the fluid 1 is a drop surrounding by the fluid 2 and both fluids rest on

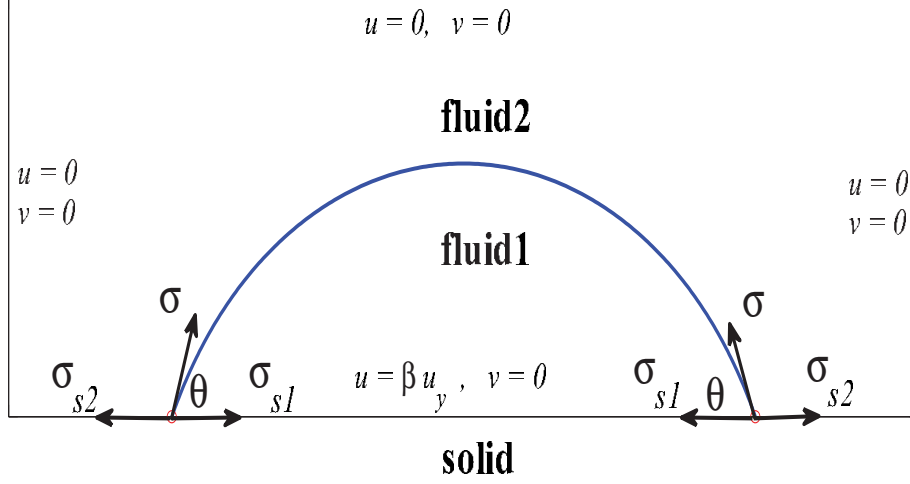


Figure 2.4: The diagram of contact lines and the problem setting.

the solid substrate; thus, the contact lines are at the bottom of the domain. Furthermore, we assume that an insoluble surfactant stays on the fluid-fluid interface so that the surface tension changes accordingly. See the diagram of the contact lines and the considered problem in detail in Figure 2.4. In this case, we simply assume that both fluids have the equal density and viscosity (Actually, it doesn't matter even when we consider different fluid properties inside and outside). The gravity is also neglected since we mainly concern about the capillary effect, especially, the effect on the contact line movements due to the existence of the surfactant. Note that the surfactant is usually soluble in fluid 2 so that it affects not only the fluid-fluid surface tension but the surface tension between fluid 2 and the solid. So, the effects of surfactant to the interfacial flow depend on the competition of  $\sigma$  and  $\sigma_{s2}$ , and the tendency of the contact angle will depend. For simplicity, we not only assume the surfactant is insoluble in fluid 1 and fluid 2 but restrict the surfactant distribute along the fluid-fluid interface, therefore, both  $\sigma_{s1}$  and  $\sigma_{s2}$  are fixed all the time such that we can predict the contact line tendency directly from the Young's condition.

Since the Young's condition is concerned with the movement of the contact line, it is related to the force balance (As before, surface tension can be regarded as energy per unit area or force per unit length) of  $\sigma$ ,  $\sigma_{s1}$ , and

$\sigma_{s2}$ , at the triple junction. From the observation of a contact line, it moves only in one direction tangent to the solid substrate, the force is balanced in the direction perpendicular to the solid substrate due to the adhesion. The force at the moving contact lines  $F_{cl}$  are only exerted along the tangential direction (that is  $x$  direction) of the solid substrate and mainly due to the unbalanced Young's force [9] and can be written as

$$F_{cl} = \sigma_{s2} - \sigma_{s1} - \sigma \cos \theta, \quad (2.29)$$

where  $\theta$  is the dynamic contact angle. Note that  $F_{cl}$  tends to zero when the dynamic contact angle  $\theta$  is getting close to the equilibrium contact angle  $\theta_e$ .

## 2.4 Governing equation of surfactant concentration

The basic equation for surfactant transport equation along a deforming interface has been derived by Scriven [46], Aris [1], and Waxman [55]. All three papers derived the surfactant equation relying heavily on differential geometry. Stone [49], however, presented a simple derivation of the time-dependent convective-diffusion equation for surfactant transport along a deforming interface. In this subsection, we present a slightly different derivation from Stone for the surfactant transport equation which will be used as one of our governing equations for numerical computation. Our derivation is in the same spirit of the immersed boundary approach. A more detailed derivation for surfactant concentration equation along a two-dimensional parametric deforming surface in three-dimensional fluid domains can be found in our recent work [19].

Let  $L(t)$  be an interfacial segment where the surfactant concentration (the mass of the surfactant per unit length) is defined. Since the surfactant remain on the material element and do not transport or diffuse to the surrounding bulk fluids, the mass on the segment is conserved

$$\frac{d}{dt} \int_{L(t)} \gamma(s, t) ds = 0, \quad (2.30)$$

where  $ds$  is the arc-length element. To apply the time derivative more easily, we rewrite the above equation in terms of the initial parameter  $\alpha$  as

$$\frac{d}{dt} \int_{L(0)} \gamma(\alpha, t) \left| \frac{\partial \mathbf{X}}{\partial \alpha} \right| d\alpha = 0. \quad (2.31)$$



By taking the time derivative inside the integral, we obtain

$$\int_{L(0)} \left( \frac{\partial \gamma}{\partial t} \left| \frac{\partial \mathbf{X}}{\partial \alpha} \right| + \gamma \frac{\partial}{\partial t} \left| \frac{\partial \mathbf{X}}{\partial \alpha} \right| \right) d\alpha = 0. \quad (2.32)$$

Note that, in our present formulation, both the interface and surfactant concentration are tracked in a Lagrangian manner. Thus, the time derivative of the first term in Eq. (2.32) is exactly the material derivative of Stone's derivation [49]. The time derivative of the second term is due to interface stretching. Now we need to compute the rate of the stretching factor, and using the fact

$$\frac{\partial \mathbf{X}}{\partial t} = \mathbf{u}(\mathbf{X}, t) = (u(\mathbf{X}, t), v(\mathbf{X}, t)), \quad (2.33)$$

we have

$$\begin{aligned} \frac{\partial}{\partial t} \left| \frac{\partial \mathbf{X}}{\partial \alpha} \right| &= \frac{\frac{\partial X}{\partial \alpha} \frac{\partial}{\partial \alpha} \left( \frac{\partial X}{\partial t} \right) + \frac{\partial Y}{\partial \alpha} \frac{\partial}{\partial \alpha} \left( \frac{\partial Y}{\partial t} \right)}{\left| \frac{\partial \mathbf{X}}{\partial \alpha} \right|} = \frac{\frac{\partial X}{\partial \alpha} \frac{\partial u}{\partial \alpha} + \frac{\partial Y}{\partial \alpha} \frac{\partial v}{\partial \alpha}}{\left| \frac{\partial \mathbf{X}}{\partial \alpha} \right|} \\ &= \frac{\frac{\partial X}{\partial \alpha} \left( \nabla \mathbf{u} \cdot \frac{\partial \mathbf{X}}{\partial \alpha} \right) + \frac{\partial Y}{\partial \alpha} \left( \nabla \mathbf{v} \cdot \frac{\partial \mathbf{X}}{\partial \alpha} \right)}{\left| \frac{\partial \mathbf{X}}{\partial \alpha} \right|} = \left( \frac{\partial \mathbf{u}}{\partial \tau} \cdot \boldsymbol{\tau} \right) \left| \frac{\partial \mathbf{X}}{\partial \alpha} \right| \\ &= (\nabla_s \cdot \mathbf{u}) \left| \frac{\partial \mathbf{X}}{\partial \alpha} \right|. \end{aligned} \quad (2.34)$$

Here, the notation  $\nabla_s \cdot \mathbf{u}$  means the surface divergence which is used commonly in the literature. Since the material segment is arbitrary, we thus have

$$\frac{\partial \gamma}{\partial t} + (\nabla_s \cdot \mathbf{u}) \gamma = 0. \quad (2.35)$$

If we allow surfactant diffusion along the interface, we obtain the surfactant transport-diffusion equation as

$$\frac{\partial \gamma}{\partial t} + (\nabla_s \cdot \mathbf{u}) \gamma = D_s \frac{\partial}{\partial \alpha} \left( \frac{\partial \gamma}{\partial \alpha} / \left| \frac{\partial \mathbf{X}}{\partial \alpha} \right| \right) / \left| \frac{\partial \mathbf{X}}{\partial \alpha} \right|, \quad (2.36)$$

where  $D_s$  is the surface diffusivity parameter [24]. We note that surface diffusion is also written in terms of initial parameter  $\alpha$ .

Let us summarize this section by pointing out the differences and similarities between our present surfactant equation (2.36) and the ones derived in literature [49, 54]. As we discussed before, the present time derivative is exactly the material derivative with the material parameter  $\alpha$  fixed, while the time derivative used in [49] is keeping the material coordinates  $\mathbf{X}$  fixed.

Wong *et al.* [54] argued that the time derivative term in Stone's surfactant equation causes ambiguity in numerical discretization since the material coordinates is time-dependent as well. Wong *et al.* [54] provide an alternative derivation for the surfactant equation, where the concentration time derivative is applied by keeping the material parameter  $s$  fixed. This is exactly what we have done here. It is interesting (but not surprising) to conclude that the surfactant concentration equation in [54] can be simplified to our present form (2.36) by substituting Eq. (2.33) into their equation.

The surface tension  $\sigma(\alpha, t)$  is related to the surfactant concentration  $\gamma(\alpha, t)$  through either linear or nonlinear approximation of Langmuir equation of state [25]

$$\sigma(\gamma) = \sigma_\infty - RTC \frac{\gamma}{\gamma_\infty}, \quad (2.37)$$

$$\sigma(\gamma) = \sigma_\infty + RTC \ln \left( 1 - \frac{\gamma}{\gamma_\infty} \right) \quad (2.38)$$

where  $\sigma_\infty$  is the surface tension of a clean interface,  $R$  is the ideal gas constant,  $T$  is a absolute temperature, and  $\gamma_\infty$  is the maximum surface packing limit such that  $\gamma$  cannot exceed this upper bound.

## 2.5 Boundary conditions

In order to gain well-posed partial differential equations and mimic the phenomena in which we are interested, appropriate boundary conditions and initial conditions should be imposed to each partial differential equations, two for momentum conservation, one for mass conservation of fluids, and one for mass conservation of surfactant equations. The unknown of fluid variables are velocity  $\mathbf{u} = (u, v)$  and pressure  $p$ , so we have three equations for three unknowns in a two-dimensional problem. In addition, the surfactant equation on the interface has only one unknown  $\gamma$ .

### 2.5.1 For Navier-Stokes equations

As before, the computational domain is still a square  $\Omega = [a, b] \times [c, d]$ , and  $\partial\Omega$  is the boundary of  $\Omega$ . There are several choices of the boundary condition for the fluid in the following.

1. **No-slip boundary condition:** No fluid penetrates the boundary and the fluid is at rest there, i.e.

$$u|_{\partial\Omega} = 0, \quad v|_{\partial\Omega} = 0. \quad (2.39)$$

2. **Inflow boundary condition:** The velocity  $\mathbf{u}$  is given, i.e.

$$u|_{\partial\Omega} = u_b, \quad v|_{\partial\Omega} = v_b. \quad (2.40)$$

Here, two specific one-variable functions  $u_b$  and  $v_b$  are given.

3. **Outflow boundary condition:** Neither velocity component changes in the direction normal to the boundary, i.e.

$$\frac{\partial u}{\partial n}|_{\partial\Omega} = 0, \quad \frac{\partial v}{\partial n}|_{\partial\Omega} = 0. \quad (2.41)$$

4. **Periodic boundary condition:** For problems which are periodic with period  $b - a$  in one coordinate direction (e.g. the flow over an undulating surface), one can restrict the computations to one period interval. The velocities and pressure must then coincide at the left and right boundary, i.e.

$$u(a, y) = u(b, y), \quad v(a, y) = v(b, y), \quad p(a, y) = p(b, y). \quad (2.42)$$

5. **Navier-slip boundary condition:** For the moving contact line problem, the no-slip boundary condition leads to the unrealistic prediction of unbounded stresses and viscous dissipation at the contact line. To avoid a non-integrable singularity, the no-slip boundary condition can be replaced with the Navier-slip boundary condition

$$\mathbf{u} \cdot \boldsymbol{\tau}|_{\partial\Omega} = \beta \nabla(\mathbf{u} \cdot \boldsymbol{\tau}) \cdot \mathbf{n}|_{\partial\Omega}, \quad (2.43)$$

where  $\mathbf{u} \cdot \boldsymbol{\tau}$  is the velocity component tangential to the surface and  $\beta$  is the slip coefficient. The slip boundary condition has been used in the previous work on the liquid spreading [11, 12, 43].

## 2.5.2 For surfactant concentration equation

Since the surfactant is insoluble and the interface is a one-dimensional curve in a two-dimensional fluid, we can simply use a parameter  $\alpha \in (0, 1)$  to define the surfactant concentration as  $\gamma(\alpha, t)$ , a function of  $\alpha$  and  $t$ .

1. **Periodic boundary condition:** When one fluid surround the interface, the interface can be seen as a simple closed curve which is parametrized as a periodic function, that is,

$$\gamma(0, t) = \gamma(1, t), \quad \text{for any } t > 0. \quad (2.44)$$

2. **No-flux boundary condition** When a moving contact line problem is considered, we use the no-flux boundary condition for the surfactant equation due to its insolubility, i.e.

$$\frac{\partial \gamma}{\partial \alpha}(0, t) = 0, \quad \frac{\partial \gamma}{\partial \alpha}(1, t) = 0. \quad (2.45)$$



# Chapter 3

## Immersed boundary method

The (IB) method was first proposed by Peskin [35] to simulate the blood-valve interaction, and has been applied successfully to other biological problems. The basic idea of the immersed boundary method is to treat the elastic material (the interface) as a part of the fluid in which additional forces (arising from the elastic stresses) are applied. The fluid equations are solved on a regular rectangular lattice (Eulerian grid), and the structure is not modified in any way by the presence of the immersed elastic material which the geometry may be very complicated. The elastic material is tracked in Lagrangian coordinate, that is, the immersed boundary is represented by a set of discrete Lagrangian markers embedding in the Eulerian fluid domain. The spatial configuration of these points is used to evaluate elastic forces, which are applied to the nearby lattice points of the fluid. The fluid velocity is updated under the influence of these forces, and the new velocity is then interpolated at the elastic material points, which are moved at the interpolated velocity to complete the time step.

The structure of this chapter arises from mathematical formulae of the equations of motion of a viscous incompressible fluid containing an immersed interface. These formulae form the foundation of the immersed boundary method, which will be presented in a dimensionless version with several dimensionless parameters. The core of the immersed boundary method is a smoothed approximation to the Dirac delta-function, the construction of which is given in the subsequent section.

### 3.1 Equation of motion

Consider a viscous two-phase incompressible fluid which contains an immersed interface (arises from two immiscible fluids). Assume that the in-

interface is pure force-generator and without mass and volume, but interacts with the fluid in which they are immersed, they form an incompressible visco-elastic material.

### 3.1.1 Derivation of interfacial forces

Let  $\Sigma$  symbolize the immersed interface whose unknown motion is represented by a Lagrangian coordinate  $\mathbf{X} = \mathbf{X}(\alpha, t) = (X(\alpha, t), Y(\alpha, t))$ ,  $0 \leq \alpha \leq L_b$ , where  $\alpha$  is the parameter of the initial configuration of the interface, and we use  $s$  as the arc-length parameter, especially. The formula of the unit tangent along the interface is given by

$$\boldsymbol{\tau} = \frac{\partial \mathbf{X} / \partial \alpha}{|\partial \mathbf{X} / \partial \alpha|}, \quad (3.1)$$

and the surface tension  $\sigma$  is given by a generalized Hook's law:

$$\sigma = S \left( \left| \frac{\partial \mathbf{X}}{\partial \alpha} \right|; \alpha, t \right) \quad (3.2)$$

Here  $\sigma ds$  is the force transmitted by a segment  $ds$  of the interface, and  $|\partial \mathbf{X} / \partial \alpha|$  determines the corresponding local strain, from which the force is computed.

Let  $I$  be an arbitrary region of the parameter interval. Consider the segment of the interface defined by  $\alpha_1 < \alpha < \alpha_2$ . Since the interface is massless, the total force acting on these segments must be zero. This total force includes both the force of the fluid on the interface and also the force transmitted across the interfaces and by the segment of the interface itself. Thus

$$0 = \text{force of fluid on the interface portion} + (\sigma \boldsymbol{\tau}) \Big|_{\alpha_1}^{\alpha_2} \quad (3.3)$$

According to Newton's third law of equal and opposite forces, and also the fundamental theorem of calculus, we may rewrite this equation as follows:

$$\text{force of the interface portion on fluid} = (\sigma \boldsymbol{\tau}) \Big|_{\alpha_2}^{\alpha_1} = \int_{\alpha_1}^{\alpha_2} \frac{\partial}{\partial \alpha} (\sigma \boldsymbol{\tau}) d\alpha. \quad (3.4)$$

Note that Eq. (3.4) is independent of the choice of the parameter  $\alpha$  due to change of variable to arc-length parameter  $s$ .

$$\int_{\alpha_1}^{\alpha_2} \frac{\partial}{\partial \alpha} (\sigma \boldsymbol{\tau}) d\alpha = \int_{\alpha_1}^{\alpha_2} \frac{\frac{\partial}{\partial \alpha} (\sigma \boldsymbol{\tau})}{|\partial \mathbf{X} / \partial \alpha|} |\partial \mathbf{X} / \partial \alpha| d\alpha = \int_I \frac{\partial}{\partial s} (\sigma \boldsymbol{\tau}) ds. \quad (3.5)$$

Since  $I$ ,  $\alpha_1$ , and  $\alpha_2$  are arbitrary, this shows that the force density of the interface with respect to the measure  $ds$  is given by

$$\mathbf{F}(\alpha, t) = \frac{\partial}{\partial \alpha} (\sigma \boldsymbol{\tau}). \quad (3.6)$$

An alternative way to derive the force is from the energy point of view, a variational method. Suppose that  $E[\mathbf{X}]$  is a given functional, the elastic potential energy of the material in configuration  $\mathbf{X}$ , we define the force from the Frechet derivative of the energy  $E$  by

$$\mathbf{F} = -\frac{\delta E[\mathbf{X}]}{\delta \mathbf{X}}. \quad (3.7)$$

If we give a specific form of energy

$$E[\mathbf{X}(\alpha, t)] = \int_{\Sigma} f \left( \left| \frac{\partial \mathbf{X}}{\partial \alpha} \right| \right) d\alpha, \quad (3.8)$$

then

$$\mathbf{F} = \frac{\partial}{\partial \alpha} \left( f' \left( \left| \frac{\partial \mathbf{X}}{\partial \alpha} \right| \right) \frac{\partial \mathbf{X} / \partial \alpha}{\left| \partial \mathbf{X} / \partial \alpha \right|} \right) \quad (3.9)$$

**proof:** let  $\alpha(\epsilon) = \delta E[\mathbf{X}] = E[\mathbf{X} + \epsilon \tilde{\mathbf{X}}]$ , then

$$\alpha'(\epsilon) = \int_{\Sigma} f' \left( \left| \frac{\partial(\mathbf{X} + \epsilon \tilde{\mathbf{X}})}{\partial \alpha} \right| \right) \frac{d}{d\epsilon} \left| \frac{\partial(\mathbf{X} + \epsilon \tilde{\mathbf{X}})}{\partial \alpha} \right| d\alpha,$$

$$\frac{d}{d\epsilon} \left| \frac{\partial(\mathbf{X} + \epsilon \tilde{\mathbf{X}})}{\partial \alpha} \right| d\alpha = \left( \frac{\partial(\mathbf{X} + \epsilon \tilde{\mathbf{X}})}{\partial \alpha} \cdot \frac{\partial \tilde{\mathbf{X}}}{\partial \alpha} \right) / \left| \frac{\partial(\mathbf{X} + \epsilon \tilde{\mathbf{X}})}{\partial \alpha} \right|,$$

$$\begin{aligned} \lim_{\epsilon \rightarrow 0} \alpha'(\epsilon) &= \int_{\Sigma} f' \left( \left| \frac{\partial \mathbf{X}}{\partial \alpha} \right| \right) \left( \frac{\partial \mathbf{X}}{\partial \alpha} \cdot \frac{\partial \tilde{\mathbf{X}}}{\partial \alpha} \right) / \left| \frac{\partial \mathbf{X}}{\partial \alpha} \right| d\alpha, \\ &= \int_{\Sigma} f' \left( \left| \frac{\partial \mathbf{X}}{\partial \alpha} \right| \right) \left( \frac{\partial \mathbf{X}}{\partial \alpha} / \left| \frac{\partial \mathbf{X}}{\partial \alpha} \right| \right) \cdot \frac{\partial \tilde{\mathbf{X}}}{\partial \alpha} d\alpha, \\ &= - \int_{\Sigma} \frac{\partial}{\partial \alpha} \left( f' \left( \left| \frac{\partial \mathbf{X}}{\partial \alpha} \right| \right) \left( \frac{\partial \mathbf{X}}{\partial \alpha} / \left| \frac{\partial \mathbf{X}}{\partial \alpha} \right| \right) \right) \cdot \tilde{\mathbf{X}} d\alpha, \\ &= - \int_{\Sigma} \frac{\partial}{\partial \alpha} \left( f' \left( \left| \frac{\partial \mathbf{X}}{\partial \alpha} \right| \right) \left( \frac{\partial \mathbf{X}}{\partial \alpha} / \left| \frac{\partial \mathbf{X}}{\partial \alpha} \right| \right) \right) \cdot \delta \mathbf{X} d\alpha, \\ \Rightarrow \mathbf{F} &= -\frac{\delta E[\mathbf{X}]}{\delta \mathbf{X}} = \frac{\partial}{\partial \alpha} \left( f' \left( \left| \frac{\partial \mathbf{X}}{\partial \alpha} \right| \right) \frac{\partial \mathbf{X} / \partial \alpha}{\left| \partial \mathbf{X} / \partial \alpha \right|} \right) \end{aligned}$$

### 3.1.2 Connection between fluid and interface

In this section, the connection between Eulerian and Lagrangian variables should be determined. To do so, take the advantage of the distinguish property of the Dirac delta function, one can evaluate a function at a point by multiplying it by an appropriately shifted delta function and integrating over the whole space. First of all, the velocities at the interface can be evaluated by integrating the product of the velocities on the lattice and the delta function:

$$\mathbf{u}(\mathbf{X}(\alpha, t), t) = \int_{\Omega} \mathbf{u}(\mathbf{x}, t) \delta(\mathbf{x} - \mathbf{X}(\alpha, t)) d\mathbf{x}. \quad (3.10)$$

On the other hand, the forces on the lattice are evaluated in this way:

$$\mathbf{f}(\mathbf{x}, t) = \int_{\Sigma} \mathbf{F}(\alpha, t) \delta(\mathbf{x} - \mathbf{X}(\alpha, t)) d\alpha. \quad (3.11)$$

Note that the integral in Eq. (3.10) is two-dimensional and gives a finite result, the velocity of the immersed interface. Unlike Eq. (3.10), the resultant  $\mathbf{f}(\mathbf{x}, t)$  of the integral in Eq. (3.11) is singular like a delta function, the singularity being supported on the immersed interface. Although  $\mathbf{f}(\mathbf{x}, t)$  is singular on the interface, the integrals over any finite volume is finite. The integral of  $\mathbf{f}(\mathbf{x}, t)$  over such a volume is the total force applied to the fluid by the part of the immersed interface contained. The important feature between the interaction equations is that Eq. (3.10) converts from Eulerian to Lagrangian variables while Eq. (3.11) converts in the other direction.

### 3.1.3 Dimensionless variables

To avoid confusion with the unit of different variables, we use the non-dimensionalization process presented in [24, 56], that is, choose several reference scales for their corresponding variables. Let  $r$  be the scale of length in space and  $U_{\infty}$  be the velocity scale. The density and viscosity are scaled by the properties of fluid 1,  $\rho_1$  and  $\mu_1$ , respectively. These lead to the inertial time scale  $r/U_{\infty}$  and the pressure scale  $\mu_1 U_{\infty}/r$ . Surface tension scale  $\sigma_{\infty}$  is the equilibrium surface tension (the surface tension corresponding to a uniformly distributed surfactant with equilibrium concentration  $\gamma_{\infty}$ , the scale of surfactant concentration). If a gravitational force is considered,  $g_{\infty}$  will be the gravity scale. Then we set

$$\begin{aligned} \mathbf{x} &= r\mathbf{x}^*, & \mathbf{u} &= U_{\infty}\mathbf{u}^*, & \rho &= \rho_1\rho^*, \\ \mu &= \mu_1\mu^*, & t &= \frac{r}{U_{\infty}}t^*, & p &= \frac{\mu_1 U_{\infty}}{r}p^*, \\ \sigma &= \sigma_{\infty}\sigma^*, & \gamma &= \gamma_{\infty}\gamma^*, & \mathbf{g} &= g_{\infty}\mathbf{g}^*, \end{aligned} \quad (3.12)$$



where variables with superscript  $*$  are dimensionless and then we have

$$\begin{aligned}
\frac{\partial \mathbf{u}}{\partial t} &= \frac{U_\infty^2}{r} \frac{\partial \mathbf{u}^*}{\partial t^*} \\
(\mathbf{u} \cdot \nabla) \mathbf{u} &= \frac{U_\infty^2}{r} (\mathbf{u}^* \cdot \nabla^*) \mathbf{u}^* \\
\nabla p &= \frac{\mu_1 U_\infty}{r^2} \nabla^* p^* \\
\nabla \cdot (2\mu E) &= \frac{\mu_1 U_\infty}{r^2} \nabla^* \cdot (2\mu^* E^*) \\
\frac{\partial \gamma}{\partial t} &= \frac{\gamma_\infty U_\infty}{r} \frac{\partial \gamma^*}{\partial t^*} \\
(\nabla_s \cdot \mathbf{u}) \gamma &= \frac{\gamma_\infty U_\infty}{r} (\nabla_s^* \cdot \mathbf{u}^*) \gamma^* \\
D_s \frac{\partial^2 \gamma}{\partial s^2} &= \frac{D_s \gamma_\infty}{r^2} \frac{\partial^2 \gamma^*}{\partial s^{*2}} \\
\rho \mathbf{g} &= \rho_1 g_\infty \rho^* \mathbf{g}^*,
\end{aligned} \tag{3.13}$$

where  $D_s$  is the surface surfactant diffusivity.

### 3.1.4 Dimensionless equations of motion

Substitute these relations above into Eqs. (2.13), (2.14), (3.10), (3.11), and (2.36), we can write down our governing equations in the usual immersed boundary formulation as follows.

$$\begin{aligned}
\rho^* \left( \frac{\partial \mathbf{u}^*}{\partial t^*} + (\mathbf{u}^* \cdot \nabla^*) \mathbf{u}^* \right) &= -\nabla^* p^* + \frac{1}{Re} \nabla^* \cdot (2\mu^* E^*) \\
&\quad + \frac{1}{ReCa} \mathbf{f}^* + \frac{E_o}{ReCa} \rho^* \mathbf{g}^*, \tag{3.14}
\end{aligned}$$

$$\nabla^* \cdot \mathbf{u}^* = 0, \tag{3.15}$$

$$\mathbf{f}^*(\mathbf{x}^*, t^*) = \int_{\Sigma^*} \mathbf{F}^*(\alpha, t^*) \delta(\mathbf{x}^* - \mathbf{X}^*(\alpha, t^*)) d\alpha, \tag{3.16}$$

$$\begin{aligned}
\frac{\partial \mathbf{X}^*(\alpha, t^*)}{\partial t^*} &= \mathbf{u}^*(\mathbf{X}^*(\alpha, t^*), t^*), \\
&= \int_{\Omega} \mathbf{u}^*(\mathbf{x}^*, t^*) \delta(\mathbf{x}^* - \mathbf{X}^*(\alpha, t^*)) d\mathbf{x}^*, \tag{3.17}
\end{aligned}$$

$$\mathbf{F}^*(\alpha, t^*) = \frac{\partial}{\partial \alpha} (\sigma^*(\gamma^*(\alpha, t^*), t^*) \boldsymbol{\tau}^*(\alpha, t^*)), \tag{3.18}$$

$$\frac{\partial \gamma}{\partial t} + (\nabla_s \cdot \mathbf{u}) \gamma = \frac{1}{Pe_s} \frac{\partial}{\partial \alpha} \left( \frac{\partial \gamma}{\partial \alpha} / \left| \frac{\partial \mathbf{X}}{\partial \alpha} \right| \right) / \left| \frac{\partial \mathbf{X}}{\partial \alpha} \right|, \tag{3.19}$$

where

$$Re = \frac{\rho_1 U_\infty r}{\mu_1}, \quad Ca = \frac{\mu_1 U_\infty}{\sigma_\infty}, \quad E_o = \frac{\rho_1 g_\infty r^2}{\sigma_\infty}, \quad Pe_s = \frac{U_\infty r}{D_s}.$$

The dimensionless numbers are the Reynolds number ( $Re$ ) describing the ratio between the inertial force and the viscous force, the capillary number ( $Ca$ ) describing the strength of the surface tension, the number ( $E_o$ ) representing the strength of the gravitational force, and the Peclet number ( $Pe_s$ ) explaining the magnitude of the diffusivity of the surfactant equation. Equations (3.16)-(3.17) represent dimensionless form of the interaction between the immersed interface and the fluids. In particular, Eq. (3.16) describes the force ( $\mathbf{f}$ ) acting on the fluid due to the interfacial force ( $\mathbf{F}^*$ ), which is defined only on the interface and must be balanced by the normal stress as shown in Eq. (2.27). Here,  $\sigma^*$  is the dimensionless surface tension, and  $\boldsymbol{\tau}^*$  is the unit tangent vector on the interface. Eq. (3.17) states that the interface moves with the fluid velocity which is consistent with (2.19). The present formulation employs a mixture of Eulerian ( $\mathbf{x}^*$ ) and Lagrangian ( $\mathbf{X}^*$ ) variables which are linked by the two-dimensional Dirac delta function  $\delta(\mathbf{x}^*) = \delta(x^*)\delta(y^*)$ .

In addition, the dimensionless surface tension  $\sigma^*$  is related to dimensionless surfactant concentration  $\gamma^*$  through the dimensionless Langmuir approximations

$$\sigma^* = 1 - \eta\gamma^*, \quad (3.20)$$

$$\sigma^* = 1 + \eta \ln(1 - \gamma^*), \quad (3.21)$$

where the elasticity number  $\eta = RT\gamma_\infty/\sigma_\infty$ .

The interfacial force  $\mathbf{F}$  arises from the surface tension and its form is derived from Laplace-Young condition [27]. One can further take derivatives explicitly so that

$$\mathbf{F}(\alpha, t) = \frac{\partial}{\partial \alpha}(\sigma \boldsymbol{\tau}) = \frac{\partial \sigma}{\partial \alpha} \boldsymbol{\tau} + \sigma \frac{\partial \boldsymbol{\tau}}{\partial \alpha} = \frac{\partial \sigma}{\partial \alpha} \boldsymbol{\tau} + \sigma \kappa \mathbf{n} \left| \frac{\partial \mathbf{X}}{\partial \alpha} \right|, \quad (3.22)$$

where  $\kappa$  is the curvature of the interface and  $\mathbf{n}$  is the unit outward normal. The first term on the right-hand side of Eq. (3.22) is the Marangoni force (the tangential force) due to the non-uniform distribution of surfactant concentration and the second one is the capillary force (the normal force) which is related to the product of the surface tension and curvature.

## 3.2 Construction of $\delta$ -function

In this section, we describe the construction of the approximation  $d_h(\mathbf{x})$ , a discrete delta function, of delta function  $\delta(\mathbf{x})$ . The choice of  $d_h(\mathbf{x})$  is used to transfer quantities on which are defined between the Eulerian and Lagrangian mesh points is an critical portion of the IB method. Peskin presents a list of discrete compatibility conditions that should be supported to the approximation  $d_h(\mathbf{x})$  to guarantee essential smoothness for the resultant of Eqs. (3.16) and (3.17). The function  $d_h(\mathbf{x})$ , an two-dimensional approximation, is required to be the form

$$d_h(\mathbf{x}) = \frac{1}{h^2} \phi\left(\frac{x}{h}\right) \phi\left(\frac{y}{h}\right), \quad (3.23)$$

where  $\mathbf{x} = (x, y)$ ,  $\phi(r)$  is a function of real number  $r$ , and  $d_h \rightarrow \delta$  as  $h \rightarrow 0$ . Actually, the product form given by Eq. (3.23) is not necessary, but it reduces all subsequent considerations to one-dimensional cases. Moreover, the scaling in (3.23) makes a simplification to reduce the parameter  $h$ .

### 3.2.1 Postulates of $\phi(r)$

Now, the construction of  $\phi(r)$  obeys the following postulates:

$$1. \quad \phi(r) \in C^0, \quad (3.24)$$

$$2. \quad \phi(r) = 0 \quad \text{for } |r| \geq 2. \quad (3.25)$$

$$3. \quad \sum_{\text{even } i} \phi(r-i) = \sum_{\text{odd } i} \phi(r-i) = 1/2 \quad \text{for all } r. \quad (3.26)$$

$$4. \quad \sum_i (r-i)\phi(r-i) = 0 \quad \text{for all } r. \quad (3.27)$$

$$5. \quad \sum_i (\phi(r-i))^2 = C \quad \text{for all } r. \quad (3.28)$$

where  $C$  is a constant.

The continuity of  $\phi(r)$  makes the coefficients of the interpolation between fluid and interface points appearing in (3.16) and (3.17) vary continuously. Then avoid jumps in velocity or force as the Lagrangian markers moves across fluid mesh.

The purpose of bounded support of  $\phi(r)$  is to reduce the computational

cost which arises from the calculation of integrals in (3.16) and (3.17). If a function with unbounded support, such as  $\exp -r^2/2$ , is present, this would involve enormous computational cost since each Lagrangian marker interacts with all grid points of the Eulerian mesh (and vice versa). Note that the choice of the support with the width  $4h$  (without scaling) is the smallest possibility maintaining consistency with the other postulates in the meantime.

Postulate 3 is called zero moment condition which is a stronger version of

$$\sum_i \phi(r - i) = 1 \quad \text{for all } r. \quad (3.29)$$

The reason why we impose the stronger conditions is for the use of the central difference operator  $\mathbf{D}^0$  in the numerical scheme. The null space of the gradient operator based on  $\mathbf{D}^0$  is four-dimensional. The separate conditions given in (3.26) ensure that all four options get the same amount of force from each Lagrangian marker, and also that each Lagrangian marker assigns equal weight to all four options when computing its interpolated velocity. This avoids oscillations from one grid point to the next that would otherwise occur, especially when localized forces are applied. Moreover, this choice guarantees that constant functions are interpolated exactly by  $d_h$  (this has the physical interpretation of conserving momentum when applied to force spread in (3.16).

Postulate 4 is the so-called first moment condition which ensures that linear functions are interpolated exactly by  $d_h$  and smooth functions are therefore interpolated with second-order accuracy (with the physical implication that angular momentum is conserved when applying forces to fluid points). Obviously, substitute (3.29) to (3.27), we obtain a simplification

$$\sum_i i\phi(r - i) = r \quad \text{for all } r. \quad (3.30)$$

This property (3.28) comes from the condition

$$\sum_i \phi(r_1 - i)\phi(r_2 - i) = \Phi(r_1 - r_2) \quad \text{for all } r_1 \text{ and } r_2, \quad (3.31)$$

where  $\Phi(r_1 - r_2)$  is a scalar function. If (3.31) is imposed (regardless of the function  $\Phi$ ), it would imply the exact translation invariance of the IB method [36]. However, (3.31) is not compatible with any other postulates. That is why we consider (3.28), a weak form of (3.31) with  $r_1 = r_2$  and  $\Phi(0) = C$ .

Though (3.28) is weak, it does give some information about the sum that appears on the left-hand side of (3.31) which implies the inequality

$$\left| \sum_i \phi(r_1 - i)\phi(r_2 - i) \right| \leq C \quad \text{for all real } r_1 \text{ and } r_2, \quad (3.32)$$

(the Schwarz inequality), which is analogous to the physically reasonable requirement that when two interface points interact, the effect of one boundary point on the other is maximized when the points coincide.

### 3.2.2 Construction of $\phi(r)$

Next, we will explain how to determine an explicit form of  $\phi(r)$  from postulates (3.24)-(3.28) and therefore  $\delta_h$ . For simplicity, let  $0 \leq r \leq 1$  and then one can express (3.24)-(3.28) in the following formulae:

$$\phi(r-2) + \phi(r) = \frac{1}{2}, \quad (3.33)$$

$$\phi(r-1) + \phi(r+1) = \frac{1}{2}, \quad (3.34)$$

$$2\phi(r-2) + \phi(r-1) - \phi(r+1) = r, \quad (3.35)$$

$$(\phi(r-2))^2 + (\phi(r-1))^2 + (\phi(r))^2 + (\phi(r+1))^2 = C. \quad (3.36)$$

Clearly, there are four equations for four unknowns  $\phi(r-2)$ ,  $\phi(r-1)$ ,  $\phi(r)$ , and  $\phi(r+1)$ . It seems easy to get an simple expression of  $\phi(r)$  from a basic idea that write  $\phi(r-2)$ ,  $\phi(r-1)$ , and  $\phi(r+1)$  in terms of  $\phi(r)$

$$\phi(r-2) = \frac{1}{2} - \phi(r), \quad (3.37)$$

$$\phi(r-1) = -\frac{1}{4} + \frac{r}{2} + \phi(r), \quad (3.38)$$

$$\phi(r+1) = \frac{3}{4} - \frac{r}{2} - \phi(r), \quad (3.39)$$

by using (3.33)-(3.35), and take (3.37)-(3.39) into (3.36) to result in a quadratic equation of  $\phi(r)$

$$4(\phi(r))^2 + (2r-3)\phi(r) + \left(\frac{7}{8} - r - \frac{1}{2}r^2\right) = C. \quad (3.40)$$

But the difficulty to solve this simple system arises from the undetermined constant  $C$ . To overcome this obstacle, a simplest way is to set  $r = 0$  so that  $\phi(-2)$  is zero due to the bounded support of  $\phi$  and hence  $\phi(0) = 1/2$ . (Meantime,  $\phi(-1) = \phi(1) = 1/4$  is obtained by solving the system of (3.34)

and (3.35) with  $r = 0$ .) Substituting  $\phi(0) = 1/2$  into (3.40), here comes out  $C = 3/8$ . With the parameter determined  $C$ , the candidates for the solution of (3.40) will be

$$\phi(r) = \frac{1}{8} \left( 3 - 2r \pm \sqrt{(2r - 3)^2 - 8(1 - r)^2} \right), \quad 0 \leq r \leq 1. \quad (3.41)$$

One can choose  $\phi(0) = 1/2$  or  $\phi(1) = 1/4$  as the reference root to gain the unique solution

$$\phi(r) = \frac{1}{8} \left( 3 - 2r + \sqrt{1 + 4r - 4r^2} \right), \quad 0 \leq r \leq 1. \quad (3.42)$$

Note that this formula is only valid for  $r \in [0, 1]$ . To determine  $\phi$  on other intervals  $[-2, -1]$ ,  $[-1, 0]$ , and  $[1, 2]$ , consider the relations in (3.37)-(3.39) and take the advantage of (3.42), for instance, if  $r \in [1, 2]$  and  $\tilde{r} = r - 1$ , then  $\tilde{r} \in [0, 1]$  and from (3.39)

$$\begin{aligned} \phi(\tilde{r} + 1) &= \frac{3}{4} - \frac{\tilde{r}}{2} - \phi(\tilde{r}) \\ &= \frac{3}{4} - \frac{\tilde{r}}{2} - \frac{1}{8} \left( 3 - 2\tilde{r} + \sqrt{1 + 4\tilde{r} - 4\tilde{r}^2} \right) \\ &= \frac{1}{8} \left( 3 - 2\tilde{r} - \sqrt{1 + 4\tilde{r} - 4\tilde{r}^2} \right), \quad 0 \leq \tilde{r} \leq 1 \\ \Rightarrow \phi(r) &= \frac{1}{8} \left( 5 - 2r - \sqrt{-7 + 12r - 4r^2} \right), \quad 1 \leq r \leq 2 \end{aligned} \quad (3.43)$$

Similarly, we can obtain formulae of  $\phi(r)$  on  $[-2, -1]$  and  $[-1, 0]$ , respectively, and simplify  $\phi(r)$  in the form

$$\begin{aligned} \phi_q(r) &= \frac{1}{8} \left( 3 - 2|r| + \sqrt{1 + 4|r| - 4r^2} \right), \quad \text{if } |r| \leq 1, \\ &= \frac{1}{8} \left( 5 - 2|r| - \sqrt{-7 + 12|r| - 4r^2} \right), \quad \text{if } 1 < |r| < 2, \\ &= 0, \quad \text{if } |r| \geq 2. \end{aligned} \quad (3.44)$$

Surprisingly, this choice of  $\phi(r)$  is symmetric with respect to  $r = 0$ . And it is easy to check that  $\phi(r)$  is not only continuous but has continuous first derivative at  $r = -2, -1, 0, 1, 2$  (at everywhere indeed).

### 3.2.3 Other conventional $\phi(r)$

First of all, a simplest linear approximation of  $\delta_h$  behaves like a hat of the form

$$\phi_l(r) = \begin{cases} 1 - |r|, & \text{if } |r| \leq 1, \\ 0, & \text{if } |r| > 1. \end{cases}$$

Note that this linear approximation obeys only the postulates 1 and 3, of course, is lack of the continuity of the first derivative.

A extreme well approximation of (3.43) is a cosine function of the form

$$\phi_c(r) = \begin{cases} \frac{1}{4} (1 + \cos(\frac{\pi r}{2})), & \text{if } |r| \leq 2, \\ 0, & \text{if } |r| > 2. \end{cases}$$

This specific choice satisfies all postulates we listed before except the first-moment condition (3.27).

Another form of  $\phi$  that satisfies a similar set of properties (3.24)-(3.28) was proposed by Roma [44]. In the construction of  $\phi(r)$ , the support was reduced from 2 to 1.5, and one replaced the even/odd distinction in (3.26) from (3.29). The derivation of this approximation is described in detail in the following. Consider  $0 \leq r \leq 1$  and then one can express (3.29), (3.30), and (3.28) as:

$$\phi(r-1) + \phi(r) + \phi(r+1) = 1, \quad (3.45)$$

$$\phi(r-1) - \phi(r+1) = r, \quad (3.46)$$

$$(\phi(r-1))^2 + (\phi(r))^2 + (\phi(r+1))^2 = C. \quad (3.47)$$

Now, there are three equations for three unknowns  $\phi(r-1)$ ,  $\phi(r)$ , and  $\phi(r+1)$ . To get the parameter  $C$ , we first write  $\phi(r-1)$  and  $\phi(r+1)$  in terms of  $\phi(r)$

$$\phi(r-1) = \frac{1}{2} (1 + r - \phi(r)), \quad (3.48)$$

$$\phi(r+1) = \frac{1}{2} (1 - r - \phi(r)), \quad (3.49)$$

and set  $r = 0.5$  to gain  $\phi(-0.5) = \phi(0.5) = 0.5$ , and hence  $C = 0.5$ . Substituting (3.48) and (3.49) into (3.47) to result in a quadratic equation of  $\phi(r)$

$$3(\phi(r))^2 - 2\phi(r) + r^2 = 0. \quad (3.50)$$

Therefore the resultant will be

$$\phi(r) = \frac{1}{3} \left( 1 + \sqrt{1 - 3r^2} \right), \quad 0 \leq r \leq 0.5. \quad (3.51)$$

where we have used the fact  $\phi(0.5) = 1/2$  to determine the sign in front of the square. Similarly, if  $-0.5 \leq r \leq 0$ , we find that the corresponding formula of  $r$  will exactly the same as Eq. (3.51). Furthermore, take the advantage

of (3.48) and (3.49), finally the approximation of delta function with 3-point support is resulted in the form

$$\begin{aligned}
 \phi_s(r) &= \frac{1}{3} \left( 1 + \sqrt{1 - 3r^2} \right), & \text{if } |r| \leq 0.5, \\
 &= \frac{1}{6} \left( 5 - 3|r| - \sqrt{1 - 3(|r| - 1)^2} \right), & \text{if } 0.5 < |r| < 1.5, \\
 &= 0, & \text{if } |r| \geq 1.5.
 \end{aligned} \tag{3.52}$$

The corresponding approximate delta function is applicable to computations on a staggered marker-and-cell grid, where the problem of decoupled pressure modes inherent in Chorin's projection scheme is not an issue.

The following is a diagram of several approximations of the delta function we listed in this chapter.

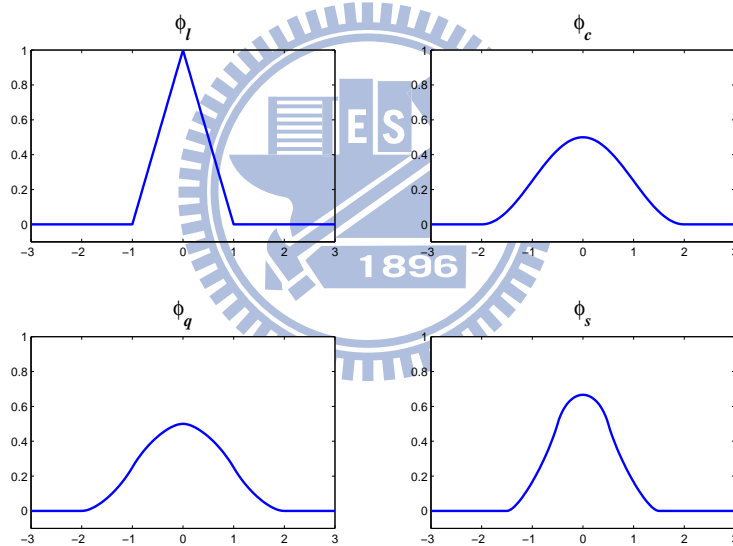


Figure 3.1: (a) Hat function. (b) Cosine approximation. (c) Second-order approximation with 4-point support. (d) Second-order approximation with 3-point support.



# Chapter 4

## Numerical method

In previous chapters, we have demonstrated what problems we are interested in and what model we will use in simulations. Now, we will give the whole numerical algorithm step by step and explain each part in detail in this chapter. First, a famous and popular MAC method combines projection method to solve variables on the fluid field. Then numerical setting for variables on the interface is present in section two. In section three, we introduce several discrete delta functions with compact support to connect variables defined on eulerian grid and lagrangian grid. A numerical scheme for artificial tangential velocity is proposed. Then a beautiful mass-preserving numerical scheme for surfactant equation will show up to fascinate the spotlight. Further, the usage of the boundary conditions and some essential approximation by the boundary conditions, such as approximation of ghost points for fluid solver, will be carried out in section four. Finally, the time integration of the whole numerical process is performed to close this chapter.

### 4.1 Fluid solver

Consider a model problem of a viscous incompressible fluid in a two-dimensional square domain  $\Omega = [a, b] \times [c, d]$ . And the unsteady flow is governed by the dimensionless momentum equations (3.14) and continuity equations (3.15). Let  $\mathbf{u}(\mathbf{x}, t) = (u(\mathbf{x}, t), v(\mathbf{x}, t))$ ,  $\mathbf{f}(\mathbf{x}, t) = (f(\mathbf{x}, t), g(\mathbf{x}, t))$ , and  $p(\mathbf{x}, t)$  be fluid velocities, external forces, and fluid pressure, respectively, where  $\mathbf{x} = (x, y)$  is the eulerian coordinate. Note that we will drop the superscript in our governing equations for convenience from now on. It is convenient to understand the numerical solver for the Navier-Stokes equations if we have the simplification of fluid properties  $\mu_1 = \mu_2 = 1$  and  $\rho_1 = \rho_2 = 1$  first. Then we can take advantage of (3.15) to simplify  $\nabla \cdot (2\mu E)$  as  $\Delta \mathbf{u}$ , and alternatively,

express the system in an explicit form

$$\frac{\partial u}{\partial t} + \frac{\partial u^2}{\partial x} + \frac{\partial uv}{\partial y} + \frac{\partial p}{\partial x} = \frac{1}{Re} \left( \frac{\partial^2 u}{\partial x^2} + \frac{\partial^2 u}{\partial y^2} \right) + \frac{1}{ReCa} f, \quad (4.1)$$

$$\frac{\partial v}{\partial t} + \frac{\partial uv}{\partial x} + \frac{\partial v^2}{\partial y} + \frac{\partial p}{\partial y} = \frac{1}{Re} \left( \frac{\partial^2 v}{\partial x^2} + \frac{\partial^2 v}{\partial y^2} \right) + \frac{1}{ReCa} g, \quad (4.2)$$

$$\frac{\partial u}{\partial x} + \frac{\partial v}{\partial y} = 0. \quad (4.3)$$

Note that we express the convection term as a conservation form. This can be recovered to original form by the use of continuity equation  $u_x + v_y = 0$ .

### 4.1.1 Staggered grid

Computational solutions of (4.1-4.3) are often obtained on a staggered grid. This implies that different dependent variables are evaluated at different grid points. Speaking in detail, the pressure is defined on the grid points labeled as  $\mathbf{x}_{i,j} = (x_i, y_j) = ((i - 1/2)h, (j - 1/2)h)$  for  $i, j = 1, 2, \dots, N$ , the velocity components  $u$  and  $v$  are defined at  $(x_{i+1/2}, y_j) = (ih, (j - 1/2)h)$  and  $(x_i, y_{j+1/2}) = ((i - 1/2)h, jh)$ , respectively, where the spacing  $h = \Delta x = \Delta y$ . A accepted staggered grid configuration is shown in Fig. 4.1. It can be seen

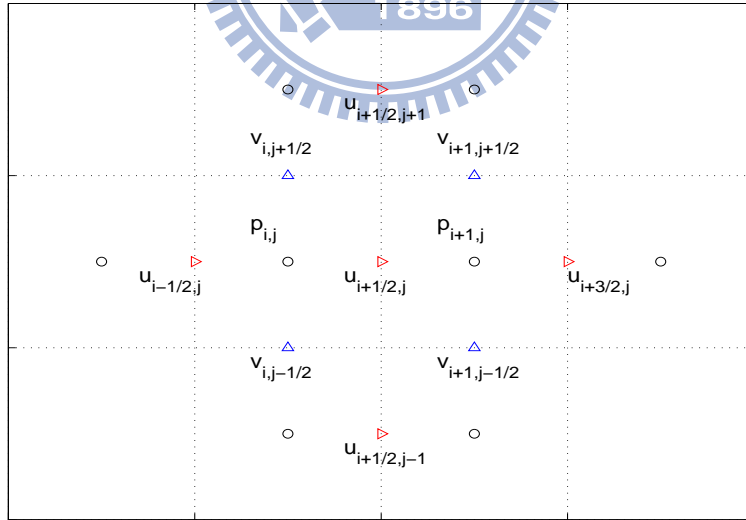


Figure 4.1: A diagram of the staggered grid.

that pressures are defined at the center of each cell while velocity components

are defined at the center of the cell faces. Discretization of (4.3) on the staggered grid shown in Fig. 4.1 gives

$$\frac{u_{i+1/2,j} - u_{i-1/2,j}}{\Delta x} + \frac{v_{i,j+1/2} - v_{i,j-1/2}}{\Delta y} = 0$$

In addition a Taylor series expansion about the cell center indicates that they have a truncation error of  $\mathcal{O}(\Delta x^2, \Delta y^2)$ , even though only four grid points are involved.

The use of the staggered grid permits coupling of the  $u$ ,  $v$  and  $p$  solutions at adjacent grid points. This in turn prevents the appearance of oscillatory solutions, particularly for  $p$ , that can occur if centered differences are used to discretize all derivatives on a non-staggered grid. The oscillatory solution is a manifestation of two separate pressure solutions associated with alternate grid points, which the use of centered differences on a non-staggered grid permits. The oscillatory behavior is usually worse at high Reynolds number where the dissipative terms, which do introduce adjacent grid point coupling for  $u$  and  $v$ , are small. Clearly, from (4.1-4.3), there are no dissipative terms for  $p$ .

Of course, the use of staggered grids has some drawbacks. Computer programs based on staggered grids tend to be harder to interpret because it is desirable to associate a cluster of dependent variables with corresponding storage locations. Thus arrays storing  $u$ ,  $v$  and  $p$  might associate storage location  $(i, j)$  with  $u_{i+1/2,j}$ , and  $v_{i,j+1/2}$  and  $p_{i,j}$  as Fig. 4.1. Generally boundary conditions are more difficult to impose consistently with a staggered grid, since at least one dependent variable,  $u$  or  $v$ , will not be defined on a particular boundary. If the grid is non-rectangular, and generalized coordinates are used, the incorporation of a staggered grid is more complicated.

Let  $\Delta t$  be the time mesh size, and  $n$  be the superscript time step index. In discretizing (4.1-4.3), the following second-order accurate finite difference expressions for derivatives with respect to space for  $(i, j)$ -cell are used [13]:

$$\begin{aligned} \left(\frac{\partial u^2}{\partial x}\right)_{i+1/2,j}^n &= \frac{(u_{i+1,j}^n)^2 - (u_{i,j}^n)^2}{\Delta x}, \\ \left(\frac{\partial uv}{\partial y}\right)_{i+1/2,j}^n &= \frac{(uv)_{i+1/2,j+1/2}^n - (uv)_{i+1/2,j-1/2}^n}{\Delta y}, \\ \left(\frac{\partial^2 u}{\partial x^2}\right)_{i+1/2,j}^n &= \frac{u_{i+3/2,j}^n - 2u_{i+1/2,j}^n + u_{i-1/2,j}^n}{\Delta x^2}, \end{aligned}$$

$$\begin{aligned}
\left(\frac{\partial^2 u}{\partial y^2}\right)_{i+1/2,j}^n &= \frac{u_{i+1/2,j+1}^n - 2u_{i+1/2,j}^n + u_{i+1/2,j-1}^n}{\Delta y^2}, \\
\left(\frac{\partial v^2}{\partial y}\right)_{i,i+1/2}^n &= \frac{(v_{i,j+1}^n)^2 - (v_{i,j}^n)^2}{\Delta y}, \\
\left(\frac{\partial uv}{\partial x}\right)_{i,j+1/2}^n &= \frac{(uv)_{i+1/2,j+1/2}^n - (uv)_{i-1/2,j+1/2}^n}{\Delta x}, \\
\left(\frac{\partial^2 v}{\partial x^2}\right)_{i,j+1/2}^n &= \frac{v_{i+1,j+1/2}^n - 2v_{i,j+1/2}^n + v_{i-1,j+1/2}^n}{\Delta x^2}, \\
\left(\frac{\partial^2 v}{\partial y^2}\right)_{i,j+1/2}^n &= \frac{v_{i,j+3/2}^n - 2v_{i,j+1/2}^n + v_{i,j-1/2}^n}{\Delta y^2}.
\end{aligned} \tag{4.4}$$

In the above expression, terms like  $u_{i,j}$ ,  $v_{i,j}$ ,  $u_{i+1/2,j+1/2}$ ,  $v_{i+1/2,j+1/2}$  appear, which are not defined in Fig. 4.1. To evaluate such terms, linear interpolation is employed, that is,

$$\begin{aligned}
u_{i,j} &= 0.5 (u_{i-1/2,j} + u_{i+1/2,j}) \\
u_{i+1/2,j+1/2} &= 0.5 (u_{i+1/2,j} + u_{i+1/2,j+1}) \\
v_{i+1/2,j+1/2} &= 0.5 (v_{i,j+1/2} + v_{i+1,j+1/2})
\end{aligned} \tag{4.5}$$

#### 4.1.2 MAC formulation

One of the earliest, and most widely used, methods for solving (4.1-4.3) is the Marker and Cell (MAC) method [17] due to Amsden and Harlow (1970). The method is characterized by the use of a staggered grid and the solution of a Poisson equation for the pressure at every time-step. Although the original form of the MAC method has certain weakness, the use of a staggered grid and a Poisson equation for the pressure has been retained in many modern methods derived from the MAC method.

In the MAC formulation the discretizations (4.4) allow the following explicit algorithm to be generated from (4.1 and 4.2):

$$u_{i+1/2,j}^{n+1} = \Delta t \left( F_{i+1/2,j}^n - \frac{p_{i+1,j}^{n+1} - p_{i,j}^{n+1}}{\Delta x} \right), \tag{4.6}$$

where

$$\begin{aligned}
F_{i+1/2,j}^n &= \frac{u_{i+1/2,j}^n}{\Delta t} - \left(\frac{\partial u^2}{\partial x}\right)_{i+1/2,j}^n - \left(\frac{\partial uv}{\partial y}\right)_{i+1/2,j}^n \\
&\quad + \frac{1}{Re} \left( \left(\frac{\partial^2 u}{\partial x^2}\right)_{i+1/2,j}^n + \left(\frac{\partial^2 u}{\partial y^2}\right)_{i+1/2,j}^n \right).
\end{aligned} \tag{4.7}$$

Similarly, the discretized form of (4.2) is written as

$$v_{i,j+1/2}^{n+1} = \Delta t \left( G_{i,j+1/2}^n - \frac{p_{i,j+1}^{n+1} - p_{i,j}^{n+1}}{\Delta y} \right), \quad (4.8)$$

where

$$G_{i,j+1/2}^n = \frac{v_{i,j+1/2}^n}{\Delta t} - \left( \frac{\partial uv}{\partial x} \right)_{i,j+1/2}^n - \left( \frac{\partial v^2}{\partial y} \right)_{i,i+1/2}^n + \frac{1}{Re} \left( \left( \frac{\partial^2 v}{\partial x^2} \right)_{i,j+1/2}^n + \left( \frac{\partial^2 v}{\partial y^2} \right)_{i,j+1/2}^n \right). \quad (4.9)$$

In (4.6 and 4.8)  $p$  appears implicitly; however,  $p^{n+1}$  is obtained before (4.6 and 4.8) are used, as follows. The continuity equation is discretized as

$$\frac{u_{i+1/2,j}^{n+1} - u_{i-1/2,j}^{n+1}}{\Delta x} + \frac{v_{i,j+1/2}^{n+1} - v_{i,j-1/2}^{n+1}}{\Delta y} = 0, \quad (4.10)$$

Substituting right-hand-side of (4.6 and 4.8) into (4.10), we rewrite (4.10) as a discrete Poisson equation for the pressure

$$\begin{aligned} & \frac{p_{i+1,j}^{n+1} - 2p_{i,j}^{n+1} + p_{i-1,j}^{n+1}}{\Delta x^2} + \frac{p_{i,j+1}^{n+1} - 2p_{i,j}^{n+1} + p_{i,j-1}^{n+1}}{\Delta y^2} \\ &= \frac{1}{\Delta t} \left( \frac{F_{i+1/2,j}^n - F_{i-1/2,j}^n}{\Delta x} + \frac{G_{i,j+1/2}^n - G_{i,j-1/2}^n}{\Delta y} \right) \end{aligned} \quad (4.11)$$

The equation is solved at every time-step using direct Poisson solver, and the solution  $p^{n+1}$  will be substituting into (4.6 and 4.8) to obtain  $u^{n+1}$  and  $v^{n+1}$ .

### 4.1.3 Projection method

An alternative way to solve the couple system (4.1-4.3) is the so-called projection method which was proposed by A. J. Chorin [6] in 1968. The general procedure for a projection method is a predictor-corrector approach. In the first step an intermediate velocity field denoted by  $\mathbf{u}^*$  is computed utilizing the momentum equations. This velocity does not satisfy the continuity equation. In the second step a Poisson equation for the pressure which is derived from the continuity equation is solved. Finally,  $\mathbf{u}^*$  is projected onto a divergence-free velocity field by the computed pressure. The three steps are now described in detail for our treatment problem.

## First-order projection method

**Step1:** This is a prediction step for  $\mathbf{u}^*$ .

$$\mathbf{u}^* = \mathbf{H}^n \quad (4.12)$$

The components of  $\mathbf{H} = (F, G)$  are expressed in (4.6 and 4.8).

**Step2:** Solve a Poisson equation for pressure by using the direct Poisson solver.

$$\Delta p^{n+1} = \frac{1}{\Delta t} \nabla \cdot \mathbf{u}^*. \quad (4.13)$$

**Step3:** The projection step.

$$\mathbf{u}^{n+1} = \mathbf{u}^* - \Delta t \nabla p^{n+1}. \quad (4.14)$$

Note that this procedure has second-order accuracy in space and first-order accuracy in time. Since the corresponding algorithms for  $u^{n+1}$  and  $v^{n+1}$  are explicit, there is a restriction on the maximum mesh size of time for a stable solution [17].

$$\begin{aligned} 0.25(|u| + |v|)^2 \Delta t Re \leq 1 \quad \text{and} \\ \Delta t / (Re \Delta x^2) \leq 0.25, \quad \text{assuming that } \Delta x^2 = \Delta y^2 \end{aligned} \quad (4.15)$$

## Second-order projection method

In order to release the restriction of the maximum mesh size of time and reduce the truncation error from the time discretization, a second-order time discretization scheme to momentum and continuity equations is intuitively considered. However, the resultant discrete formulation of Navier-Stokes equations

$$\begin{aligned} \frac{3\mathbf{u}^{n+1} - 4\mathbf{u}^n + \mathbf{u}^{n-1}}{2\Delta t} + 2(\mathbf{u}^n \cdot \nabla)\mathbf{u}^n - (\mathbf{u}^{n-1} \cdot \nabla)\mathbf{u}^{n-1} + \nabla p^{n+1} \\ = \frac{1}{Re} \Delta \mathbf{u}^{n+1} + \frac{1}{ReCa} (2\mathbf{f}^n - \mathbf{f}^{n-1}) \end{aligned} \quad (4.16)$$

is a coupled system of the velocity field  $\mathbf{u}$  and the pressure  $p$ . Note that non-linear terms such as advection terms and external forces are approximated by a conventional extrapolation evaluated at  $t = n\Delta t$ , that is, the approximation of a function  $\psi$  at  $t = (n+1)\Delta t$  simply comes from the average form  $\psi^n \approx 0.5(\psi^{n+1} + \psi^{n-1})$ . To decouple the above numerical scheme, we

introduce a second-order projection method which is based on the idea of the first-order projection method. The detailed procedures are described as the following steps.

**Step1:** This is a prediction step to evaluate the intermediate velocity field  $\mathbf{u}^*$  by the Helmholtz-type solver.

$$\begin{aligned} \frac{3\mathbf{u}^* - 4\mathbf{u}^n + \mathbf{u}^{n-1}}{2\Delta t} + 2(\mathbf{u}^n \cdot \nabla)\mathbf{u}^n - (\mathbf{u}^{n-1} \cdot \nabla)\mathbf{u}^{n-1} + \nabla p^n \\ = \frac{1}{Re}\Delta\mathbf{u}^* + \frac{1}{ReCa}(2\mathbf{f}^n - \mathbf{f}^{n-1}) \end{aligned} \quad (4.17)$$

or simply

$$\Delta\mathbf{u}^* - \frac{3Re}{2\Delta t}\mathbf{u}^* = Re\mathbf{H}^n \quad (4.18)$$

where

$$\mathbf{H}^n = \frac{\mathbf{u}^{n-1} - 4\mathbf{u}^n}{2\Delta t} + 2(\mathbf{u}^n \cdot \nabla)\mathbf{u}^n - (\mathbf{u}^{n-1} \cdot \nabla)\mathbf{u}^{n-1} + \nabla p^n - \frac{1}{ReCa}(2\mathbf{f}^n - \mathbf{f}^{n-1}) \quad (4.19)$$

In this step the unknown  $\mathbf{u}^*$  is treated implicitly, so we can relax the restriction of upper bound of time mesh. Moreover, this algorithm is second-order accurate in time.

**Step2:** By the Hodge decomposition there exists a potential function  $\phi$  and a divergence-free velocity field  $\mathbf{u}^{n+1}$  such that

$$\mathbf{u}^* = \mathbf{u}^{n+1} + \frac{2\Delta t}{3}\Delta\phi^{n+1}. \quad (4.20)$$

Taking the divergence operator to both sides of (4.20) and using the divergence-free property, we have

$$\Delta\phi^{n+1} = \frac{3}{2\Delta t}\nabla \cdot \mathbf{u}^* \quad (4.21)$$

Furthermore, a Poisson solver is used again to obtain  $\phi^{n+1}$ .

**Step3:** Project  $\mathbf{u}^*$  onto  $\mathbf{u}^{n+1}$  as

$$\mathbf{u}^{n+1} = \mathbf{u}^* - \frac{2\Delta t}{3}\Delta\phi^{n+1}. \quad (4.22)$$

Now we already updated  $\mathbf{u}^{n+1}$ , and solve a Poisson equation of potential function  $\phi^{n+1}$  instead of the one of pressure  $p^{n+1}$ . Obviously,  $p^{n+1}$  can be obtained from  $\phi^{n+1}$  by substituting Eq. (4.20) into Eq. (4.17) and comparing the resultant formulation with Eq. (4.16). Therefore,

$$\nabla p^{n+1} = \nabla p^n + \nabla\phi^{n+1} - \frac{1}{Re}\Delta\mathbf{u}^*. \quad (4.23)$$

## 4.2 Lagrangian manners

For the immersed interface, we use a collection of discrete points  $\alpha_k = k\Delta\alpha, k = 0, 1, \dots, M$  such that the Lagrangian markers are denoted by  $\mathbf{X}_k = \mathbf{X}(\alpha_k) = (X_k, Y_k)$ . The force density  $\mathbf{F}$  and velocity  $\mathbf{U}$  are always defined on position  $\mathbf{X}_k$  such that  $\mathbf{F}_k = \mathbf{F}(\alpha_k) = (F_k, G_k)$  and  $\mathbf{U}_k = \mathbf{U}(\alpha_k) = (U_k, V_k)$ . However, there are two types of interfaces in our numerical simulations, a bubble which is a simple closed curve and a drop which attaches on the solid wall, some of quantities defined on the interface may be evaluated on the position different from  $\mathbf{X}_k$  due to the problem. No matter what kind of problem we treat, the calculation of the derivative of a variable along the interface plays a very important role to the dynamic of the interface. Here, we provide two choices of approach to compute the derivatives of a function along the interface. Without loss of generality, for any function defined on the interface  $\psi(\alpha)$ , we approximate the partial derivative  $\frac{\partial\psi}{\partial\alpha}$  by

### Finite difference approach

$$D_\alpha\psi(\alpha) = \frac{\psi(\alpha + \Delta\alpha/2) - \psi(\alpha - \Delta\alpha/2)}{\Delta\alpha}. \quad (4.24)$$

and

### Cubic spline approach

$$D_{cs}(\psi(\alpha)), \quad (4.25)$$

where  $D_{cs}$  is an operator of derivative from cubic splines.

### A bubble

In this case, the bubble can be seen as a periodic parametric function of  $\alpha$ , i.e.  $\mathbf{X}_0 = \mathbf{X}_M$ . The unit tangent  $\boldsymbol{\tau}$ , the surfactant concentration  $\gamma$ , surface tension  $\sigma$  are defined at the ‘‘half-integer’’ points given by  $\alpha_{k+1/2} = (k + 1/2)\Delta\alpha$ . Then  $\boldsymbol{\tau}_{k+1/2} = \boldsymbol{\tau}(\alpha_{k+1/2})$ ,  $\gamma_{k+1/2} = \gamma(\alpha_{k+1/2})$ , and  $\sigma_{k+1/2} = \sigma(\alpha_{k+1/2})$ . For this setting,  $\boldsymbol{\tau}_{k+1/2}$  is simply evaluated from the derivative of  $\mathbf{X}$  with respect to  $\alpha$  by the center difference method. And  $\mathbf{F}_k$  will be obtained from  $\boldsymbol{\tau}_{k+1/2}$  in the same process. Alternatively, one can use cubic spline method for the derivative of variables along the interface, however, it is convenient to define  $\boldsymbol{\tau}$  and  $\sigma$  at the integer-points but keep  $\gamma$  at the half-integer points for numerically preserving the total mass of surfactant concentration.



## A drop contacts a solid wall

When a drop contact a solid wall, the interface is no longer a simple closed curve and two end-points are always located on the solid wall with  $\mathbf{X}_0 \neq \mathbf{X}_M$ . Again, the surfactant concentration  $\gamma_{k-1/2}$ , is still defined at the “half-integer” points given by  $\alpha_{k-1/2} = (k - 1/2)\Delta\alpha$ . However, the unit tangent  $\boldsymbol{\tau}$  and surface tension  $\sigma$  are defined at  $\alpha_k = k\Delta\alpha$ . Since center difference approach to derivatives on the interface is not good enough to catch the behavior of the interface, instead, we use a natural cubic spline to fit the interface. Although this approach need more computational cost, it makes the interface behave as a piecewise cubic polynomial so that unit tangent  $\boldsymbol{\tau}_k$ , unit normal  $\mathbf{n}_k$ , and curvature  $\kappa_k$  are provided automatically.

## 4.3 Connection between fluid and interface

Recall that (3.16) represents a transformation from lagrangian variables to eulerian variables while (3.17) seems to be a transfer to interpolate fluid velocity to the position of the interface. And we have proposed several one dimensional delta functions at the end of last chapter. Since we only consider two-dimensional problem here, the delta function should be given as a product of one-variable functions that scale with the mesh width  $h$  as  $\delta(\mathbf{x}) = \frac{1}{h^2}\phi(x)\phi(y)$ . This means that the delta function allows us to treat each component of  $\mathbf{x} - \mathbf{X}$  individually and the resultant comes from their product.

## 4.4 An equi-distributed technique for Lagrangian markers

In the context of immersed boundary simulations, the interface is tracked in a Lagrangian manner. Once the Lagrangian markers have been chosen initially, the movement of those markers are based on the interpolating local fluid velocity. Very often, as time evolves, those Lagrangian markers will be either clustered together or diluted so the overall numerical stability or accuracy can be affected significantly. Therefore, certain grid redistribution technique must be adopted to preserve better resolution. In our previous immersed boundary simulation for a drop in a shear flow [31], the marker points will gradually sweep into the tips so we need to add or delete the grid points based on the distances of the markers. In this paper, we introduce another convenient way to dynamically control the Lagrangian markers so

that they can be equally distributed for all time.

In order to remove the stiffness from the interfacial flows with surface tension more easily, Hou, Lowengrub and Shelly [18] introduced an artificial tangential velocity into their  $\theta - L$  formulation of boundary integral methods so that the particles can be uniformly distributed. Following the same idea of [18] and modifying it to the framework of the immersed boundary method, we propose the following technique to enforce Lagrangian markers equally distributed.

As we know,  $|\mathbf{X}_\alpha|$  is the local stretching factor of the interface. The idea is to introduce an artificial tangential velocity  $U^A(\alpha, t)$  in Eq. (3.17) as

$$\frac{\partial \mathbf{X}(\alpha, t)}{\partial t} = \mathbf{U}(\alpha, t) + U^A(\alpha, t) \boldsymbol{\tau}, \quad (4.26)$$

so that  $|\mathbf{X}_\alpha|$  is independent of  $\alpha$ , but is dependent of  $t$ . It is quite apparent that there should be no artificial tangential velocity at moving contact lines ( $\alpha = 0$  and  $\alpha = L_b$ ) since the contact lines should move with their own speed determined by the fluid system. Thus, we have  $U^A(0, t) = U^A(L_b, t) = 0$ . Here, we need to impose  $|\mathbf{X}_\alpha|_\alpha = 0$  so we have  $|\mathbf{X}_\alpha| = \frac{1}{L_b} \int_0^{L_b} |\mathbf{X}_{\alpha'}| d\alpha'$ . Taking the derivative with respect to  $t$ , we have  $|\mathbf{X}_\alpha|_t = \frac{1}{L_b} \int_0^{L_b} |\mathbf{X}_{\alpha'}|_t d\alpha'$ . Since

$$\begin{aligned} S_{\alpha t} &= \frac{\partial |\mathbf{X}_\alpha|}{\partial t} = \mathbf{X}_{\alpha t} \cdot \boldsymbol{\tau} = \left( \frac{\partial \mathbf{U}}{\partial \alpha} + \frac{\partial U^A}{\partial \alpha} \boldsymbol{\tau} + U^A \frac{\partial \boldsymbol{\tau}}{\partial \alpha} \right) \cdot \boldsymbol{\tau} \\ &= \left( \frac{\partial \mathbf{U}}{\partial \alpha} + \frac{\partial U^A}{\partial \alpha} \boldsymbol{\tau} + U^A \kappa S_\alpha \mathbf{n} \right) \cdot \boldsymbol{\tau} = \frac{\partial \mathbf{U}}{\partial \alpha} \cdot \boldsymbol{\tau} + \frac{\partial U^A}{\partial \alpha}, \\ &= (\nabla_s \cdot \mathbf{U}) |\mathbf{X}_\alpha| + \frac{\partial U^A}{\partial \alpha} \end{aligned} \quad (4.27)$$

we have

$$\frac{\partial U^A}{\partial \alpha} = \frac{1}{L_b} \int_0^{L_b} \left( \frac{\partial \mathbf{U}}{\partial \alpha'} \cdot \boldsymbol{\tau}' + \frac{\partial U^A}{\partial \alpha'} \right) d\alpha' - \frac{\partial \mathbf{U}}{\partial \alpha} \cdot \boldsymbol{\tau}. \quad (4.28)$$

Integrating with respect to  $\alpha$  and using the fact of  $U^A(0, t) = U^A(L_b, t) = 0$ , we obtain

$$U^A(\alpha, t) = \frac{\alpha}{L_b} \int_0^{L_b} \frac{\partial \mathbf{U}}{\partial \alpha'} \cdot \boldsymbol{\tau}' d\alpha' - \int_0^\alpha \frac{\partial \mathbf{U}}{\partial \alpha'} \cdot \boldsymbol{\tau}' d\alpha'. \quad (4.29)$$

It is important to mention that an alternative formula for above artificial tangential velocity has been derived by Cenicerros [5] in a similar front-tracking

manner. However, unlike the derivation in [5], the present formula (4.29) does not need to compute the curvature of the interface.

Furthermore, the numerical formulation of (4.29) can be written as

$$(U^A)_k^{n+1} = \frac{\Delta\alpha}{L_b} C - \sum_{i=0}^{k'} \left( \frac{\partial \mathbf{U}}{\partial \alpha} \cdot \boldsymbol{\tau} \right)_i^{n+1} \Delta\alpha. \quad (4.30)$$

where  $\sum_{i=0}^{k'} a_i = 0.5a_0 + a_1 + \dots + a_{k-1} + 0.5a_k$  and  $C$  is the integrand of  $S_{\alpha t}$  over  $[0, L_b]$ . Actually,  $C$  is evaluated by the use of (4.30) as following

$$C = \frac{L_b}{\Delta\alpha} \sum_{i=0}^{M'} \left( \frac{\partial \mathbf{U}}{\partial \alpha} \cdot \boldsymbol{\tau} \right)_i^{n+1} \Delta\alpha. \quad (4.31)$$

Note that this artificial velocity will affect not only the position of markers  $\mathbf{X}_k$  on the interface but the distribution of the surfactant concentration  $\gamma_{k+1/2}$ . We will put the effect of the artificial velocity into the surfactant equation and give a mass-preserving numerical scheme in next section.

## 4.5 Modified surfactant concentration equation

By taking the artificial velocity  $U^A$  into account, the material derivative now becomes

$$\frac{D\gamma}{Dt} = \frac{\partial\gamma}{\partial t} - U^A \boldsymbol{\tau} \cdot \nabla_s \gamma. \quad (4.32)$$

So the surfactant equation (2.36) has to be modified to

$$\frac{\partial\gamma}{\partial t} - U^A \boldsymbol{\tau} \cdot \nabla_s \gamma + (\nabla_s \cdot \mathbf{U}) \gamma = \frac{1}{Pe_s} \nabla_s^2 \gamma. \quad (4.33)$$

Multiplying the stretching factor  $|\mathbf{X}_\alpha|$  on both sides of the above equation, we obtain

$$\frac{\partial\gamma}{\partial t} |\mathbf{X}_\alpha| - U^A \frac{\partial\gamma}{\partial\alpha} + (\nabla_s \cdot \mathbf{U}) |\mathbf{X}_\alpha| \gamma = \frac{1}{Pe_s} \nabla_s^2 \gamma |\mathbf{X}_\alpha|. \quad (4.34)$$

By writing the surface derivatives in terms of  $\alpha$  explicitly and using the identity of Eq. (4.27), we obtain

$$\frac{\partial\gamma}{\partial t} |\mathbf{X}_\alpha| + \frac{\partial|\mathbf{X}_\alpha|}{\partial t} \gamma - \frac{\partial(U^A \gamma)}{\partial\alpha} = \frac{1}{Pe_s} \frac{\partial}{\partial\alpha} \left( \frac{\partial\gamma}{\partial\alpha} / |\mathbf{X}_\alpha| \right). \quad (4.35)$$

The finite difference discretization for the surfactant equation in next section should be based on the above formulation. Notice that, when the artificial tangential velocity  $U^A$  is set to be zero, the above equation can be recovered to the original surfactant equation derived in [31]. We should also mention that a similar modified surfactant equation (by taking the artificial velocity into account) with curvature term can be found in [5] as well.

## 4.6 Mass-preserving numerical scheme for surfactant equation

Since the surfactant is insoluble, the total mass on the interface must be conserved. Thus, it is important to develop a numerical scheme for the surfactant concentration equation to preserve the total mass. This can be done as follows.

For the sake of convenience, we use  $S_\alpha$  to denote the stretching factor  $|\mathbf{X}_\alpha|$ , and rewrite the surfactant concentration equation (4.35) as

$$\frac{\partial \gamma}{\partial t} S_\alpha + \frac{\partial S_\alpha}{\partial t} \gamma - \frac{\partial(U^A \gamma)}{\partial \alpha} = \frac{1}{Pe_s} \frac{\partial}{\partial \alpha} \left( \frac{\partial \gamma}{\partial \alpha} / S_\alpha \right). \quad (4.36)$$

Now we discretize the above equation by the Crank-Nicholson scheme in a symmetric way as

$$\begin{aligned} & \frac{\gamma_{k+\frac{1}{2}}^{n+1} - \gamma_{k+\frac{1}{2}}^n}{\Delta t} \frac{(S_\alpha)_{k+\frac{1}{2}}^{n+1} + (S_\alpha)_{k+\frac{1}{2}}^n}{2} + \frac{(S_\alpha)_{k+\frac{1}{2}}^{n+1} - (S_\alpha)_{k+\frac{1}{2}}^n}{\Delta t} \frac{\gamma_{k+\frac{1}{2}}^{n+1} + \gamma_{k+\frac{1}{2}}^n}{2} \\ & - \frac{1}{2} \left( \frac{(U^A)_{k+1}^{n+1} \gamma_{k+1}^{n+1} - (U^A)_k^{n+1} \gamma_k^{n+1}}{\Delta \alpha} + \frac{(U^A)_{k+1}^n \gamma_{k+1}^n + \gamma_k^n - (U^A)_k^n \gamma_k^n}{\Delta \alpha} \right) \\ & = \frac{1}{2 Pe_s} \frac{1}{\Delta \alpha} \left( \frac{(\gamma_{k+\frac{3}{2}}^{n+1} - \gamma_{k+\frac{1}{2}}^{n+1})}{\Delta \alpha} / (S_\alpha)_{k+1}^{n+1} - \frac{(\gamma_{k+\frac{1}{2}}^{n+1} - \gamma_{k-\frac{1}{2}}^{n+1})}{\Delta \alpha} / (S_\alpha)_k^{n+1} \right) \\ & + \frac{1}{2 Pe_s} \frac{1}{\Delta \alpha} \left( \frac{(\gamma_{k+\frac{3}{2}}^n - \gamma_{k+\frac{1}{2}}^n)}{\Delta \alpha} / (S_\alpha)_{k+1}^n - \frac{(\gamma_{k+\frac{1}{2}}^n - \gamma_{k-\frac{1}{2}}^n)}{\Delta \alpha} / (S_\alpha)_k^n \right) \end{aligned} \quad (4.37)$$

where  $(S_\alpha)_{k+\frac{1}{2}} \approx 0.5((S_\alpha)_k + (S_\alpha)_{k+1})$  and  $\gamma_k \approx 0.5(\gamma_{k-\frac{1}{2}} + \gamma_{k+\frac{1}{2}})$ .

Since the new interface marker location  $\mathbf{X}_k^{n+1}$  is obtained in the previous step, the above discretization results in a symmetric tri-diagonal linear system

which can be solved easily. More importantly, the total mass of surfactant is conserved numerically; that is,

$$\sum_k \gamma_{k+\frac{1}{2}}^{n+1} (S_\alpha)_{k+\frac{1}{2}}^{n+1} \Delta\alpha = \sum_k \gamma_{k+\frac{1}{2}}^n (S_\alpha)_{k+\frac{1}{2}}^n \Delta\alpha. \quad (4.38)$$

(Note that, the summation is exactly the mid-point rule discretization for the integral in Eq. (2.30).) The above equality can be easily derived by taking the summation of both sides of Eq. (4.37) and using the no flux boundary condition (or periodic boundary condition) of  $\gamma$ .

## 4.7 Ghost values from boundary conditions

In this section, we demonstrate approximation of ghost values which are used in the computation of fluid solver. Since the fluid mesh is staggered, velocity components  $u$  and  $v$ , and pressure  $p$  are defined on the center of the faces of the cell  $(i, j)$  and the center of the cell  $(i, j)$ , respectively. Discrete values  $u_{1/2,j}$ ,  $u_{M+1/2,j}$ ,  $v_{i,1/2}$ , and  $v_{i,M+1/2}$  are evaluated at their corresponding boundaries, respectively. However,  $u_{i+1/2,0}$ ,  $u_{i+1/2,M+1}$ ,  $v_{0,j+1/2}$ , and  $v_{M+1,j+1/2}$  are so-called the ghost values approximated by the use of the boundary conditions on its adjacent boundary.

### A bubble in a shear flow

The first numerical experiment in next chapter is concerned with a bubble in a shear flow. In this case, the initial condition of a shear flow  $\mathbf{u} = r(y, 0)$  is applied in the beginning, and boundary conditions for the fluid velocities are given as values of the initial velocity at the boundary of the computational domain  $[a, b] \times [c, d]$ . That is,  $u(x, c) = rc$ ,  $u(x, d) = rd$ ,  $u(a, y) = u(b, y) = ry$ , and  $v(x, c) = v(x, d) = v(a, y) = v(b, y) = 0$ . Then approximations for ghost values from linear extrapolation are given in the following.

$$\begin{aligned} u_{i+1/2,0} &= 2u(i\Delta x, c) - u_{i+1/2,1} = 2rc - u_{i+1/2,1}, \\ u_{i+1/2,M+1} &= 2u(i\Delta x, d) - u_{i+1/2,M} = 2rd - u_{i+1/2,M}, \\ v_{0,j+1/2} &= -v_{1,j+1/2}, \\ v_{M+1,j+1/2} &= -v_{M,j+1/2}. \end{aligned} \quad (4.39)$$

Note that  $u_{i+1/2,1}$ ,  $u_{i+1/2,M}$ ,  $v_{1,j+1/2}$ , and  $v_{M,j+1/2}$  are unknowns for the system when these ghost values are used. Therefore, the effect of these ghost values will appear in the right-hand side of the linear system and simultaneously affect the coefficients of the matrix of the linear system.

## A drop adheres to a solid wall

For the moving contact line problem, the no-slip boundary condition should be replaced with the Navier-slip boundary condition (2.43). For simplicity, consider a drop adheres the bottom of a box  $[a, b] \times [c, d]$ , then Navier-slip boundary condition will be imposed at  $y = c$  while no-slip boundary conditions are imposed at  $x = a$ ,  $x = b$ , and  $y = d$ . (Obviously, ghost values corresponding to boundaries with no-slip boundary conditions, in fact, are approximated in similar way to last case). We can simplify (2.43) as

$$u(x, c) = \beta \frac{\partial u}{\partial y}(x, c), \quad (4.40)$$

where  $\beta$  is the slip coefficient of magnitude around  $0.5\Delta y$ . A discrete form of Eq. (4.40) is

$$\frac{u_{i+1/2,1} + u_{i+1/2,0}}{2} = \beta \frac{u_{i+1/2,1} - u_{i+1/2,0}}{\Delta y} + O(\Delta y^2), \quad (4.41)$$

therefore, we obtain a second-order approximation

$$u_{i+1/2,0} = \left( \frac{\beta - \Delta y/2}{\beta + \Delta y/2} \right) u_{i+1/2,1}. \quad (4.42)$$

## 4.8 Indicator function

Since the density and viscosity are discontinuous constants across the interface, they can be represented by the approximate form

$$\mu(\mathbf{x}, t) = \mu_2 + (\mu_1 - \mu_2) I(\mathbf{x}, t), \quad (4.43)$$

$$\rho(\mathbf{x}, t) = \rho_2 + (\rho_1 - \rho_2) I(\mathbf{x}, t), \quad (4.44)$$

where the indicator function is found using Tryggvason's approach in [52]. In detail, the indicator function can be written as an integral of the two-dimensional Dirac-delta function on the region  $\Sigma(t)$

$$\begin{aligned} I(\mathbf{x}, t) &= \int_{\Sigma(t)} \delta(\mathbf{x} - \mathbf{x}') d\mathbf{x}', \\ \nabla I(\mathbf{x}, t) &= - \int_{\partial\Sigma(t)} \delta(\mathbf{x} - \mathbf{X}(\alpha, t)) \mathbf{n} d\alpha, \\ \Rightarrow \Delta I(\mathbf{x}, t) &= -\nabla \cdot \int_{\partial\Sigma(t)} \delta(\mathbf{x} - \mathbf{X}(\alpha, t)) \mathbf{n} d\alpha. \end{aligned} \quad (4.45)$$

## 4.9 Numerical time integration

At the beginning of each time step, e.g., step  $n$ , the variables  $\mathbf{X}_k^n = \mathbf{X}(\alpha_k, n\Delta t)$ ,  $\gamma_{k+1/2}^n = \gamma(\alpha_{k+1/2}, n\Delta t)$ ,  $\mathbf{u}^n = \mathbf{u}(\mathbf{x}, n\Delta t)$ , and  $p^{n-1/2} = p(\mathbf{x}, (n-1/2)\Delta t)$  are all given. The details of the numerical time integration are as follows.

1. Compute the surface tension and unit tangent on the interface.

**For a bubble:**

$$\sigma_{k+1/2}^n = \sigma_c (1 + \ln(1 - \eta\gamma_{k+1/2}^n)) \quad (4.46)$$

$$\boldsymbol{\tau}_{k+1/2}^n = \frac{D_\alpha \mathbf{X}_k^n}{|D_\alpha \mathbf{X}_k^n|} \quad (4.47)$$

both of which hold for  $\alpha_{k+1/2} = (k+1/2)\Delta\alpha$ . Then the interfacial force at the fluid/fluid markers  $\mathbf{X}_k$ ,  $k = 1, \dots, M$  are given by

$$\mathbf{F}_k^n = D_\alpha (\sigma_{k+1/2}^n \boldsymbol{\tau}_{k+1/2}^n). \quad (4.48)$$

Note that  $\mathbf{F}_0^n = \mathbf{F}_M^n$  due to the periodicity of  $\mathbf{F}$ .

**For a drop:**

$$\sigma_k^n = \sigma_c (1 + \ln(1 - \eta\gamma_k^n)) \quad (4.49)$$

$$\boldsymbol{\tau}_k^n = \frac{D_s \mathbf{X}_k^n}{|D_s \mathbf{X}_k^n|} \quad (4.50)$$

both of which hold for  $\alpha_k = k\Delta\alpha$ , and  $\gamma_k^n$  is simply approximated by the average of  $\gamma_{k-1/2}^n$  and  $\gamma_{k+1/2}^n$ . Then we compute the interfacial force at the fluid/fluid markers  $\mathbf{X}_k$ ,  $k = 1, \dots, M-1$  by

$$\mathbf{F}_k^n = D_s (\sigma_k^n \boldsymbol{\tau}_k^n). \quad (4.51)$$

The unbalanced Young force at the contact lines ( $k = 0$  and  $k = M$ ) can be computed by

$$\mathbf{F}_0^n = (\sigma_{s2} - \sigma_{s1} - \sigma_0^n \cos \theta_0^n) \mathbf{e}_1 \quad (4.52)$$

$$\mathbf{F}_M^n = -(\sigma_{s2} - \sigma_{s1} - \sigma_M^n \cos \theta_M^n) \mathbf{e}_1 \quad (4.53)$$

where  $\mathbf{e}_1 = (1, 0)$  and  $\cos \theta_k^n = -\boldsymbol{\tau}_k^n \cdot \mathbf{e}_1$ .

2. Distribute the force from the markers to the fluid by

$$\mathbf{f}^n(\mathbf{x}) = \sum_{k=1}^{M-1} \mathbf{F}_k^n \delta_h(\mathbf{x} - \mathbf{X}_k^n) \Delta\alpha + C \sum_{k=0, M} \mathbf{F}_k^n \delta_h(\mathbf{x} - \mathbf{X}_k^n), \quad (4.54)$$

where the smooth version of Dirac delta function in [36] is used. Here,  $C = 0.5$  is used for a bubble enclosed in a fluid while  $C = 1$  is used in the moving contact line problem.

3. Solve the Navier-Stokes equations. This can be done by the following second-order accurate projection method [2], where the nonlinear term is approximated by the Adams-Bashforth scheme and the viscous term is approximated by the Crank-Nicholson scheme. For convenience, we use a simple notation  $\psi|_{a[n-1]}^{b[n]}$  to represent  $b\psi^n - a\psi^{n-1}$ .

$$\nabla_h \cdot (\mu \nabla_h \mathbf{u}^*) - \frac{3Re}{2\Delta t} \mathbf{u}^* = Re \mathbf{H}^n \quad (4.55)$$

where

$$\begin{aligned} \mathbf{H}^n &= \frac{\mathbf{u}^{n-1} - 4\mathbf{u}^n}{2\Delta t} + ((\mathbf{u} \cdot \nabla_h) \mathbf{u})|_{[n-1]}^{2[n]} + \nabla_h p^n \\ &\quad - \frac{1}{Re} (\nabla_h \cdot (\mu \nabla_h \mathbf{u}^T))|_{[n-1]}^{2[n]} - \frac{1}{ReCa} \mathbf{f}|_{[n-1]}^{2[n]} \end{aligned} \quad (4.56)$$

**BCs for a shear flow:**

$$\begin{aligned} u^* &= ry, & \text{on } x = a \text{ and } x = b, \\ u^* &= rc, & \text{on } y = c, \\ u^* &= rd, & \text{on } y = d, \\ v^* &= 0, & \text{on } \partial\Omega \end{aligned} \quad (4.57)$$

**BCs for a moving contact line problem:**

$$\begin{aligned} u^* &= \beta \frac{\partial u^*}{\partial y}, \quad v^* = 0, & \text{on } y = c, \\ \mathbf{u}^* &= 0, & \text{otherwise} \end{aligned} \quad (4.58)$$

$$\nabla_h^2 \phi^{n+1} = \frac{\nabla_h \cdot \mathbf{u}^*}{2\Delta t/3}, \quad \frac{\partial \phi^{n+1}}{\partial n} = 0, \quad \text{on } \partial\Omega \quad (4.59)$$

$$\mathbf{u}^{n+1} = \mathbf{u}^* - \frac{2\Delta t}{3} \nabla_h \phi^{n+1}, \quad (4.60)$$

$$p^{n+1} = p^n + \phi^{n+1} - \frac{1}{Re} \nabla_h \cdot \mathbf{u}^*. \quad (4.61)$$

Here,  $\nabla_h$  is the standard centered difference operator on the staggered grid. One can see that the above Navier-Stokes solver involves solving two Helmholtz equations for velocity  $\mathbf{u}^* = (u^*, v^*)$  and one Poisson equation for pressure. These elliptic equations are solved by using the geometric multigrid solver.



4. Interpolate the new velocity on the fluid lattice points onto the marker points  $\mathbf{U}_k = (U_k, V_k)$  and move the marker points  $\mathbf{X}_k = (X_k, Y_k)$  to new positions.

$$\mathbf{U}_k^{n+1} = \sum_{\mathbf{x}} \mathbf{u}^{n+1} \delta_h(\mathbf{x} - \mathbf{X}_k^n) h^2 \quad k = 0, 1, \dots, M \quad (4.62)$$

$$\mathbf{X}_k^{n+1} = \mathbf{X}_k^n + \Delta t (\mathbf{U}_k^{n+1} + (U^A)_k^{n+1} \boldsymbol{\tau}_k^n), k = 1, \dots, M - 1 \quad (4.63)$$

$$X_k^{n+1} = X_k^n + \Delta t U_k^{n+1}, k = 0, M \quad (4.64)$$

where  $(U^A)_k^{n+1}$  is computed by a mid-point integration rule of Eq. (4.29). It is worth noting that at the positions of contact lines  $k = 0$  and  $k = M$ , we only update the  $x$  coordinates by the velocity along the solid wall, and keep their  $y$  coordinates fixed as  $Y_0^{n+1} = Y_M^{n+1} = c$ . This is consistent with the unbalanced Young forces which are applied only along the solid wall ( $x$  direction) as shown in Eqs. (4.52)-(4.53). As mentioned before, there is no artificial velocity applied at the moving contact lines; that is,  $(U^A)_0^{n+1} = (U^A)_M^{n+1} = 0$ .

5. Update surfactant concentration distribution  $\gamma_k^{n+1}$  by the numerical algorithm (4.37). Basically, we can rearrange (4.37) to a simpler form

$$\begin{aligned} & \left( \frac{1}{(S_\alpha)_{k+1}^{n+1}} \gamma_{k+\frac{3}{2}}^{n+1} - \left( \frac{1}{(S_\alpha)_{k+1}^{n+1}} + \frac{1}{(S_\alpha)_k^{n+1}} + \frac{\zeta(S_\alpha)_{k+\frac{1}{2}}^{n+1}}{\Delta t} \right) \gamma_{k+\frac{1}{2}}^{n+1} + \frac{1}{(S_\alpha)_k^{n+1}} \gamma_{k-\frac{1}{2}}^{n+1} \right) \\ &= \left( \frac{-1}{(S_\alpha)_{k+1}^n} \gamma_{k+\frac{3}{2}}^n + \left( \frac{1}{(S_\alpha)_{k+1}^n} + \frac{1}{(S_\alpha)_k^n} - \frac{\zeta(S_\alpha)_{k+\frac{1}{2}}^n}{\Delta t} \right) \gamma_{k+\frac{1}{2}}^n + \frac{-1}{(S_\alpha)_k^n} \gamma_{k-\frac{1}{2}}^n \right) \\ & \quad - \frac{\zeta}{2} \left( \frac{(u^A)_{k+1}^{n+1} \gamma_{k+1}^{n+1} - (u^A)_k^{n+1} \gamma_k^{n+1}}{\Delta \alpha} + \frac{(u^A)_{k+1}^n \gamma_{k+1}^n - (u^A)_k^n \gamma_k^n}{\Delta \alpha} \right) \end{aligned} \quad (4.65)$$

where  $\zeta = 2Pe_s \Delta \alpha^2$ ,  $(S_\alpha)_{k+\frac{1}{2}} \approx 0.5((S_\alpha)_k + (S_\alpha)_{k+1})$ , and  $\gamma_k \approx 0.5(\gamma_{k-\frac{1}{2}} + \gamma_{k+\frac{1}{2}})$ . Note that the unknown  $\gamma^{n+1}$  appears only on the left-hand side of the above equation, we simply have a linear system  $A\gamma = b$ . Since the essential data  $\mathbf{X}^{n+1}$  and  $(U^A)^{n+1}$  are obtained in previous steps, we can get  $S_\alpha^{n+1}$  involving to the tri-diagonal matrix  $A$  and the right-hand side of the system. The resultant symmetric tri-diagonal linear system can be solved easily by the Thomas algorithm.

# Chapter 5

## Numerical results

In this chapter, we first verify the convergence of our numerical schemes for the concerning problems, a bubble in a shear flow and a drop adheres to a solid substrate. If the surface tension is a constant, the motion of the interface is affected only by the curvature force in the normal direction (Capillary effect only), a corresponding benchmark will be shown after convergence test. When the interface is contaminated by surfactants, the surface tension can be altered and regarded as a function of surfactant which is derived by a linear or nonlinear Langmuir equation, therefore the maragoni effect appears. In the consequent, the effect of the surfactant for a bubble in a shear flow will be presented. Also, several moving contact line phenomena which are derived by the unbalanced Young's forces will attract one's attention. Finally, we consider a two-phase flow with different fluid properties (both of the viscosity and density are piecewise constant functions). In this run, not only the surface tension evolve the interface but an external force (gravity) will affect the evolution of entire fluid field.

### 5.1 Convergent test

#### 5.1.1 For a bubble in a shear flow

First of all, we carry out the parameter setting in the convergence study of the present method. Here, we perform different computations with varying Cartesian meshes  $h = \Delta x = \Delta y = 0.04, 0.02, 0.01, 0.005$ . The Lagrangian mesh is chosen as  $\Delta s \approx h/2$  and the time step size is  $\Delta t = h/8$ . The solutions are computed up to time  $T = 1$ .

Since the analytical solution is not available in these simulations, we choose the results obtained from the finest mesh as our reference solution

and compute the  $L_2$  error between the reference solution and the solution obtained from the coarser grid. Table 5.2 shows the mesh refinement analysis of the velocity  $u$ ,  $v$ , and the surfactant concentration  $\gamma$ . One can see that

$h$	$\ u - u_{ref}\ _2$	rate	$\ v - v_{ref}\ _2$	rate	$\ \gamma - \gamma_{ref}\ _2$	rate
0.04	4.9739E-03	-	4.1656E-03	-	1.4551E-02	-
0.02	2.1476E-03	1.21	1.8169E-03	1.20	6.3542E-03	1.20
0.01	6.9859E-04	1.62	6.2180E-04	1.55	2.2329E-03	1.51

Table 5.1: The mesh refinement analysis of the velocity  $u$ ,  $v$ , and the surfactant concentration  $\gamma$ .

the error decreases substantially when the mesh is refined, and the rate of convergence is about 1.5. Notice that, the fluid variables are defined at the staggered grid and the surfactant concentration is defined at "half-integer" indices of the grid, so when we refine the mesh, the numerical solutions will not coincide with the same grid locations. In these runs, we simply use a linear interpolation to compute the solutions at the desired locations. We attribute this is part of the reason why the rate of convergence behaves less than second-order. However, we believe that the key factor reducing the rate of convergence comes from using the discrete delta function, a function with compact support and only  $C^1$  smoothness.

### 5.1.2 For the moving contact line problem

Since the motion of the interface in the moving contact line problem involves not only fluid-fluid surface tension but surface tension between fluid and solid near the contact line points. There are additional treatments in the numerical processes, that is why we have two verifications for the convergence of the numerical schemes.

We consider a computational domain  $\Omega = [-1, 1] \times [0, 1]$  where a half of circular drop with radius 0.5 is initially attached on the bottom of the domain, and both left and right contact angles are  $\pi/2$  initially. The initial fluid velocity are all set to be zero. The surface tension is affected by the surfactants following the equation of state given by Eq. (2.38), here,  $\sigma_c = 1$  and  $\eta = 0.3$ . Other parameters are initial surfactant concentration  $\gamma(\alpha, 0) = 1$ , the Reynolds number  $Re = 10$ , the capillary number  $Ca = 0.1$ , the surface Peclet number  $Pe_s = 20$ , and the slip length  $\beta = h/4$ , where  $h$  is the mesh width. Here, we perform four different computations with varying Cartesian mesh  $h = \Delta x = \Delta y = 1/32, 1/64, 1/128, 1/256$ . The Lagrangian mesh

h	$\ u - u_{ref}\ _2$	rate	$\ v - v_{ref}\ _2$	rate	$\ \gamma - \gamma_{ref}\ _2$	rate
1/16	5.8079e-03	-	3.3148e-03	-	3.1818e-02	-
1/32	2.9639e-03	0.97	1.9179e-03	0.79	1.7977e-02	0.82
1/64	1.4773e-03	1.00	1.0805e-03	0.82	9.8698e-03	0.86
1/128	5.9179e-04	1.32	4.6628e-04	1.21	4.2087e-03	1.23

Table 5.2: The mesh refinement analysis of the velocity  $u$ ,  $v$ , and the surfactant concentration  $\gamma$ .

h	$\ \mathbf{X} - \mathbf{X}_{ref}\ _\infty$	rate	$ \cos(\theta) - \cos(\theta_{ref}) $	rate	$ A - A_{ref} /A_{ref}$	rate
1/16	4.7646e-02	-	1.0285e-01	-	1.1476e-01	-
1/32	2.4225e-02	0.98	6.3948e-02	0.69	5.6724e-02	1.02
1/64	1.1426e-02	1.08	3.6915e-02	0.79	2.7473e-02	1.05
1/128	4.1700e-03	1.45	2.1708e-02	0.77	1.3145e-02	1.05

Table 5.3: The mesh refinement analysis of interface positions, the contact angles, and the area of drop.

is chosen as  $\Delta\alpha \approx h$  and the time mesh size is  $\Delta t = h/10$ . The solutions are computed up to time  $T = 6.25$ . Again, the analytical solution is not available in these simulations, we choose the results obtained from the finest mesh as our reference solution and compute the  $L_2$  error between the reference solution and the solution obtained from the coarser grid. Table 5.2 shows the mesh refinement analysis of the velocity  $u$ ,  $v$ , and the surfactant concentration  $\gamma$ . One can see that the error decreases substantially when the mesh is refined, and the rate of convergence is about first-order. Notice that, the fluid variables are defined at the staggered grid and the surfactant concentration is defined at "half-integer" indices of grid, so when we refine the mesh, the numerical solutions will not coincide with the same grid locations. In these runs, we simply use a linear interpolation to compute the solutions at the desired locations. Table 5.3 shows the  $L_\infty$  errors of the interface positions, the cosine value of the contact angles, and the area loss of the drop for different meshes. One can see the rate of convergence is about first-order which is consistent with the results shown in Table 5.2.

During the drop deformation, the Lagrangian markers will gradually sweep into contact lines and cause clustered distribution near those points. Fig. 5.1 shows the comparison of the local stretching factor  $|\mathbf{X}_\alpha| = S_\alpha$  at  $T = 6.25$  with (solid line) or without (dashed line) the implementation of

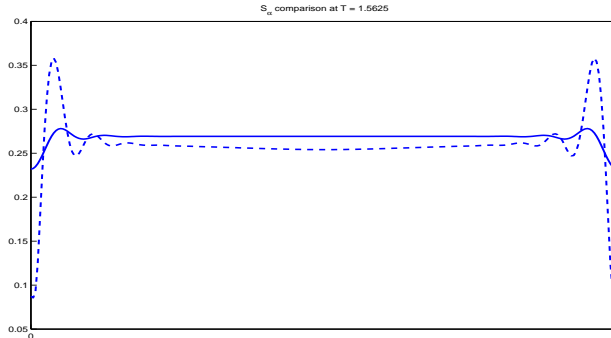


Figure 5.1: Comparison of stretching factor  $|\mathbf{X}_\alpha|$  with ( $U^A = 0$ , dashed line) and ( $U^A \neq 0$ , solid line), where  $h = 1/128$ .

equi-distributed technique of Lagrangian markers. Here, we only show the case with surfactant  $\eta = 0.3$ . One can see this technique does preserve the markers more uniformly.

In addition, it is well-known that the fluid leakage often appears in the simulation of immersed boundary method. In [37], Peskin and Printz proposed an improved volume (area in 2D) conservation scheme for the immersed boundary method by constructing a discrete divergence operator based on the interpolation scheme. Here, however, the area loss is not that significant, thus no modification is applied. One should mention that with the implementation of present dynamical control of Lagrangian markers, one can reduce the area loss significantly than without implementing it.

## 5.2 Capillary and Maragoni effect

In this section, we aim to numerically verify the concept of Capillary and Maragoni effects in the evolution of a bubble immersed in a fluid. First of all, we consider a benchmark which is an ellipse generated only by Capillary forces ( $\sigma$  is independent of surfactants) in a quiescent flow. The basic setups in this experiment are the computational domain  $\Omega = [-1.28, 1.28] \times [-0.64, 0.64]$ , aspect ratio of the initial configuration 2 : 1, the surface tension  $\sigma = 1$ , the mesh size  $h = 1/128$ , and the mesh of time is  $t = h/10$ . About the fluid properties, we choose  $\mu_1 = \mu_2 = 0.1$  and  $\rho_1 = \rho_2 = 1$  so that Reynolds number  $Re = 10$  and Capillary number  $Ca = 0.1$ .

Since curvatures are bigger at the tips of the bubble, the magnitude of

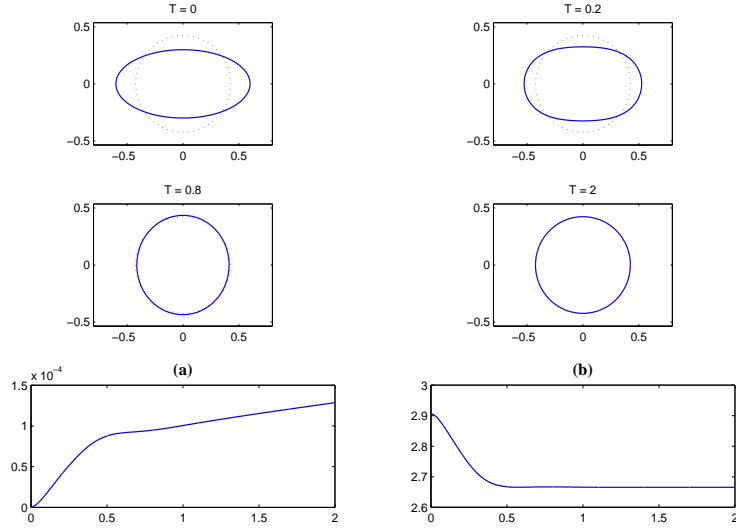


Figure 5.2: The time evolution of a bubble in a quiescent flow. The dash-line is the configuration of the steady state which is a circle with  $r_e = 0.4243$ . (a) Relative error of area loss. (b) Total length of the bubble.

forces at the tips are greater than ones close to the bottom and top zones. As expected, the ellipse will shrink gradually to a circle. Fig. 5.2 shows the evolution of an elliptical bubble and the corresponding area loss and total length of the bubble. Moreover, we can verify how accurate of this simulation by considering the incompressibility of the bubble. If the area inside the bubble is preserved well, then the radius  $r_e$  of the steady state, a circle, can be obtained by taking the square root of the area over  $\pi$ . In Fig. 5.2(a), we observe that the relative error of the area enclosed the bubble is within 0.015% and the area of the initial configuration is 0.5655 so that  $r_e = \sqrt{0.5665/\pi} = 0.4243$ . The evolution of the total length of the bubble reaches an equilibrium 2.6655 which matches well to the corresponding perimeter of the steady state  $2\pi r_e = 2.6657$ , see Fig. 5.2(b).

Base on the same setting above except to replace the initial configuration of a circle with radius 0.35, we add nonuniform distribution of surfactant concentration to the interface as follows.

$$\gamma(\alpha, 0) = 0.8 (1.1 - \tanh(2(\alpha - 0.5\pi)(\alpha - \pi))), \quad \alpha \in [0, 2\pi], \quad (5.1)$$

$$\gamma(\alpha, 0) = 0.8 (1.1 - \tanh(2(\alpha - \pi)(\alpha - 1.5\pi))), \quad \alpha \in [0, 2\pi], \quad (5.2)$$

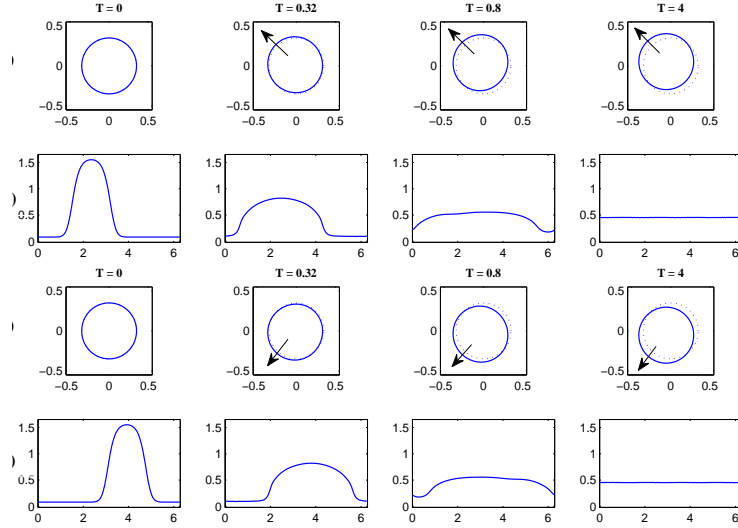


Figure 5.3: (a) A bubble with bulk surfactant in the second quadrant moves to the left-top corner of the box. (b) The corresponding evolution of surfactant concentration of (a). (c) A bubble with bulk surfactant in the third quadrant moves to the left-bottom corner of the box. (d) The corresponding evolution of surfactant concentration of (c).

that one has bulk surfactant in  $\alpha \in [0.5\pi, \pi]$ , and the other concentrates in  $\alpha \in [\pi, 1.5\pi]$ . In the former case, surfactants initially aggregate in the second quadrant, see the first figure in Fig. 5.3(b), and reduce more surface tension, the surface tension along the other quadrant gives more contribution to the bubble in the beginning and the bubble moves toward the left-top direction, see Fig. 5.3(a). Later, surfactants diffuse to the area with lower concentration to produce a uniform distribution of surfactant, and the surface tension becomes almost constant along the interface so that the bubble stops moving, see Fig. 5.3 (a) and (b). Similarly, the bubble moves to the left-bottom corner of the box when the surfactant initially bulk in the third quadrant, the corresponding evolutions of the bubble motion and the distribution of the surfactant are shown in Fig 5.3 (c) and (d), respectively. Note that the leakage of the area in both case is less than 0.01% probably due to the invariant of the shape, and the total mass of the surfactant is preserved numerically (up to machine accuracy).

## 5.3 Deformation of a bubble in a shear flow

The effect of surfactant on the deformation of a drop is of considerable interest in polymer and emulsion industries. It is also a good theoretical model for illustrating subtle physics in viscous interfacial flow. In this section, the immersed boundary method is applied to study the effect of surfactant on the deformation of a bubble in Navier-Stokes flows.

Following the set up in [56], we consider a computational domain  $\Omega = [-5, 5] \times [-2, 2]$  where a circular bubble of radius one is initially located at the center of the domain. We apply a steady shear flow to the bubble; that is, we set the boundary condition  $\mathbf{u}_b = (0.5y, 0)$ , for  $-2 \leq y \leq 2$ . For comparison purposes, both clean (without surfactant) and contaminated (with surfactant) bubbles are used in these computations. Using the equation of state given by Eq. (2.37),  $\eta = 0$  implies no contamination, in which case we do not need to solve the surfactant equation (2.36). Throughout this section, we set  $\sigma_c = 1$  so the clean interface has a uniform surface tension  $\sigma = \sigma_c$ . For the contaminated case, the initial surfactant concentration is uniformly distributed along the interface such that  $\gamma(\alpha, 0) = 1$ . Unless otherwise, we set the Reynolds number  $Re = 10$ , the capillary number  $Ca = 0.5$ , the surface Peclet number  $Pe_s = 10$ , and the parameter  $\eta = 0.25$ .

### 5.3.1 Clean vs. contaminated interface

To examine the effect of the surfactant on interfacial dynamics, we compare a bubble with and without surfactant in a steady shear flow. When the surfactant are present in the interface, the surface tension can be reduced significantly, cf. equation of state (2.37). Throughout the rest of this section, we use a uniform Cartesian mesh  $h = \Delta x = \Delta y = 0.02$ , and a Lagrangian grid with size  $\Delta s \approx h/2$ . The mesh size of time is set to be  $\Delta t = h/8$ .

Fig. 5.14 shows the time evolution plots of deformation of the bubble in a steady shear flow field. Here, we consider three different values of  $\eta$  in Eq. (2.37); namely,  $\eta = 0$  (dotted, clean interface),  $\eta = 0.25$  (dash-dotted), and  $\eta = 0.5$  (solid). As expected, the magnitude of deformation of the bubble increases when the value of  $\eta$  increases, as in the case of Stokes flow [56]. Fig. 5.5 shows the vorticity plot for the bubble with surfactant near the left and the right tips. One can see that two vortices with positive and negative signs are generated near the tips of the bubble.

During the deformation of the bubble, the Lagrangian markers will gradually sweep into the tips and cause clustered distribution near the tips. If the



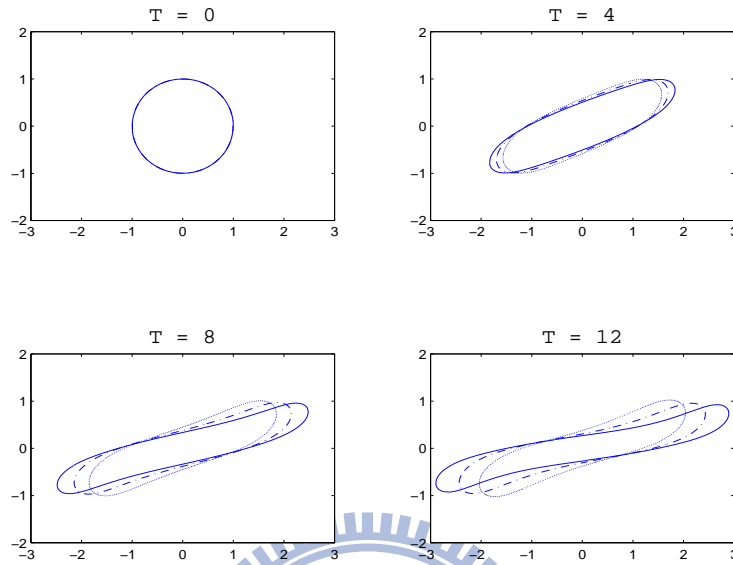


Figure 5.4: The time evolution of a drop in a shear flow with clean ( $\eta = 0$ , '-') and contaminated interface ( $\eta = 0.25$ , '-.',  $\eta = 0.5$ , '-').

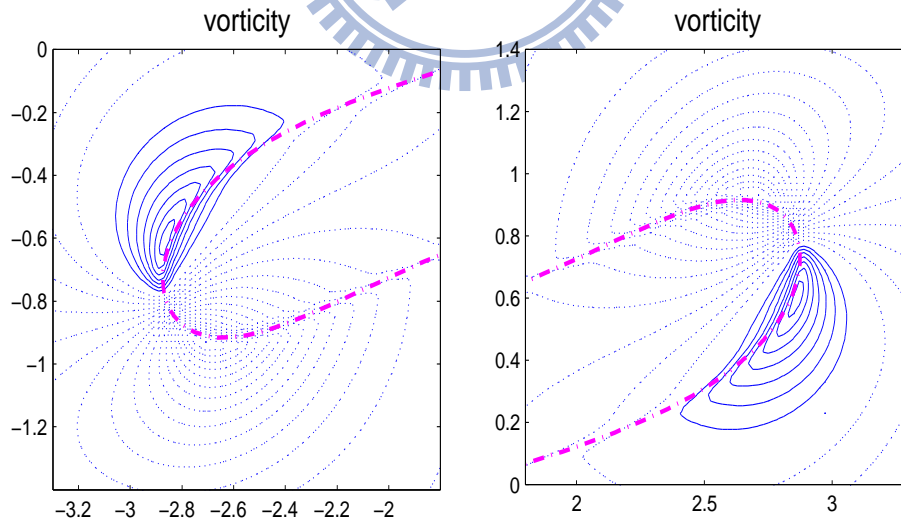


Figure 5.5: The vorticity plot for the drop with surfactant near the left and right tips ( $\eta = 0.5, T = 12$ ).

markers become too crowdedly or too coarsely distributed, it will affect the numerical accuracy. Thus, in order to maintain the numerical stability and accuracy, we need to apply the equi-distributed technique we performed in previous chapter, moreover, if necessary, we will double the number of grid when the bubble is over stretched. The detail is given as follows.

In each time step, we first apply the equi-distributed technique to get an artificial velocity and compute the resultant distance between two adjacent markers. If the distance is less than  $0.75h$ , then we basically keep the original resolution. However, if the distance is greater than  $0.75h$ , then we double the number of the grid. (Should be clarified. One important thing during the grid redistribution process is to keep the mass conservation of the surfactant. This can be done in a local way. For instance, in the segment of adding more grid points, we simply distribute the surfactant mass into those points uniformly. On the other hand, in the segment of removing grid points, we add up those surfactant mass to be a new surfactant concentration in the new combining segment. Thus, the overall surfactant mass is conserved exactly without any scaling.)

Plots of the corresponding surfactant concentration (left column) and surface tension (right column) versus arc-length are given in Fig. 5.16. For the surfactant concentration plot, we omit the case of clean interface since the concentration is zero everywhere on the interface. It can be seen from this figure, the bubble is elongated by the shear flow so that the total length of the interface is increased from the rest state. Since there is no surfactant transferred between the interface and the fluid, the surfactant concentration is diluted on a portion of the interface, partly due to the elongation of the interface, but mainly because it is swept to the tips of the bubble. As a result, the smallest surface tension occurs at the tips. One can also see that the value of  $\eta$  affects the surfactant concentration by shifting the distributions slightly along the length of the bubble. Once again, we confirm the same qualitative behavior as in [56].

In Fig. 5.7, the corresponding capillary (defined as  $\sigma\kappa|\frac{\partial\mathbf{X}}{\partial\alpha}|/(ReCa)$ , left column) and the Marangoni forces (defined as  $\frac{\partial\sigma}{\partial\alpha}/(ReCa)$ , right column) are plotted versus the arc-length for different cases of  $\eta$ . Since the capillary force depends on the curvature and surface tension, we see that the largest capillary force occurs at the tips of the bubble due to the high curvature there. For clean interface, the Marangoni force is obviously zero.

In Fig. 5.17, we present four different plots; namely, (a) total mass of the surfactant, (b) the error of total mass,  $m(t) - m(0)$ , (c) total area of

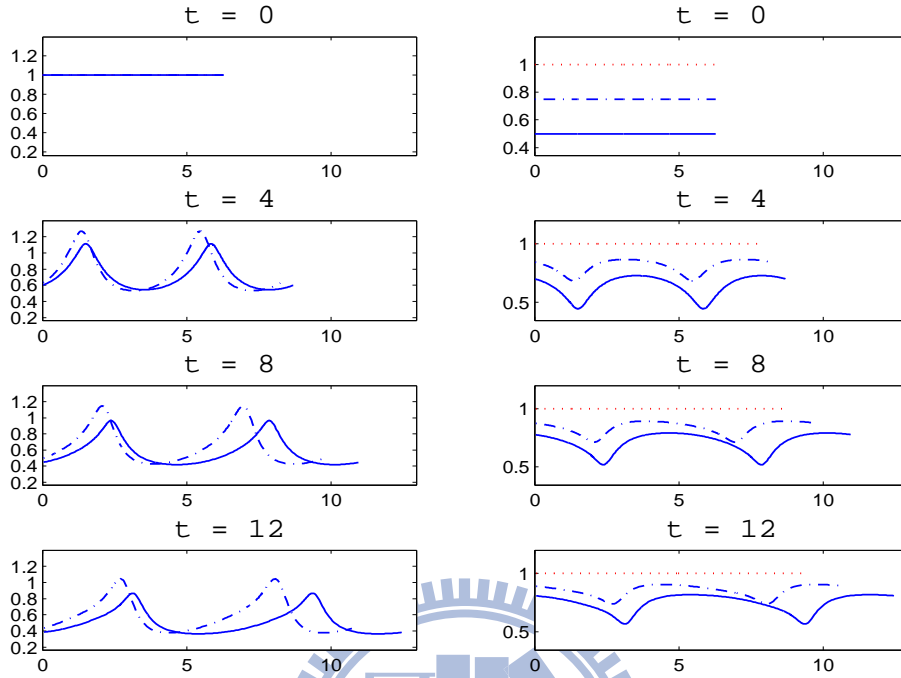


Figure 5.6: Distributions of the surfactant concentration (left) and the corresponding surface tension (right). Notations and parameters are same as in Fig. 5.14.

the bubble, (d) total length of the interface. Clearly, the present method preserves the total surfactant mass and the errors reach machine precision. However, there is a slight area losing or fluid leakage inside the bubble as shown in Fig. 5.17(c). It seems that the bubble without surfactant has a more serious leakage than the ones with surfactant. Here, the area loss is not that significant, thus no modification is applied. Once again, we can see from Fig. 5.17(d) that the bubble with surfactant has larger deformation than the one without surfactant due to the increase of total length of the interface.

### 5.3.2 Linear vs. nonlinear equation of state

In this test, we use the same set up as in the previous one except that a simplified form of nonlinear Langmuir equation of state  $\sigma(\gamma) = \sigma_c (1 + \ln(1 - \eta\gamma))$  is used and compared with the results of the linear equation of the state. In Fig. 5.9, the evolution of the bubble under steady shear flow is shown at different times using the linear (dotted) and nonlinear (solid) equations of state with  $\eta = 0.5$ . Once again, our results are consistent with those in [56],

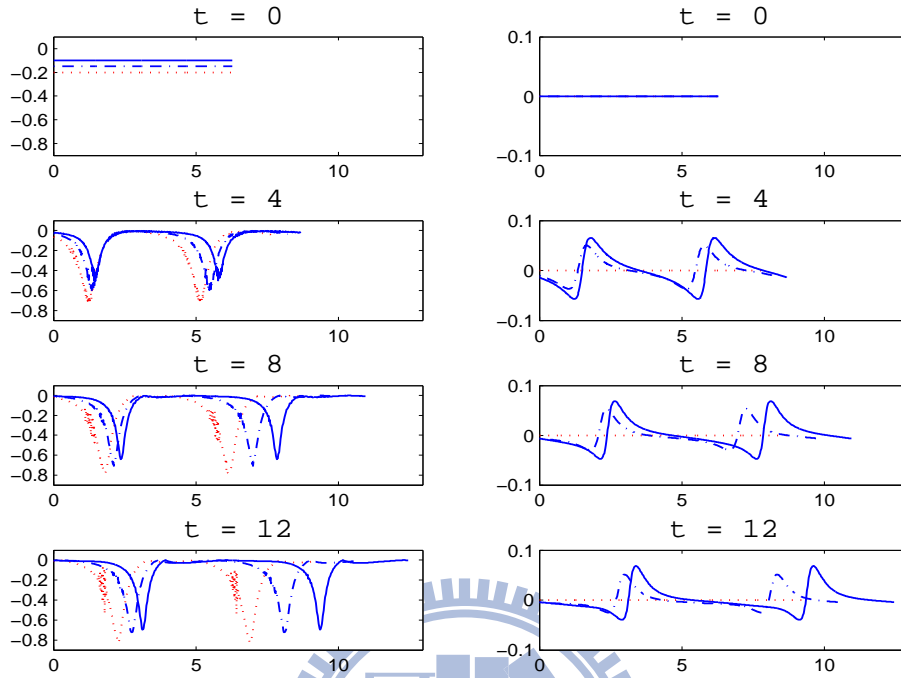


Figure 5.7: The corresponding capillary force (left) and Marangoni force (right). Notations and parameters are same as in Fig. 5.14.

i.e., deformation of the bubble increases when the nonlinear equation of state is used. The corresponding surfactant concentrations and surface tensions are shown in Fig. 5.10. One can easily see that the nonlinear equation of state generates smaller surface tension at tips of the bubble which leads to a larger deformation. As shown in Fig. 5.11, the capillary forces are roughly similar but the Marangoni force for the nonlinear case is slightly larger at tips of the bubble. The four different plots for both linear and nonlinear cases including the total mass of the surfactant, the error of total mass, the total area of the bubble, and the total length of the bubble are shown in Fig. 5.12.

### 5.3.3 Effect of capillary number on drop deformation

As the last test, we perform the study on how different capillary numbers affect the deformation of the bubble. Here, we fix the Reynolds number  $Re = 10$  and the surface Peclet number  $Pe_s = 10$ . We vary the capillary number as  $Ca = 0.05, 0.25, 0.5, 1.0$  and perform our runs up to time  $T = 4$ . As confirmed in previous literature such as [30], a larger capillary number means a smaller surface tension (with the viscosity fixed) so the bubble un-

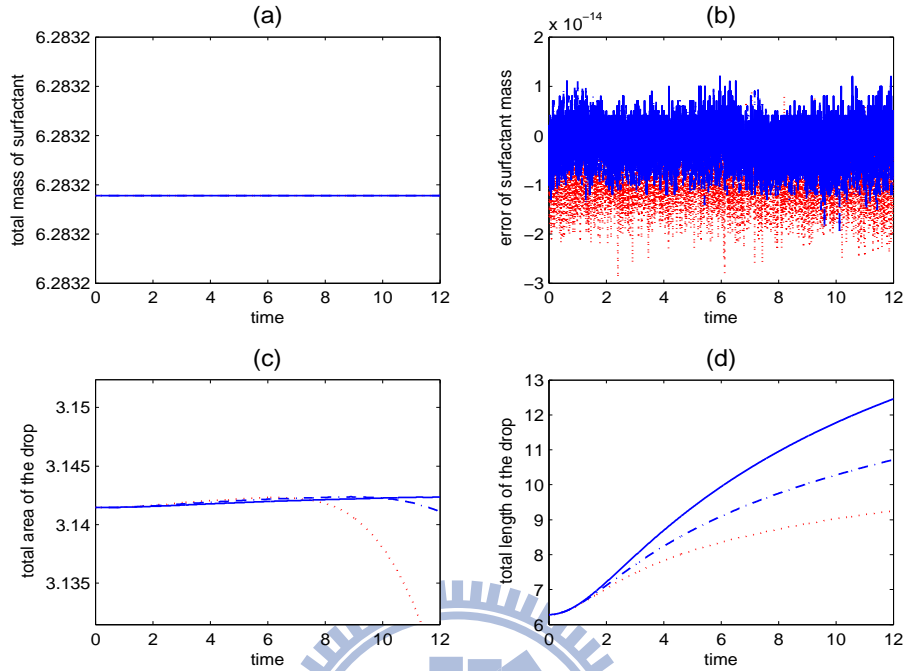


Figure 5.8: (a) Total mass of the surfactant. (b) Time plot of  $m(t) - m(0)$ . (c) Total area of the bubble. (d) Total length of the interface. Notations and parameters are same as in Fig. 5.14.

der shear flow can deform more substantially. This is exactly what we see in our simulations as illustrated in Fig. 5.13. We also make runs by varying the different surface Peclet number while keeping the Reynolds and capillary numbers fixed. However, the effect of surface Peclet number is not as significant as the effect of the capillary number on the deformation of the bubble, so we omit the results here.

## 5.4 A drop adheres to a solid surface

In this section, we perform several numerical experiments to test our scheme described in previous chapter. We consider a computational domain  $\Omega = [-1, 1] \times [0, 1]$  where a half of circular drop with radius 0.5 is initially attached on the bottom of the domain, and both left and right contact angles are  $\pi/2$  initially. The initial fluid velocity are all set to be zero. We like to see how the surfactant affects the motion of the interface so both clean (without surfactant) and contaminated (with surfactant) drops are used in these

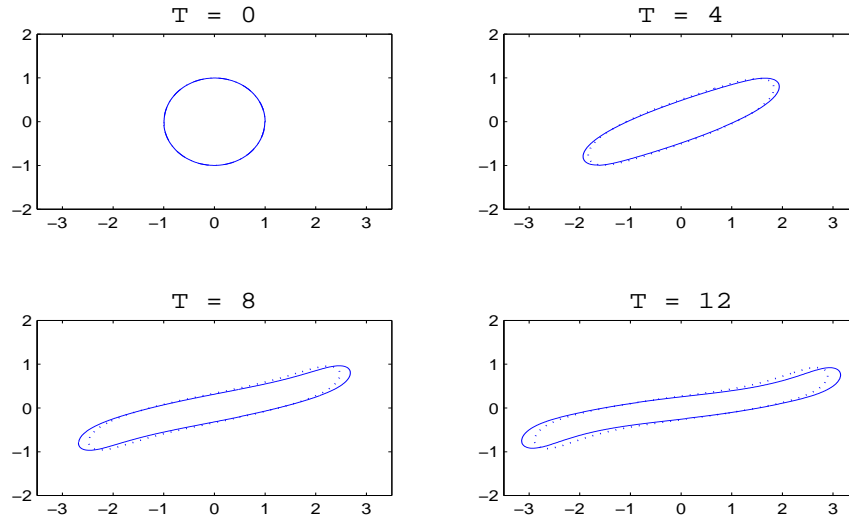


Figure 5.9: The time evolution of a bubble under a shear flow with linear (‘.’) and nonlinear (‘-’) equation of state.

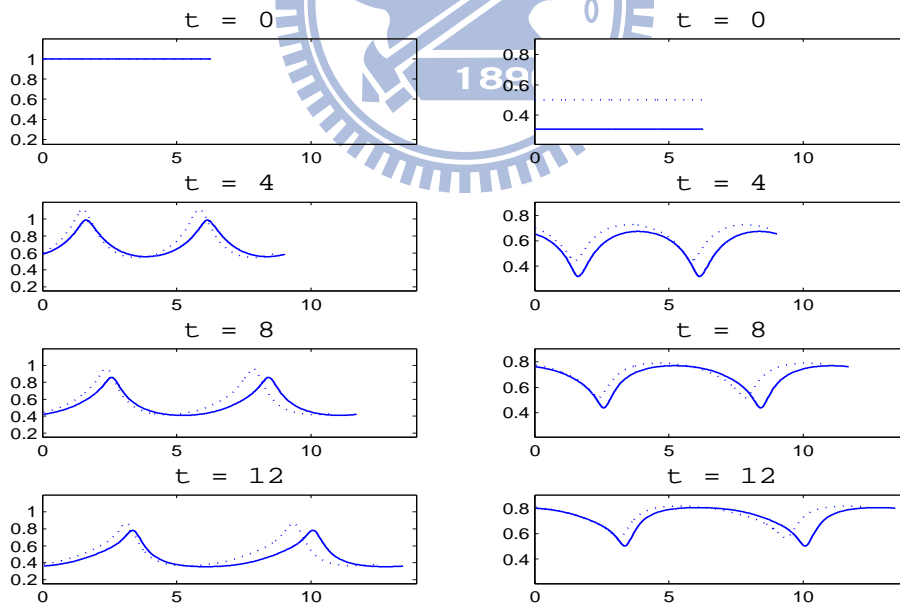


Figure 5.10: Distributions of the surfactant concentration (left) and the corresponding surface tension (right). Notations and parameters are same as in Fig. 5.9.

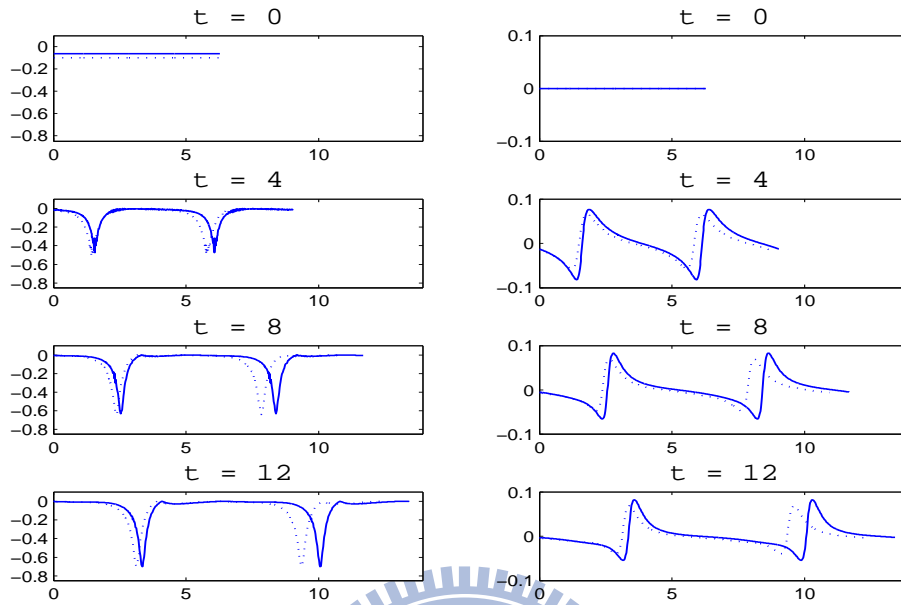


Figure 5.11: The corresponding capillary force (left) and Marangoni force (right). Notations and parameters are same as in Fig. 5.9.

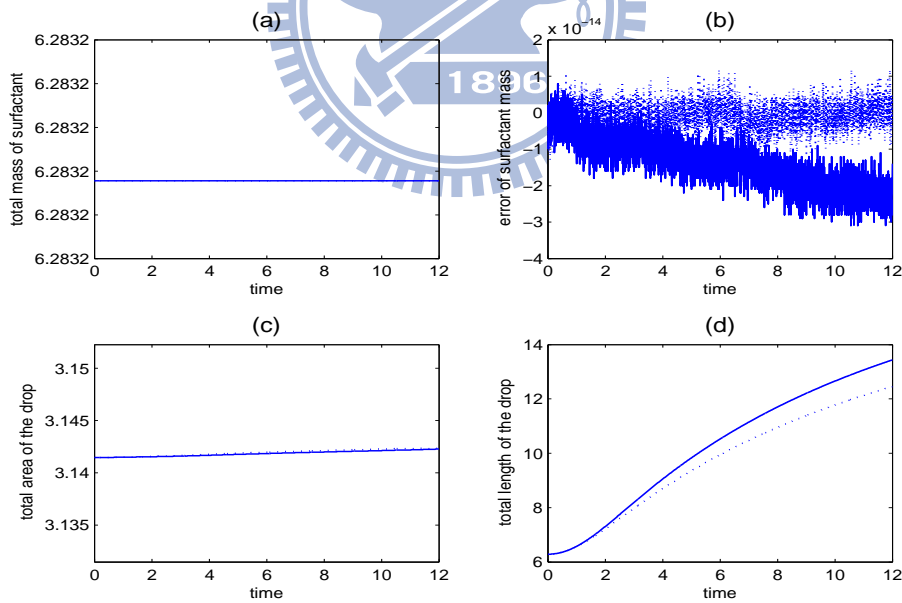


Figure 5.12: (a) Total mass of the surfactant. (b) Time plot of  $m(t) - m(0)$ . (c) Total area of the bubble. (d) Total length of the interface. Notations and parameters are same as in Fig. 5.9.

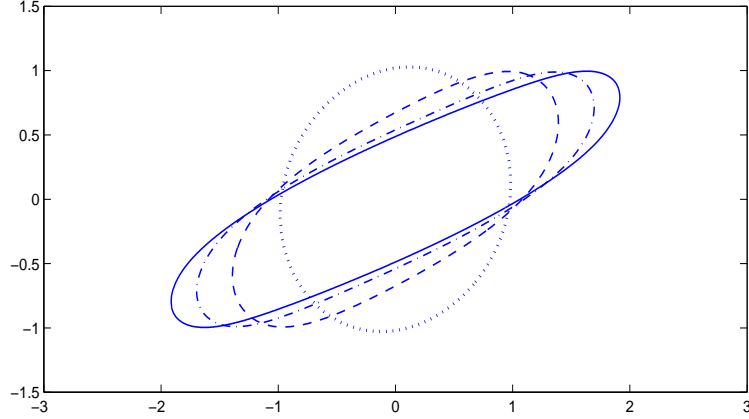


Figure 5.13: The effect of capillary number  $Ca$  on the deformation of the bubble. ( $Ca = 0.05$  : '·',  $Ca = 0.25$ : '- ·',  $Ca = 0.5$ : '- · ·',  $Ca = 1.0$ : '-')

computations. Using the equation of state given by Eq. (2.38),  $\eta = 0$  implies no surfactant, in which case we do not need to solve the surfactant equation (4.35). Throughout this section, we set  $\sigma_c = 1$  so the clean interface has a uniform surface tension  $\sigma = \sigma_c$ . For the contaminated case, the initial surfactant concentration is uniformly distributed along the interface such that  $\gamma(\alpha, 0) = 1$ . Unless otherwise, we set the Reynolds number  $Re = 10$ , the capillary number  $Ca = 0.1$ , the surface Peclet number  $Pe_s = 20$ . The slip length used in Navier-slip boundary condition is chosen as  $\beta = h/4$ , where  $h$  is the mesh width.

### 5.4.1 Hydrophilic case

To examine the effect of the surfactant on interfacial dynamics, we compare a hydrophilic drop with and without surfactant in a quiescent flow. When the surfactant are present in the interface, the surface tension can be reduced significantly, cf. equation of state (2.38). In this case, we choose  $\sigma_{s2} = 1$ ,  $\sigma_{s1} = 0.5$  so that the equilibrium contact angle is  $\theta_e = \pi/3$  for the clean interface. Here, we choose a uniform Cartesian mesh  $h = \Delta x = \Delta y = 1/128$ ,



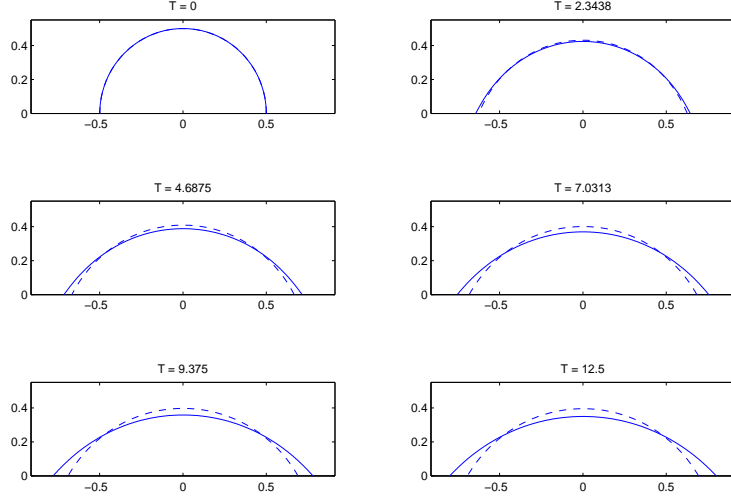


Figure 5.14: The time evolution of a hydrophilic drop with clean ( $\eta = 0$ , dashed line) and contaminated interface ( $\eta = 0.3$ , solid line).

and a Lagrangian grid with size  $\Delta\alpha \approx h$ . The mesh size of time is set to be  $\Delta t = h/10$ .

Fig. 5.14 shows the time evolution plots of a hydrophilic drop in a quiescent flow field. Here, we distinguish the clean ( $\eta = 0$ ) and contaminated ( $\eta = 0.3$ ) drop interfaces by the "dashed" and "solid" lines, respectively. As expected, both drops will start wetting on the solid substrate. The clean drop moves gradually to a state with the contact angle approaching to equilibrium  $\theta \approx \pi/3$ , while the contaminated one wets further than the clean one to reach a state with  $\theta \approx \pi/4$ . This drop behavior can be easily explained by Eq. (2.28). The surfactant is insoluble and affects only the surface tension between liquid phase 1 and liquid phase 2. Therefore, both  $\sigma_{s2}$  and  $\sigma_{s1}$  remain the same and so is their difference, but the surface tension  $\sigma$  at the right and left contact lines are always smaller than  $\sigma_c$ . As a result, the dynamic contact angle  $\theta$  becomes a function of  $t$  as  $\theta(t) = \arccos((\sigma_{s2} - \sigma_{s1})/\sigma) \leq \pi/3$ . Thus, the contaminated drop becomes more wetting than the clean one. It is also interesting to mention that the larger value of  $\eta$ , the more wetting of the drop since the surface tension  $\sigma$  decreases more.

Fig. 5.15 shows the velocity plots for the drop with surfactant near the

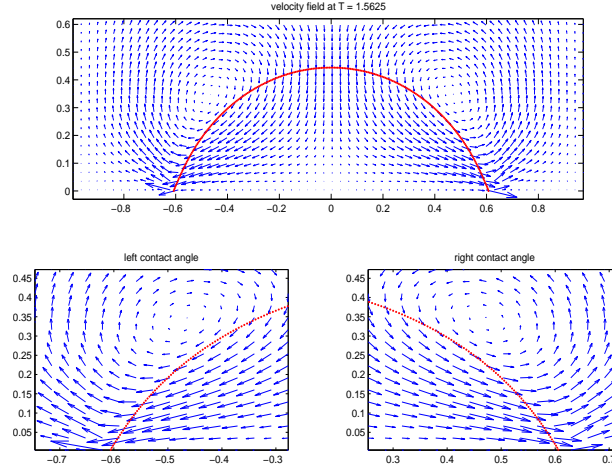


Figure 5.15: The velocity field for the drop with surfactant near the left and right contact lines ( $\eta = 0.3$ ,  $T = 1.5625$ ).

left and the right contact lines at time  $T = 1.5625$ . One can see significant contact line velocity pointing outward to the dry region (fluid 2) has been observed during the wetting process.

Plots of the corresponding surfactant concentration (top column) and surface tension (bottom column) versus arc-length for the contaminated case are given in Fig. 5.16. It can be observed although the initial surfactant is uniformly distributed, the later concentration at the contact lines are higher than other places of the interface. This is because during the wetting process, the surfactant are swept into the contact lines. As a result, the smallest surface tension occurs near the contact points. However, the distribution of the surfactant concentration will finally reach a uniform distribution again due to the diffusion process. The present method preserves the total surfactant mass exactly and the error reaches the machine precision, i.e.  $|m(t) - m(0)| \approx 10^{-14}$ .

In Fig. 5.17, we present four different time evolutionary plots; namely, (a) left contact line speed; (b) right contact line speed; (c) the contact angles; and (d) the total length of the drop. Fig. 5.17-(a) and (b) show the evolution of left and right contact line speed, respectively. Since the initial contact angle deviates the equilibrium angle more, the unbalanced Young force is larger in the beginning and so is the contact line speed. However, as

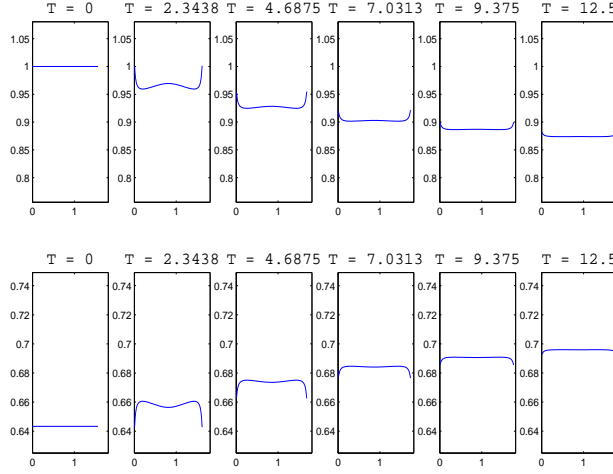


Figure 5.16: Distribution of the surfactant concentration (top) and the corresponding surface tension (bottom).

time evolves, the contact line speed is slowing down and tends to zero when the drop reaches its steady state. The corresponding evolution of contact angle is shown in Fig. 5.17-(c). In fact, evolutions of the left and right contact angles in the corresponding run are almost the same due to the symmetry of the drop and the same setting of equilibrium of both contact angles. The final dynamic contact angle of the clean drop approaches to  $\pi/3$  as expected, while the contaminated one approaches to  $\pi/4$ . Fig. 5.17-(d) shows that the drop with surfactant wets more than the one without surfactant due to the increase of total length of the interface.

## 5.4.2 Hydrophobic case

In this case, we keep almost the same setup as previous example but change the surface tensions to  $\sigma_{s2} = 0.1557$  and  $\sigma_{s1} = 1$  so that the equilibrium contact angle for a clean interface is  $\theta_e = 0.82\pi$  which corresponds to a hydrophobic drop.

Fig. 5.18 shows the time evolution plots of a hydrophobic drop in a quiescent flow field. Again, we distinguish the clean ( $\eta = 0$ ) and contaminated ( $\eta = 0.3$ ) drop interfaces by the "dashed" and "solid" lines, respectively. In this case, both drops start to contact. From Eq. (2.28), the dynamic contact angle  $\theta$  evolves following  $\theta(t) = \arccos((\sigma_{s2} - \sigma_{s1})/\sigma) \geq 0.82\pi$  so

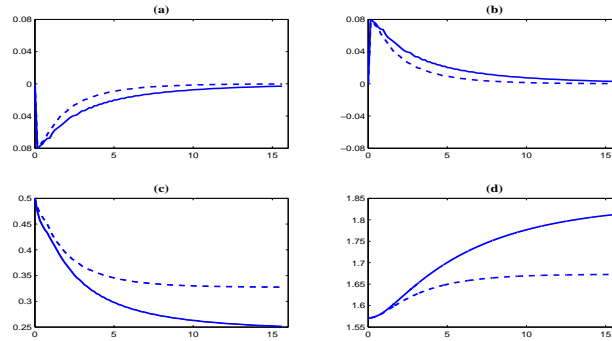


Figure 5.17: (a) Left contact line speed of the drop. (b) Right contact line speed of the drop. (c) Contact angle of the drop. (d) Total length of the drop. Notations and parameters are same as in Fig. 5.14.

the contaminated drop becomes more hydrophobic due to the reduction of surface tension. Thus, while the clean drop moves gradually to approach to a state with equilibrium contact angle, the contaminated one goes further to become a nearly non-wetting state. Once again, the larger value of  $\eta$ , the more hydrophobic the drop becomes as the surface tension  $\sigma$  is reduced by contamination.

Fig. 5.19 shows the plots for the drop with surfactant near the left and the right contact lines at time  $T = 2.3438$ . Significant contact line velocity pointing inward to the wet region (fluid 1) has been observed during the non-wetting process. Plots of the corresponding surfactant concentration and surface tension are similar to the hydrophilic case and omitted here.

In Fig. 5.20, we present time evolutionary plots for the comparison of clean and contaminated hydrophobic drops; namely, (a) left contact line speed; (b) right contact line speed; (c) the contact angles in units of  $\pi$ ; and (d) the total length of the drop. Fig. 5.20-(a) and (b) show the evolution of left and right contact line speed, respectively. As in the hydrophilic case, the initial contact angle deviates the equilibrium angle more, the unbalanced Youngs force is larger in the very beginning and so is the contact line speed. Now, this is a hydrophobic case so the contact line speed for left angle is positive while the right one is negative. Furthermore, the magnitude of contact line speed for the contaminated drop is larger than the clean one since the contaminated drop becomes more non-wetting. As time evolves, the contact lines slow down and approach to zero when the drop reaches its steady state.

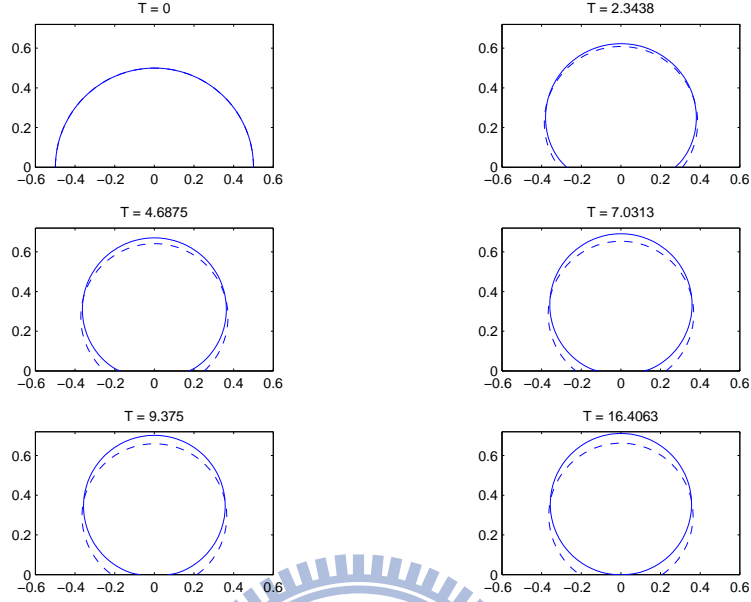


Figure 5.18: The time evolution of a hydrophobic drop with clean ( $\eta = 0$ , dashed line) and contaminated interface ( $\eta = 0.3$ , solid line).

The corresponding evolutions for left and right contact angles in units of  $\pi$  are shown in Fig. 5.20-(c). The final dynamic contact angle of the clean drop approaches to  $0.82\pi$  as expected, while the contaminated one approaches to  $\pi$ .

### 5.4.3 Hydrophobic-hydrophilic case

Now, we consider a substrate that has different wettability by defining  $\sigma_{s2}(x)$ ,  $x \in [-1, 1]$  as

$$\sigma_{s2}(x) = \begin{cases} 0.191, & \text{Hydrophobic} & x \in I_1 = [-1, -0.65] \\ 5.59(x + 0.65) + 0.191, & & x \in I_2 = (-0.65, -0.45) \\ 1.309, & \text{Hydrophilic} & x \in I_3 = [-0.45, 1]. \end{cases}$$

We simply choose  $\sigma_{s1} = 1$  so that the static contact angles (clean interface) for  $\sigma_{s2} = 0.191$  and  $1.309$  are  $\theta_e = 4\pi/5$  and  $2\pi/5$ , respectively. Roughly speaking, this set up mimics the situation that the solid surface has a combining hydrophobic (zone  $I_1$ ) and hydrophilic (zone  $I_3$ ) feature. Initially, we put a half circular drop with radius  $0.5$  and centered at  $(-0.25, 0)$  in the

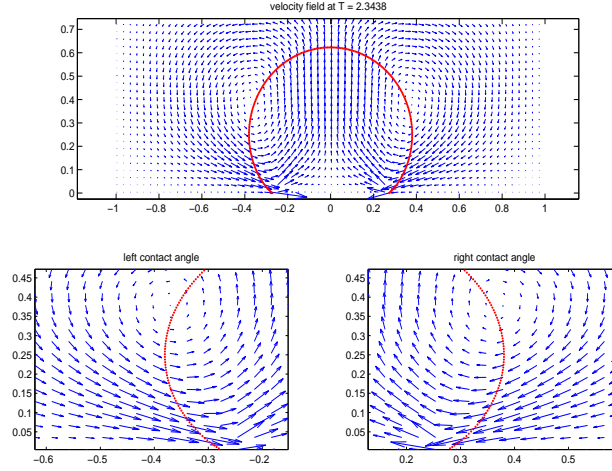


Figure 5.19: The velocity field for the drop with surfactant near the left and right contact lines ( $\eta = 0.3, T = 1.5625$ ).

domain so that the left and right contact lines are located in zone  $I_1$  and  $I_3$ , respectively. See the corresponding diagram in Fig. 5.21 in detail.

Along the circular interface, we choose a nonuniform initial surfactant concentration as

$$\gamma(\alpha) = -\frac{8}{5\pi^3}\alpha^3 + \frac{12}{5\pi^2}\alpha^2 + 0.5, \quad \alpha \in (0, \pi).$$

Fig. 5.22 shows the time evolution plots of the hydrophobic-hydrophilic drop with ( $\eta = 0.3$ , solid line) or without ( $\eta = 0$ , dashed line) surfactant effect. Basically, the existence of surfactant does not make significant difference in present set up. Initially, the motion of the contact line is mainly derived by the contribution of the unbalance Young force. The left contact angle deviates from its equilibrium more than the right contact angle, so the left unbalanced Young force is larger than the right one at the earlier time. Therefore, in the beginning, the left contact line speed is larger than the right one as shown in top row in Fig. 5.23 or Fig. 5.25-(a) and (b). One can also see from Fig. 5.22, at the earlier time, the left portion of drop tends to become non-wetting while the right portion tends to be wetting as expected. This makes the drop look curvier near left contact line and the mass center of the drop shifts a little bit to the left of the drop. When the left contact line arrives at zone  $I_2$  (a continuous transition region from hydrophobic to hydrophilic) around  $t = 1$ , the unbalanced Young force is getting smaller and

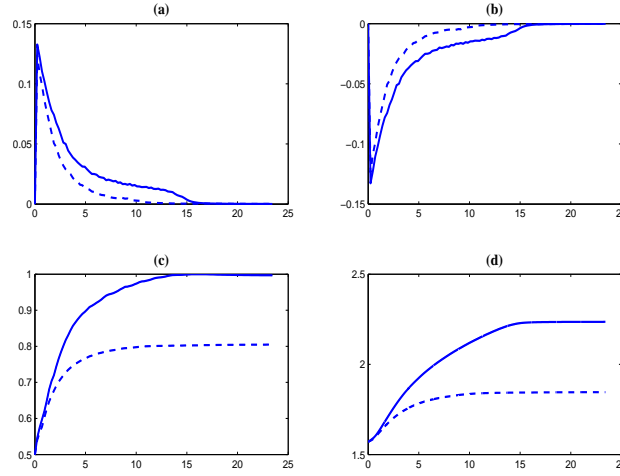


Figure 5.20: (a) Left contact line speed of the drop. (b) Right contact line speed of the drop. (c) Contact angles of the drop. (d) Total length of the drop. Notations and parameters are same as in Fig. 5.18.

smaller, and so is the corresponding contact line speed. Meanwhile, the effect of surface tension becomes apparent and keeps reducing the curvature in the left side of the drop. At the same time, the fluid inside is pushed from left to the right due to the incompressibility of the fluid and then the right contact angle is increasing slightly (away from its corresponding equilibrium), this implies an increase of Young force and leads an increasing contact line speed in a short time, see Fig. 5.25-(a) and (b). After the left contact line crosses the middle of  $I_2$  (around  $t = 3.6$ ), the entire drop falls into a hydrophilic zone, and the rest drop behavior is similar to the hydrophilic wetting case.

In Fig. 5.25, we present four different time evolutionary plots; namely, (a) left contact line speed, (b) right contact line speed, (c) left contact angle, and (d) right contact angle for this hydrophobic case. The contact angles of clean drop match very well to  $0.4\pi$ , while contact angles of the contaminated drop tend to reach  $\theta \approx 0.35\pi$ .

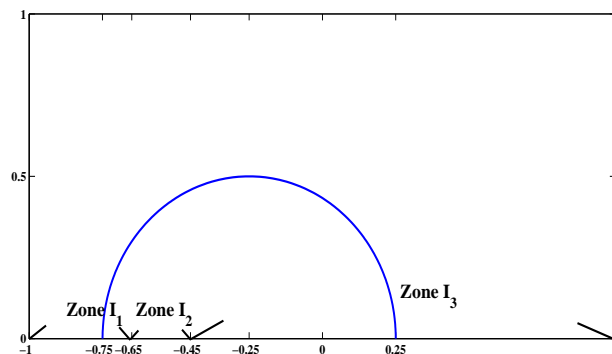


Figure 5.21: Wettability and the initial drop set up.

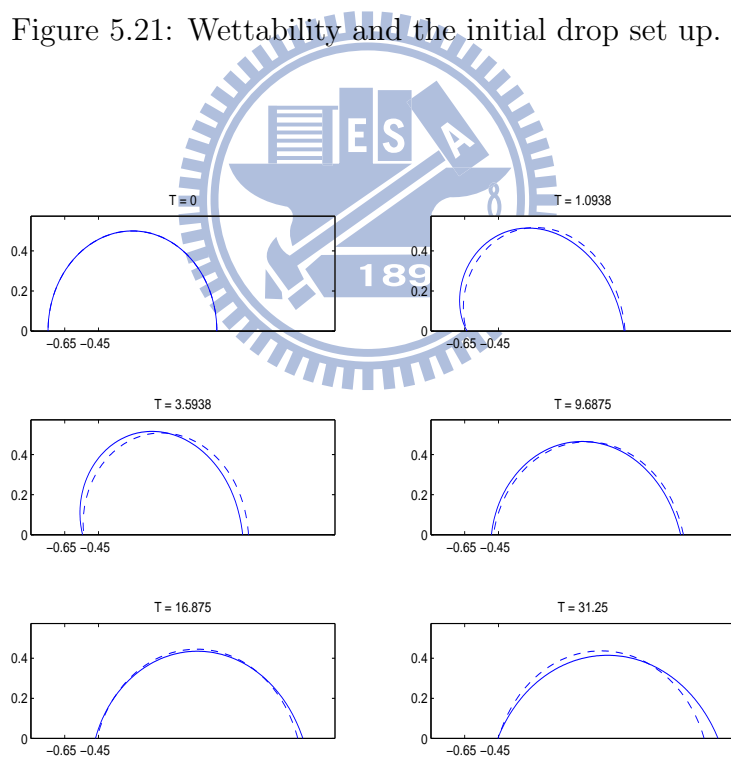


Figure 5.22: The time evolution of a hydrophilic drop with clean ( $\eta = 0$ , dashed line) and contaminated interface ( $\eta = 0.3$ , solid line).



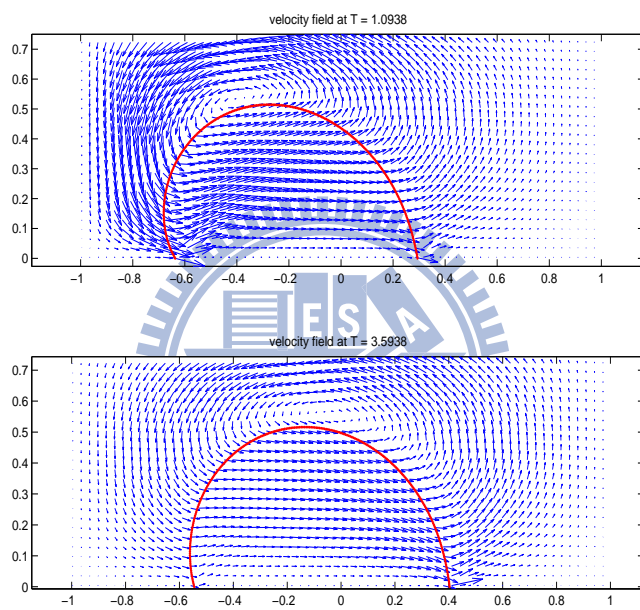


Figure 5.23: The velocity field for the drop with surfactant near the left and right contact lines at  $T = 1.0938, 3.5938$ .

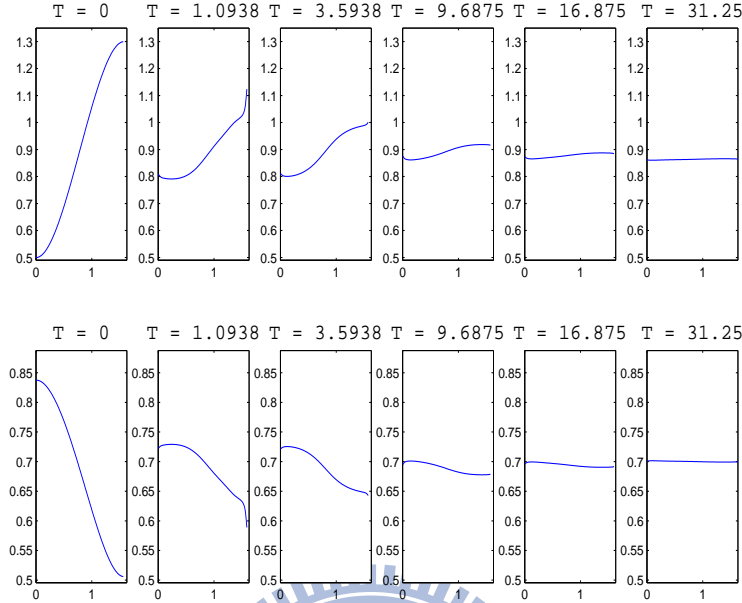


Figure 5.24: Distribution of the surfactant concentration (top) and the corresponding surface tension (bottom).

## 5.5 A rising bubble in a fluid with gravity effect

In this section, we aim to validate that our numerical method can be extended straightforward to more realistic interfacial flow problems, that is, the fluids inside and outside the interface have different fluid properties (density and viscosity), although we consider only constant fluid properties in all previous sections. Basically, we just need to consider an extra indicator function  $I(\mathbf{x}, t)$  evaluated by solving a Poisson equation in Eq. (4.45) to determine where is fluid 1 and where is fluid 2 and use Eqs. (4.44) and (4.43) to update the density and viscosity, respectively. Since we now have different fluid properties, the fast direct solver we used to solve linear systems in the projection method is no longer available due to variable coefficient of the diffusion operator. Alternatively, an iterative solver, based on a semi-coarsening geometric multigrid method [3, 32], replaces to solve these linear systems. In this test, we consider the motion of a liquid bubble rising in a two-dimensional domain  $\Omega = [-0.64, 0.64] \times [-0.64, 1.92]$  due to gravity

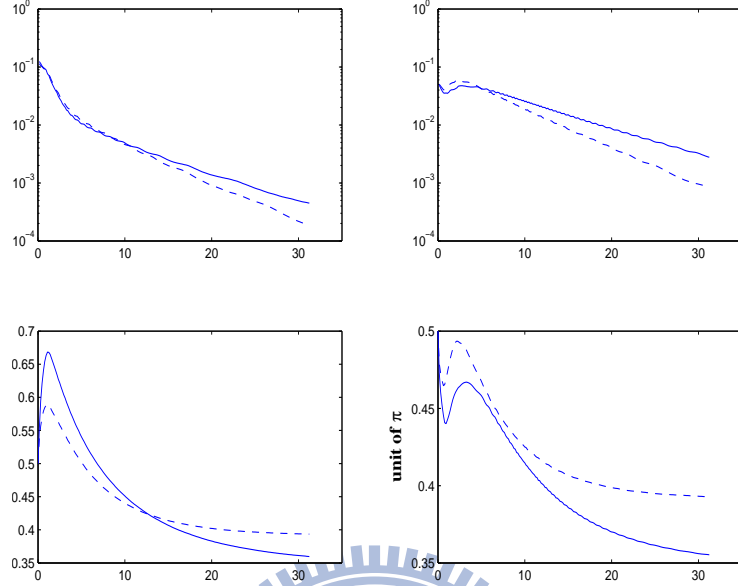


Figure 5.25: (a) Left contact line speed of the drop. (b) Right contact line speed of the drop. (c) Left contact angle of the drop. (d) Right contact angle of the drop.

$g_\infty = 1$ . The radius of the liquid bubble set to be  $R = 0.35$ . The boundary conditions are given as  $\mathbf{u}(\mathbf{x}; t)|_{\partial\Omega} = 0$  and the initial conditions are  $u(\mathbf{x}; 0) = v(\mathbf{x}; 0) = 0$ . The density and viscosity ratios  $\rho_2/\rho_1 = \mu_2/\mu_1 = 10$ , where subscripts 1 and 2 stand for values inside and outside the bubble, respectively. In addition, we set  $\rho_1 = 10$  and  $\mu_1 = 0.01$ . The surface tension  $\sigma$  is varied as it determines the shape of the interface separating the two fluids. More precisely, we use a non-dimensional parameter called the Eotvos number  $Eo$ , which is the ratio of the gravity and the surface tension force.

Fig. 5.26(a) is the evolution of the interface which separates the two fluids at  $t = 0, t = 7, t = 14$ , and  $t = 20$  with  $Eo = 0.1$  while the shape of the rising bubble with  $Eo = 10$  at the same time intervals is shown in Fig. 5.26(b). In each case, the leakage of the area inside the bubble is within 0.5%. It can be seen that the shape of the bubble is clearly affected by the value of the Eotvos number. The shape of the liquid drop remains circular when the Eotvos number is small (corresponding to a large surface tension coefficient). When the Eotvos number is large (corresponding to a small surface tension

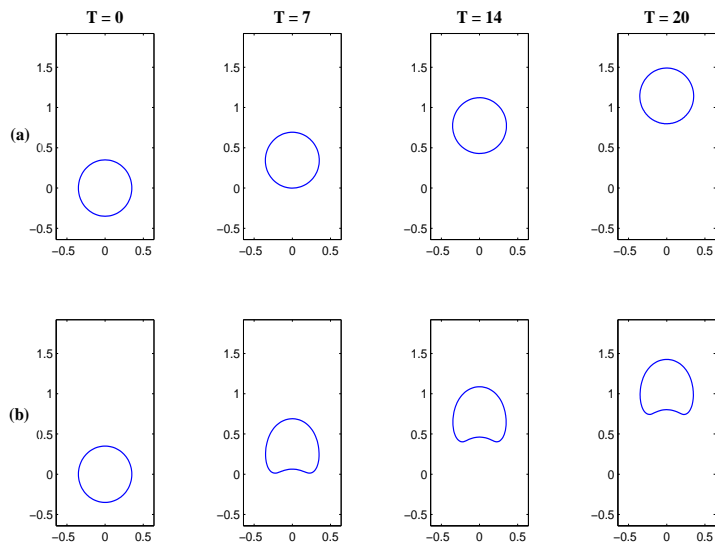


Figure 5.26: (a) A rising bubble with  $E_o = 0.1$ . (b) A rising bubble with  $E_o = 10$ .

coefficient), however, significant deformation can be observed. In another words, the surface tension affects the shape of the bubble. This is consistent with experimental observations.

# Chapter 6

## Summary and future work

In this dissertation, we introduced a mathematical model for the interfacial flow problems such as a bubble in a shear flow and the moving contact line problems. We have developed an immersed boundary method for two-dimensional interfacial flows with insoluble surfactant. The governing equations (Navier-Stokes equations) are formulated in a usual immersed boundary framework where a mixture of Eulerian fluid and Lagrangian interfacial variables are used, with the linkage between those two different variables is provided by the Dirac delta function. The immersed boundary force comes from the nonhomogeneous surface tension which is affected by the distribution of surfactants along the interface. In addition, the unbalanced Young force should be applied at the contact lines to mimic the tendency to the equilibrium in the moving contact line problems (Navier-slip boundary conditions should be imposed on the solid substrate which contact lines adhere to). By tracking the interface in a Lagrangian manner, a simplified surfactant concentration equation can be obtained. The numerical method involves solving the Navier-Stokes equations on a staggered grid by a semi-implicit pressure increment projection method where the immersed interfacial forces are calculated at the beginning of each time step. Once the velocity values and interfacial configurations are obtained, a dynamical control of Lagrangian markers is introduced so that the physical spacing of the markers can be kept uniformly. Then the corresponding modified surfactant equation is solved in a new symmetric discretization such that the total mass of surfactant along the interface is conserved numerically. Numerical results include the convergence analysis, a bubble with surfactant in a shear flow, the effect of the surfactant for hydrophilic and hydrophobic drops, and a rising bubble in a flow with gravitational effect. These numerical results match mathematical predictions well, and show that one can trustfully use the method we presented here to simulate related interfacial flow problems or extend the idea

of this work to predict phenomena with more complicated effects.

As a next step, we will generalize the present algorithm to simulate two phase flows with distinct densities and viscosities for the moving contact line problems. In particular, we plan to study the effect of soluble surfactant on drop detachment from a solid surface, i.e., a problem with moving contact points/lines. We also like to extend the idea of this work to first three-dimensional axi-symmetric flows, and then we plan to generalize the current work to general 3D simulations.



# Bibliography

- [1] R. Aris, *Vectors, Tensors, and the Basic Equations of Fluid Mechanics*, Prentice-Hall, Englewood Cliffs, NJ, 1962.
- [2] D. L. Brown, R. Cortez, M. L. Minion, Accurate projection methods for the incompressible Navier-Stokes equations, *J. Comput. Phys.*, 168 (2001) 464–499.
- [3] W. L. Briggs, V. E. Henson, S. F. McCormick, *A multigrid tutorial*, SIAM, 1987.
- [4] J. U. Brackbill, D. B. Kothe, C. Zemach, A continuum method for modeling surface tension, *J. Comput. Phys.*, 100 (1992) 335–254.
- [5] H. D. Ceniceros, The effects of surfactants on the formation and evolution of capillary waves, *Phys. Fluids*, 15(1), (2003) 245–256.
- [6] A. J. Choirn, Numerical Solution of the Navier-Stokes Equations, *Math. Comp.*, 22 (1968) 745–762.
- [7] L. G. Currie, *Fundamental mechanics of fluids*, McGraw-Hill, 1993.
- [8] S.H. Davis, G.K. Batchelor, H.K. Moffatt, M.G. Worster (Eds.), *Perspectives in Fluid Dynamics*, Cambridge University Press, Cambridge, 2002.
- [9] P. G. De Gennes, F. Brochard, D. Quere, *Gouttes, Bulles, Perles Ondes*, Edition Berlin, 2002.
- [10] M. A. Drumright-Clarke, Y. Renardy, The effect of insoluble surfactant at dilute concentration on drop breakup under shear with inertia, *Phys. Fluids*, 16(1), (2004) 14–21.
- [11] E. B. Dussan V., The moving contact line: the slip boundary condition, *J. Fluid Mech.*, 77, (1976), 665–684.

- [12] E. B. Dussan V., On the spreading of liquids on a solid surface: static and dynamic contact lines, *Ann. Rev. Fluid Mech.*, 11, (1979), 371–400.
- [13] C. A. J. Fletcher, *Computational techniques for fluid dynamics: fundamental and general techniques*, Berlin: Springer-Verlag, 1991.
- [14] P. G. de Gennes, Wetting: statics and dynamics, *Rev. Mod. Phys.*, 57(3), (1985) 827–863.
- [15] M. Griebel, T. Dornseifer, T. Neunhoeffer, *Numerical simulation in fluid dynamics: a practical introduction*, SIAM, 1998.
- [16] S. Ganesan, L. Tobiska, Modelling and simulation of moving contact line problems with wetting effects, *Comput. Visual Sci.*, DOI 10.1007/s00791-008-0111-3, (2008).
- [17] F. H. Harlow, J. E. Welsh, Numerical calculation of time-dependent viscous incompressible flow of fluid with a free surface, *Phys. Fluids*, 8 (1965) 2181–2189.
- [18] T. Y. Hou, J. S. Lowengrub, M. J. Shelley, Removing the stiffness from interfacial flows with surface tension, *J. Comput. Phys.*, 114 (1994), 312–338.
- [19] H. Huang, M.-C. Lai, H.-C. Tseng, A parametric derivation of the surfactant transport equation along a deforming fluid interface, *Frontiers of Applied and Computational Mathematics*, (2008), 198–205.
- [20] H. Huang, D. Liang, B. Wetton, Computation of a moving drop/bubble on a solid surface using a front-tracking method, *Comm. Math. Sci.* 2(4) (2004) 535–552.
- [21] C. Huh, L. E. Scriven, Hydrodynamic model of steady movement of a solid/liquid/fluid contact line, *J. Colloid Interf. Sci.* 35 (1971), 85–101.
- [22] M. Hameed, M. Siegel, Y.-N. Young, J. Li, M. R. Booty, D. T. Papageorgiou, Influence of insoluble surfactant on the deformation and breakup of a bubble or thread in a viscous fluid, *J. Fluid Mech.*, in press.
- [23] D. Jacqmin, Contact-line dynamics of a diffuse fluid interface, *J. Fluid Mech.*, 402 (2000), 57–88.
- [24] A. J. James, J. S. Lowengrub, A surfactant-conserving volume-of-fluid method for interfacial flows with insoluble surfactant, *J. Comput. Phys.*, 201 (2004) 685–722.



- [25] V. G. Levich, *Physicochemical Hydrodynamics*, Prentice Hall, 1962.
- [26] H. Liu, S. Krishnan, S. Marella, H. S. Udaykumar, Sharp interface Cartesian grid method II: A technique for simulating droplet interactions with surfaces of arbitrary shape, *J. Comput. Phys.*, 210 (2005), 32–54.
- [27] L. D. Landau, E. M. Lifshitz, *Fluid Mechanics*, Pergamon Press, New York, 1958.
- [28] R. LeVeque, Z. Li, The immersed interface method for elliptic equations with discontinuous coefficients and singular sources, *SIAM J. Numer. Anal.*, 31 (1994) 1019–1044.
- [29] X. Li, C. Pozrikidis, Shear flow over a liquid drop adhering to a solid surface, *J. Fluid Mech.*, 307 (1996) 167–190.
- [30] J. Lee, C. Pozrikidis, Effect of surfactants on the deformation of drops and bubbles in Navier-Stokes flow, *Comput. Fluids*, 35 (2006) 43–60.
- [31] M.-C. Lai, Y.-H. Tseng, H. Huang, An immersed boundary method for interfacial flow with insoluble surfactant, *J. Comput. Phys.* 227 (2008) 7279–7293.
- [32] M.-C. Lai, C.-T. Wu, Y.-H. Tseng, An efficient semi-coarsening multi-grid method for variable diffusion problems in cylindrical coordinates, *Appl. Numer. Math.* 57 (2007) 801–810.
- [33] M. Muradoglu, G. Tryggvason, A front-tracking method for computations of interfacial flows with soluble surfactants, *J. Comput. Phys.*, 227 (2008) 2238–2262.
- [34] A. Oron, S. H. Davis, S. G. Bankoff, Long-scale evolution of thin liquid films, *Rev. Mod. Phys.*, 69 (1997), 931–980.
- [35] C. S. Peskin, Flow patterns around heart valves: a numerical method, *J. Comput. Phys.* 10 (1972) 252.
- [36] C. S. Peskin, The immersed boundary method, *Acta Numerica*, 1–39, (2002).
- [37] C. S. Peskin, B. F. Printz, Improved volume conservation in the computation of flows with immersed elastic boundaries, *J. Comput. Phys.* 105 (1993) 33–36.

- [38] Y. Pawar, K. J. Stebe, Marangoni effects on drop deformation in an extensional flow: the role of surfactant physical chemistry, I. Insoluble surfactants, *Phys. Fluids*, 8 (1996) 1738.
- [39] C. A. Powell, M. D. Savage, Numerical simulation of transient free surface flow with moving contact lines, *Commun. Numer. Meth. Engng*, 17 (2001) 581–588.
- [40] T. Qian, X.-P. Wang, P. Sheng, Molecular scale contact line hydrodynamics of immiscible flows, *Phys. Rev. E* 68, (2003) 016306.
- [41] T. Qian, X.-P. Wang, P. Sheng, Power-law slip profile of the moving contact line in two-phase immiscible flows, *Phys. Rev. Lett.* 93(9), (2004) 094501.
- [42] T. Qian, X.-P. Wang, P. Sheng, Molecular hydrodynamics of the moving contact line in two-phase immiscible flows, *Commun. Comput. Phys.*, Vol 1, No 1, pp. 1–52 (2006).
- [43] W. Ren, W. E, Boundary conditions for moving contact line problem, *Phys. Fluids* 19, (2007) 022101.
- [44] A. M. Roma, C. S. Peskin, M. J. Berger (1999), An adaptive version of the immersed boundary method. *J. Comput. Phys.* 153 (1999) 509–534.
- [45] M. Renardy, Y. Renardy, J. Li, Numerical simulation of moving contact line problems using a volume-of fluid method, *J. Comput. Phys.*, 171 (2001), 243–263.
- [46] L. E. Scriven, Dynamics of a fluid interface, *Chem. Eng. Sci.* 12 (1960) 98.
- [47] Y. D. Shikhmurzaev, *Capillary Flows with Forming Interfaces*, Chapman & Hall/CRC Press, 2008.
- [48] Peter D.M. Spelt, A level-set approach for simulations of flows with multiple moving contact lines with hysteresis, *J. Comput. Phys.* 207 (2005) 389–404.
- [49] H. A. Stone, A simple derivation of the time-dependent convective-diffusion equation for surfactant transport along a deforming interface, *Phys. Fluids A* 2(1), (1990) 111–112.

- [50] S. Sikalo, H.-D. Wilhelm, I. V. Roisman, S. Jakirlic, C. Tropea, Dynamic contact angle of spreading droplets: Experiments and simulations, *Phys. Fluids* 17, (2005) 062103.
- [51] P. Tabeling, *Introduction to Microfluidics*, Oxford University Press, 2005.
- [52] G. Tryggvason, B. Bunner, A. Esmaeeli, D. Juric, N. Al-Rawahi, W. Tauber, J. Han, S. Nas, Y.-J. Jan, A front-tracking method for the computations of multiphase flow, *J. Comput. Phys.*, 169 (2001) 708–759.
- [53] S. O. Unverdi, G. Tryggvason, A front-tracking method for viscous incompressible multi-fluid flows, *J. Comput. Phys.*, 100 (1992) 25–37.
- [54] H. Wong, D. Rumschitzki and C. Maldarelli, On the surfactant mass balance at a deforming fluid interface, *Phys. Fluids*, 8(11) (1996) 3203–3204.
- [55] A. M. Waxman, Dynamics of a couple-stress fluid membrane, *Stud. Appl. Math.* 70, (1984) 63.
- [56] J.-J. Xu, Z. Li, J. S. Lowengrub, H.-K. Zhao, A level-set method for interfacial flows with surfactant, *J. Comput. Phys.*, 212 (2006) 590–616.
- [57] J.-J. Xu, H.-K. Zhao, An Eulerian formulation for solving partial differential equations along a moving interface, *J. Sci. Comput.*, 19 (2003) 573–593.
- [58] K. Yokoi, D. Vadillo, J. Hinch, I. Hutchings, Numerical studies of the influence of the dynamic contact angle on a droplet impacting on a dry surface, *submitted to Physics of Fluids* (2009).